# MEMBRANE PERMEABILITY AND TRANSPORT STUDIES OF COENZYME A, ITS PRECURSORS AND ANTIMETABOLITES

**Koketso Seipelo Precious Mogwera**

Dissertation presented for the degree of Doctor of Philosophy (Biochemistry) in the Faculty of Natural Sciences at Stellenbosch University

**Supervisor: Professor Erick Strauss**
Department of Biochemistry, Stellenbosch University

**Co-Supervisor: Dr Marianne de Villiers**
Department of Biochemistry, Stellenbosch University

March 2020

# Declaration

By submitting this dissertation electronically, I declare that the entirety of the work contained therein is my own, original work, that I am the sole author thereof (save to the extent explicitly otherwise stated), that reproduction and publication thereof by Stellenbosch University will not infringe any third party rights and that I have not previously in its entirety or in part submitted it for obtaining any qualification.

March 2020

*For my Parents: Matshediso le Motshidisi Mogwera*

*BoKorwe lo tlhokile go ja ba bapalela nna tsetsi,*

*BoKgaka kgolo lo tlhokile mebala gore nna kgakana ke nne le mebala.*

*Moremogolo go betlwa wa taola, wa motho o a ipetla.*

# Acknowledgements

I want to thank my heavenly father, in whom everything is created. He is with me all the time – *O ntwetse dintwa.* I also want to thank my supervisor Prof Erick Strauss for giving me a chance at a time when I had really lost confidence in my capabilities as a scientist. I also want to thank my co-supervisor Dr. Marianne de Villiers for being more than just a science mentor, for your words of encouragement and practical advice. I also want to thank our lab manager Dr. Helba Bredell – you made a difficult load seem lighter with your presence and charm. I would also like to thank the Strauss-de Villiers research lab members and the alumni for cultivating a good work environment. A special thank you to Konnie, Sarah and Blake for making the thesis writing a "pleasant" experience – *Montsamaisa bosigo ke mo leboga bo sele.* I also want to thank the Rautenbach lab members – for the many great engagements through the years. I want to thank the Biochemistry department at Stellenbosch University for a culture of excellence that it has embodied in its members. I also want to thank my family at Christ Church Stellenbosch for allowing me to be a part of something so much greater than myself. To my friends – Tebogo, Precious and Tshegofatso, even when you did not fully understand, you listened to my grievances, and celebrated with me when a celebration was warranted. Thank you so much for always reminding me of my true identity – for always reminding me that I am fearfully and wonderfully made. I thank the lord for the gift of your time and love in this journey called life. I also want to thank my parents – *Bokgaka kgolo lo tlhokileng mebala gore nna ke nne le mebala.* Thank you for supporting me, for believing even when you did not understand where this journey could take me, thank you for standing with me through the darkest of hours – I thank the Lord that you are still here to witness the end of journey, and the beginning of another. To my brother Motheo – I went before you so that you could know that you have permission to dream and breathe life into those dreams, it is all within reach. I would also like to thank everyone else I came across on this journey for adding color to this picture. It was more than just an academic journey – it was a journey of redemption, of self-discovery, of creating. As I stand on top of this hill in euphoria, I am fully aware that there are even greater mountains to climb – the mountains that I now I have the confidence to climb because I now know that I have what it takes. E ya tlhatlhoga Kgabo!

# Abstract

Coenzyme A (CoA) is a cofactor essential to several metabolic processes, including central energy and fatty acid metabolism. In addition, there is increasing evidence that CoA also plays an important role in the rate of neurodegeneration and aging. CoA is usually biosynthesized from vitamin B5, but recently it was shown that dietary CoA can also replenish intracellular CoA levels through degradation of exogenous CoA by ecto-nucleoside pyrophosphatases into 3',5'-ADP and 4'-phosphopantetheine (P-PantSH), which is subsequently taken up by cells. Importantly, permeability studies suggested that this uptake occurs by passive diffusion, an observation that was further confirmed by nutrient complementation studies in *Drosophila* S2 cells containing a mutation that results in CoA depletion. Moreover, investigation of CoA homeostasis in *Escherichia coli* suggested that this bacterium irreversibly exports P-PantSH to regulate intracellular CoA levels. This suggests an interplay between eukaryotes and their microbiome regarding the maintenance of levels of this cofactor through the exchange of P-PantSH as a likely nexus metabolite in CoA biosynthesis.

In this study we used a systematic biophysical approach to investigate the determinants of P-PantSH permeability, and whether this relates to the structure of the molecule, or a certain specific membrane composition. This was achieved by devising a new assay specific for determining the membrane permeability of thiolated metabolites (such as P-PantSH), and subsequently applying this assay in studying the permeability of P-PantSH and its structural analogues in model membranes. Our results indicate that the permeability of P-PantSH is dependent on the fluidity of the membranes in question, and that manipulation of membrane composition to affect membrane fluidity offers a new mechanism to regulate the maintenance of CoA levels from exogenous sources. Using the same assay, we were also able to study a mitochondrial solute carrier protein that is apparently involved in the regulation of CoA levels in the mitochondria. ADP-dependent efflux of P-PantSH was observed for the transporter, and this constitutes preliminary evidence of the implied role of P-PantSH as a nexus metabolite of CoA metabolism.

These findings have important implications for the development of drugs that target CoA biosynthesis and utilization, whether in the context of human diseases for the treatment or delay of neurodegenerative diseases, or alternatively as antimicrobials for the treatment of infectious diseases.

# Opsomming

Koënsiem A (KoA) is 'n kofaktor wat noodsaaklik is vir verskeie metaboliese prosesse, waaronder sentrale energie en vetsuurmetabolisme. Daarbenewens is daar toenemende bewyse dat KoA ook 'n belangrike rol speel in die tempo van neurodegenerasie en veroudering. KoA word gewoonlik gebiosintetiseer vanaf vitamien B5, maar onlangs is aangetoon dat KoA in die dieet ook intrasellulêre KoA-vlakke kan aanvul deur die afbraak van eksogene KoA deur ekto-nukleosied pirofosfatases na 3',5'-ADP en 4'-fosfopanteteïen (P-PantSH), wat gevolglik deur selle opgeneem word. Meer belangrik, deurlaatbaarheidstudies het aangetoon dat hierdie opname plaasvind deur passiewe diffusie, 'n waarneming wat verder bevestig is deur voedingsaanvullingsstudies in *Drosophila* S2-selle wat 'n mutasie bevat wat tot die uitputting KoA-reserwes lei. Verder het die ondersoek na KoA-homeostase in *Escherichia coli* voorgestel dat hierdie bakterie P-PantSH onomkeerbaar uitvoer om intrasellulêre KoA-vlakke te reguleer. Dit dui op 'n wisselwerking tussen eukariote en hul mikrobioom t.ov. die handhawing van die vlakke van hierdie kofaktor deur die uitruil van P-PantSH as 'n waarskynlike verbindingsmetaboliet in KoA-biosintese.

In hierdie studie het ons 'n sistematiese biofisiese benadering gebruik om die determinante van P-PantSH-deurlaatbaarheid te ondersoek, en of dit verband hou met die struktuur van die molekule, of 'n spesifieke membraansamestelling. Dit is bewerkstellig deur 'n nuwe toets te ontwerp wat spesifiek is vir die bepaling van die membraandeurlaatbaarheid van tiol-bevattende metaboliete (soos P-PantSH), waarna hierdie toets gebruik is vir die bestudering van die deurlaatbaarheid van P-PantSH en strukturele analoë daarvan in modelmembrane. Ons resultate dui aan dat die deurlaatbaarheid van P-PantSH afhanklik is van die vloeibaarheid van die betrokke membrane, en dat die manipulering van die membraansamestelling om die membraanvloeibaarheid te beïnvloed 'n nuwe meganisme bied om die handhawing van KoA-vlakke vanuit eksogene bronne te reguleer. Met behulp van dieselfde toets kon ons ook 'n mitochondriale vervoerproteïen bestudeer wat betrokke blyk te wees by die regulering van KoA-vlakke in die mitochondria. ADP-afhanklike uitvloei van P-PantSH is waargeneem vir die vervoerproteïen, en hierdie resultaat vorm 'n voorlopige bewys van die implisiete rol van P-PantSH as 'n verbindingsmetaboliet van KoA-metabolisme.

Hierdie bevindings het belangrike implikasies vir die ontwikkeling van medikasie wat KoA-biosintese en -benutting teiken, hetsy in die konteks van menslike siektes vir die behandeling of vertraging van neurodegeneratiewe siektes, of alternatiewelik as antimikrobiese middels vir die behandeling van aansteeklike siektes.

# Table of Contents

# Abbreviations

| | |
|---|---|
| ACPs | Acyl carrier proteins |
| AcpH | ACP hydrolase |
| ADP | Adenosine diphosphate |
| ALP | Alkaline phosphatase |
| AMP | Adenosine monophosphate |
| ATP | Adenosine triphosphate |
| BSA | Bovine serum albumin |
| $CaCl_2$ | Calcium chloride |
| CL | Cardiolipin |
| CAF | Central Analytical Facility |
| Chol | Cholesterol |
| CoaA | Pantothenate kinase |
| CoaB | Phosphopantothenoylcysteine synthetase |
| CoaC | Phosphopantothenoylcysteine decarboxylase |
| CoaD | Phosphopantetheine adenylyltransferase |
| CoaE | Dephospho-CoA kinase |
| CoA | Coenzyme A |
| CoASy | CoA synthase |
| CoPAN | CoASy associated neurodegeneration |
| CPM | 7-diethylamino-3-(4-maleimidophenyl)-4-methylcoumarin |
| dePCoA | Dephospho-CoA |
| DSC | Differential scanning calorimetry |
| DMSO | Dimethyl sulfoxide |
| DMP | Dimethoxypyrimidine |
| DTT | Dithiothreitol |
| DPPC | Dipalmitoylphosphatidylcholine |
| DPCK | Dephospho-CoA kinase |
| DLS | Dynamic light scattering |
| ENPP | Ectonucleo-pyrophosphatases |
| EDTA | Ethylenediaminetetraacetic acid |
| *Ec*PanK | *Escherichia coli* pantothenate kinase |
| FDA | Food and Drug Administration |
| FTIR | Fourier transform infrared spectroscopy |
| GP | Generalized polarization |
| GPL | Glycerophospholipids |

| | |
|---|---|
| G6P | Glucose-6-phosphate |
| GSH | Glutathione |
| h | hour |
| HPLC | High performance liquid chromatography |
| HPTS | 8-hydroxypyrene-1,3,6-trisulfonate (pyranine) |
| HTS | High throughput screening |
| IB | Inclusion body |
| IMAC | Immobilized metal affinity chromatography |
| IPTG | Isopropyl β-d-1-thiogalactopyranoside |
| kDa | kilodalton |
| LDH | Lactate dehydrogenase |
| LPS | Lipopolysaccharide |
| MES | 2-(*N*-morpholino)ethanesulfonic acid |
| MCs | Mitochondrial carriers |
| MOA | Mode of action |
| MWCO | Molecular weight cut off |
| H-SNAC | *N*-acetylcysteamine |
| N7-Pan | N-heptyl pantothenamide |
| N5-Pan | *N*-pentyl pantothenamide |
| *N*-PE-Pan | *N*-phenethyl pantothenamide |
| NADH | nicotinamide adenine dinucleotide, reduced |
| NBIA | Neurodegeneration by brain iron accumulation |
| NMR | Nuclear Magnetic Resonance |
| NPPs | New permeability pathways |
| α-PanAm | *N*-substituted α-pantothenamides |
| *n*-PanAm | *N*-substituted pantothenamides (also just PanAm) |
| HoPanAm | *N*-substituted homopantothenamides |
| PAGE | Polyacrylamide gel electrophoresis |
| PAMPA | Parallel artificial membrane permeability assay |
| PantSH | Pantetheine |
| PanCOOH | Pantothenic acid |
| PanF | Pantothenate permease |
| PanK | Pantothenate kinase (bacterial) |
| PANK | Pantothenate kinase (mammalian) |
| $PanK_{I}$ | Pantothenate kinase type I |
| $PanK_{II}$ | Pantothenate kinase type II |
| $PanK_{III}$ | Pantothenate kinase type III |

| | |
|---|---|
| PKAN | Pantothenate kinase associated neurodegeneration |
| PantOH | Pantothenol |
| PEP | Phosphoenolpyruvate |
| pNPP | *p*-nitrophenyl phosphate |
| P-N5-Pan | 4'-Phospho-*N*-pentyl pantothenamide |
| P-PE-Pan | 4'-Phospho-*N*-phenethyl pantothenamide |
| P-PanCOOH | 4'-Phosphopantothenic acid |
| P-PanOH | 4'-Phosphopantothenol |
| P-PanCys | 4'-phosphopantothenoylcysteine |
| P-PantSH | 4'-Phosphopantetheine |
| PPAT | Phosphopantetheine adenylyltransferase |
| PPCDC | Phosphopantothenoylcysteine decarboxylase |
| PPCS | Phosphopantothenoylcysteine synthetase |
| POPC | 1-palmitoyl-2-oleoyl-sn-glycero-3-phosphocholine |
| POPE | 1-palmitoyl-2-oleoyl-sn-glycero-3-phosphoethanolamine |
| POPG | 1-palmitoyl-2-oleoyl-sn-glycero-3-phosphoglycerol |
| PSA | Polar surface area |
| KCl | Potassium chloride |
| PAP | 3'-Phosphoadenosine-5'-phosphosulfate |
| $PP_i$ | Pyrophosphate |
| PK | Pyruvate kinase |
| Pyr | Pyruvate |
| Ro5 | Lipinski rule of 5 |
| rpm | Revolutions per minute |
| SDEV | Standard deviation |
| SEM | Standard error of the mean |
| SMVT | Sodium dependent multivitamin transporter |
| SLC25 | Solute carrier family 25 |
| SAS | Small angle scattering |
| SDS | Sodium dodecyl sulfate |
| SEM | Scanning electron microscopy |
| SUVs | Small unilamellar vesicles |
| TPP | Thiamine pyrophosphate |
| TCEP | Tris(2-carboxyethyl) phosphine |
| Tris | Tris(hydroxymethyl)aminomethane |

# List of Figures

# 1 Introduction and Literature Review

## 1.1 Poor permeability is still a great barrier to overcome in drug discovery

Before the 1970s drug discovery involved phenotype-based approaches which were very empirical[1]. It was informed by published work, existing drugs and natural products. Screening techniques then involved lower through-put *in vitro* assays that required no understanding of molecular mechanisms of action, as well as *in vivo* phenotype assessments in which activity could be translated into therapeutic impact of a given disease state[2]. As a result, the drug discovery processes were inherently biased towards compounds that were soluble in aqueous conditions and were also bioavailable[1]. This approach was very successful and produced most of the therapeutics still in use today[2,3]. Nonetheless, the drawback of this approach is that it is often challenging to optimize the molecular properties of candidate drug molecules as there is no prior knowledge of the molecular mechanisms of action[2]. Incorporating new technologies into this drug discovery approach is another challenge that is often encountered[2].

Advances in molecular genetics saw the evolution of drug discovery to become more target-based[2,3]. With it came a shift towards protein targets with key roles in pathogenesis, as well as screening for compounds that interact with these targets[4–6]. Current drug discovery processes can therefore be summarised to consist of the following steps[3]:

1. Basic research which involves target identification and selection
    - This is usually based on a hypothesis that inhibition of a certain protein or pathway will result in a therapeutic effect in a disease state.
    - A target is then selected and validated based on this hypothesis.
2. Lead discovery and candidate selection
    - This involves an intensive search to find ‘drug-like’ small molecules or biological therapeutic agent also known as development candidates.
3. Pre-clinical development
    - Identification of a “hit” compound which has the desired effect and the activity of which has been confirmed by further retesting.
4. Clinical development
5. Food and Drug Administration (FDA) filing

The first two steps of this process involve screening of compounds for potential therapeutic properties. There are several approaches that can be used for this, and these include the following[3]:

1. Knowledge-based screening[7,8]

- It involves selection of a small subset of molecules from a large chemical library. The selection is based on knowledge of the target protein, examples from the literature or on molecules of a similar class previously shown to possess the desired activity.

2. Physiological screening
    - This is a tissue-based approach that looks for a response more aligned with the desired *in vivo* effect rather than targeting one specific molecular component.
3. Fragment-based screening[9]
    - Involves the generation of small molecule libraries which are then screened at high concentrations as potential therapeutics.
    - This process is usually accompanied by generation of protein structures by structure-based tools such as X-ray crystallography and computational modelling. The chemical libraries are then screened against structures to identify potential "hits".
4. High-throughput screening (HTS)[10]
    - This is currently the most popular approach and involves screens of entire compound libraries directly against the drug target using more complex assay systems.

HTS became more popular in the 1980s were the advent of technology brought with it automation, which encouraged the development of libraries of chemical compounds using combinatorial chemistry[1,11]. This saw a shift in drug development strategies to focus more on optimization of binding affinity whilst overlooking binding kinetics and conformation of the potential drug molecule to the target. Therefore, more emphasis was placed on chemical functionalization to improve potency of the potential drug molecule towards the target rather than on solubility that would ensure drug bioavailability *in vivo*[1].

Despite their potency *in vitro*, it is now apparent that compounds which demonstrate poor solubility and bioavailability are unlikely to become drug molecules. It has also come to light that efficient membrane permeation maybe necessary for bioavailability[12]. Taken together, these suggest that solubility and permeability assessments may be crucial in identifying a potential drug molecule.

Whilst studies or practices that focus directly on the permeability of potential drug molecules are scarce, guidelines like the Lipinski rule of five (Ro5) has served as good substitutes for predicting this property. Ro5 predicts the therapeutic potential of molecules, and does so in a

manner that takes into account their solubility and permeability characteristics. It stipulates that an ideal drug molecule should have the following features[13]:

- 5 or less hydrogen bond donors
- a molecular mass of 500 or below
- a calculated LogP of 500 or less
- a sum of nitrogen and oxygen atoms (hydrogen bond acceptors) that is equivalent to 10 or less'

Additionally, alternative metrics such as the polar surface area (PSA) were also developed to compliment the Ro5[12,14]. Together these have been successfully applied in the evaluation of orally bioavailable drug molecules.

Nonetheless, in the recent years, many of the FDA approved drug molecules were found to be non-Ro5 compliant. Therefore, it is evident that guidelines like the Ro5 cannot be interpreted in a literal, inflexible manner as that could stunt innovation in drug discovery[1]. Conversely, making it a more common practice to perform comprehensive enquiries into permeability of pontetial drug molecules may be more beneficial for drug discovery: Such enquiries will not only aid in understanding the mechanisms by which drug molecules permeate cells, but can also inform strategies for mitigating poor permeability. This can in turn lead to the repurposing of lead compounds that were dismissed from clinical trial due to poor permeability.

## 1.2 How do small molecules enter the cell?

Small molecules of moderate polarity can readily cross membranes by passive diffusion[15]. For instance small non-polar gases can rapidly cross membranes with a high permeability coefficient of $3.5\times10^{-1}$ cm.s$^{-1}$ reported for $CO_2$[16], whilst even slightly larger polar molecules like urea have lower permeability with a permeability coefficient of $1.35\times10^{-6}$ cm.s$^{-1}$[17]. Conversely, larger molecules of relatively high polarity such as sugars and peptides to name a few, cannot permeate cells by passive diffusion but require transporter-mediated membrane permeation[15]. There are two modes of transporter-mediated cell entry, categorized according to their energy requirement as active transport and facilitated diffusion[15].

Active transport involves translocation of molecules against a concentration gradient and requires energy input. Examples of protein transporters involved in this mode of transport include:

- Ion pumps: these proteins transport ions against their concentration gradients. An example thereof is the $Na^+/K^+$ ATPase which transports three $Na^+$ ions into the cell, and two $K^+$ ions out of the cell for every ATP molecule that is hydrolyzed[18].

On the other hand, facilitated diffusion involves transporter-mediated membrane translocation of molecules in the direction of their concentration gradient, and does not require external energy input[15]. Examples are:

- GLUT transporter family: This group of transporters are responsible for transmembrane import of glucose, galactose and fructose[19].
- Ion channels: allow passive diffusion of inorganic ions with high specificity[20].
- Ionophores: bacteria can synthesize ionophores which facilitate the diffusion of ions across the membrane by complexing and shuttling ions[21].
- Aquaporins: facilitate the transport of water and hydrophilic solutes across the membrane[22].

In addition to these, some organisms also have dedicated efflux systems that are responsible for removal of toxins and other xenobiotics from the cells[22]. The most common of these is the ABC transporter family (e.g.: TolC pump) which is involved in the efflux of structurally diverse *compounds*[23].

### 1.2.1 The outer membrane of Gram-negative bacteria gives intrinsic resistance to antibiotics

Membrane composition is a major determinant of the distinct permeability profiles observed for organisms. Membrane lipids are amphipathic molecules that self-assemble into supramolecular structures such as bilayers. The lipid bilayer is a functional barrier between subcellular compartments, and between the cell and its environment[15,24].

The following gives a brief description of the membrane composition of mammalian and bacterial cells with specific focus on the ability of Gram-negative bacteria to alter the permeability profile of the membranes as a line of defense against antibiotics and other molecules perceived as hostile towards the organism.

#### *1.2.1.1 Mammalian cells*

The plasma membrane is a dynamic bilayer with a thickness of about 5 nm, and is made up of multiple lipid species and membrane proteins[15,24]. The lipids are distributed asymmetrically in the bilayer and can be grouped into three main classes as follows:

- Glycerophospholipids (GPLs): These are made up of fatty acyl chains with a phosphatidyl ester attached to the terminal carbon. The phosphate ester group can either be an ethanolamine, choline, serine or inositol. The fatty acid chains range in size from 16-24 carbons, and can be saturated, mono- or poly-unsaturated[25,26].

- Sphingolipids: these are also phospholipids but with no glycerol backbone. Long fatty acyl chains combine with sphingosine to make up sphingolipids. Sphingosine is made from palmitoyl-CoA and serine[25,26].

- Cholesterol: this is a sterol type lipid which modulates the fluidity of a membrane over a range of physiological temperatures[25].

The best-studied model for eukaryotic membranes is the red blood cell membrane[25,2728]. It is characteristically asymmetric, with the outer leaflet enriched in sphingomyelin and phosphatidylcholine, and the inner leaflet in phosphatidylserine, phosphatidylethanolamine and phosphatidylinositol. Cholesterol is also enriched in the outer leaflet of these membranes.

#### *1.2.1.2 Bacterial cell envelope*

Gram-negative bacteria have a cell envelope made up of two membranes—a cytoplasmic and an outer membrane—separated by a layer of peptidoglycan, as well as a cellular compartment called the periplasm[29].

- Cytoplasmic membrane: This is generally a phospholipid bilayer heavily populated with membrane proteins. Unlike the mammalian plasma membrane, it is exclusively made of GPLs and has no sterols or sphingolipids[26]. The main functions thereof include nutrient import and export of toxins, as well as all membrane-related functions that would be associated with organelles in eukaryotic cells, the most notable of which is energy metabolism[30]. It also serves as barrier to hydrophilic and charged molecules this is especially the case in artificial membranes where protein transporters are absent. The *E. coli* cytoplasmic membrane consists of the following GPLs: phosphatidylethanolamine, phosphatidylglycerol and cardiolipin. Furthermore, the most abundant fatty acids in this organism include palmitic acid (16:0), palmitoleic acid (16:1) and vaccenic acid (18:1) – where (x:y) refers to chain length and number of unsaturated bonds, respectively[31].

- The outer membrane: It can be divided into outer leaflet largely made up of lipopolysaccharide (LPS), and the inner leaflet made up of phospholipids[31].

- The peptidoglycan layer: It is a cell wall that serves a rigid exoskeleton. Gram-positive bacteria, such as *Staphylococcus aureus*, do not have an outer membrane, but have a thick peptidoglycan layer which distinguishes it from Gram-negative bacteria[30].
- The periplasm: it consists of densely packed proteins and as a result is more viscous than the cytoplasm[30,32].

LPS constitutes the outer leaflet of the outer membrane of the cell envelope. This molecule is exclusively found in Gram-negative bacteria is an amphiphilic molecule which carries a negative charge at physiological pH. This in turn gives Gram-negative cells a relatively strong negative charge[29]. As result, the outer membrane is generally resistant to hydrophobic antibiotics, bile salts, detergents and other molecules perceived as hostile by the bacteria. It is therefore presumed that the outer membrane is responsible for the intrinsic resistance to antibiotics that is often observed in Gram-negative bacteria[29,32,33].

In addition to this, Gram-negative bacteria have elaborate efflux systems made up of tripartite structures that span the entire cross-section of the cell envelope[34–36]. These consist of a transporter protein located in the inner cytoplasmic membrane, an accessory protein located in the periplasmic space, and an outer membrane channel (Figure 1-1). These effectively shorten the distance between the cytoplasm and the extracellular space, which in turn translate to efficient efflux rates. The most common example of these outer membrane channels is the TolC protein (Figure 1-1)[37]. These channels are promiscuous and can interact with a wide range of inner membrane transporters.

Gram positive membranes do not have the outer membrane of LPS and phospholipids, and as a result also have a thin periplasm sandwiched between the cytoplasmic membrane and a thick layer of peptidoglycan. This difference in architecture make tripartite efflux systems found in Gram negative bacteria, unnecessary in Gram-positive bacteria. As such, Gram-positive bacteria lack the outer membrane channels which are constituents of the tripartite efflux system in Gram-negative bacteria[38].

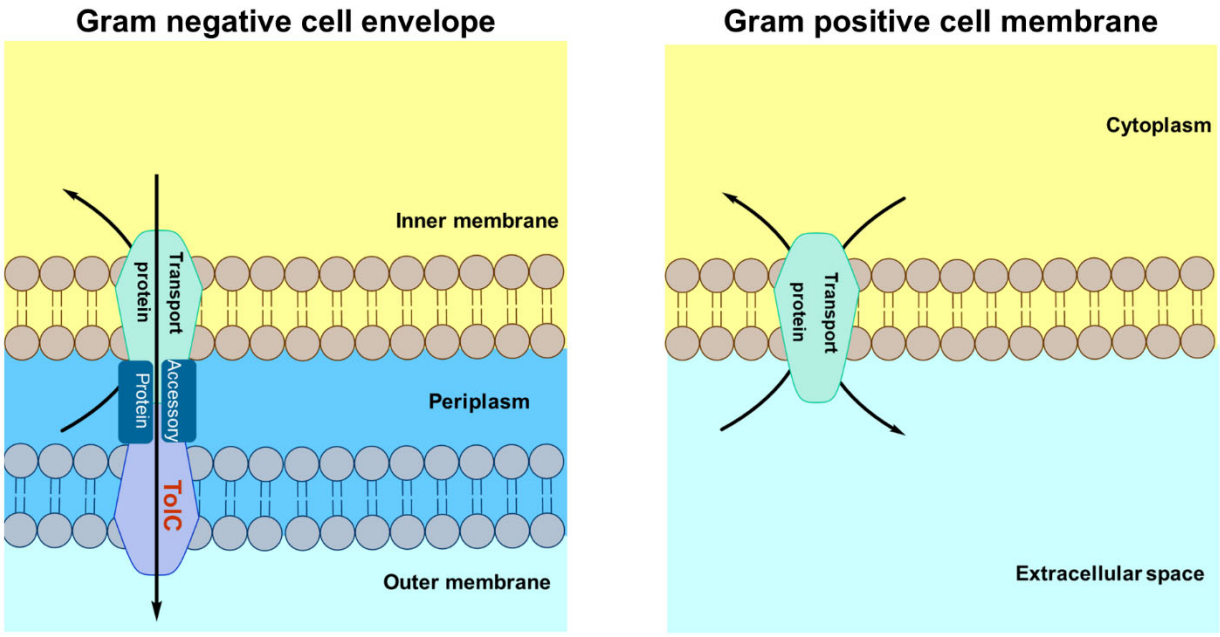


**Figure 1-1: The difference in membrane architecture necessitates tripartite efflux systems in Gram-negative but not Gram-positive bacteria.** Gram-negative bacteria have tripartite efflux systems that span the width of the cell envelope consisting of a transport protein, an accessory protein and the TolC efflux pump situated in the inner membrane, periplasm and outer membrane, respectively. Gram-positive organisms do not have the outer membrane and therefore lack the TolC efflux pump that is often associated with the intrinsic resistance of Gram-negative bacteria to antibiotics. Adapted from Piddock[38].

### 1.2.2 Drug molecules should ideally permeate molecules by passive diffusion

Our current knowledge indicates that Gram-negative bacteria are inherently resistant to antibiotics as a result of poor permeability of the outer membrane. Moreover, the elaborate efflux systems on the cell envelopes of Gram-negative bacteria also make it easy for these organisms to acquire resistance to additional classes of antibiotics. Therefore, the ideal drug molecule against these organisms should be able to permeate the cell envelope, and having done so should remain unrecognizable to the efflux systems. This insaturable mode of entry would enable intracellular accumulation of the drug to concentrations which are sufficient to elicit the desired therapeutic effect. This suggests that the ideal drug molecule should preferably permeate the cell by passive diffusion.

Passive diffusion refers to the movement of molecules across the cell membrane driven by ion or solute gradients[16]. This process is described as passive since there is no external energy input or output required to affect the transport.

According to the solubility-diffusion theory, membrane translocation by passive diffusion occurs in a three-step process summarized as follows: first, the molecule partitions through the membrane, second it diffuses across the membrane, and third it is finally released into the cytoplasm[39,40]. It further states that the permeability of a molecule directly relates to its oil-

water partition coefficient as well as its molecular radius, the latter describing the measure of steric hindrance a molecule will encounter when crossing the bilayer[39,40].

#### *1.2.2.1 Membrane fluidity modulates membrane permeation by passive diffusion*

The solubility-diffusion theory suggests a close relationship between membrane fluidity and permeability of a molecule[39,40] It states that membrane fluidity influences permeability by determining the diffusion rate of the target molecule through the bilayer. Lower membrane fluidity will therefore result in low molecule permeability. This can be explained by the small aqueous filled cavities that form transiently in different regions of the bilayer. These include the interface between the phospholipid head groups and the aqueous medium, as well as the portion of the hydrocarbon chain that is adjacent to the head groups. According to the solubility-diffusion theory, solutes dissolve into the cavities and so permeate the membrane. Membrane regions with lower fluidity has less of these cavities, which in turn translate to lower solute permeability[39,40].

Membrane fluidity is in turn modulated by membrane composition: GLPs are the most abundant type of lipids in membranes, and its main components include two acyl (fatty acid-derived) chains and a hydrophilic head group[25,26,41].The head group generally determines the molecular geometry of the phospholipid, which in turn determines membrane fluidity, as shown in Figure 1-2. For example, lysophospholipids, which play a major role in signaling, adopt a conical geometry (Figure 1-2 A). Phosphatidylcholine, which is a major constituent of eukaryotic membranes, has a cylindrical shape (Figure 1-2 B), while another common bilayer constituent, phosphatidylethanolamine, –has a small head group that gives it inverted cone geometry (Figure 1-2 C)[26]. The phospholipids with cylindrical geometry can pack tight together and tend to produce solid “gel-like” membranes (Figure 1-2 D), whereas conical shaped phospholipids tend to increase membrane curvature, which also appears to be important for insertion of membrane proteins[26,40,42]. Moreover, combinations and ratios of saturated to unsaturated fatty acid chains also determine lipid packing, membrane viscosity, as well as water permeability in the membrane[26,40,43,44]. GPLs with long saturated fatty acid chains tend to produce thicker, relatively rigid membranes (Figure 1-2 D). This is because the saturated fatty acid chains pack tightly together. On the other hand, the double bonds of the unsaturated fatty acids cause kinks which prevent tight packing of the membrane thereby making the membrane more fluid (Figure 1-2 E). The introduction of sterol lipids such a cholesterol also have “fluidizing” effects that produce relatively fluid membranes that also tend to be thicker than non-sterol containing membranes (Figure 1-2 F)[26,40,43,44].

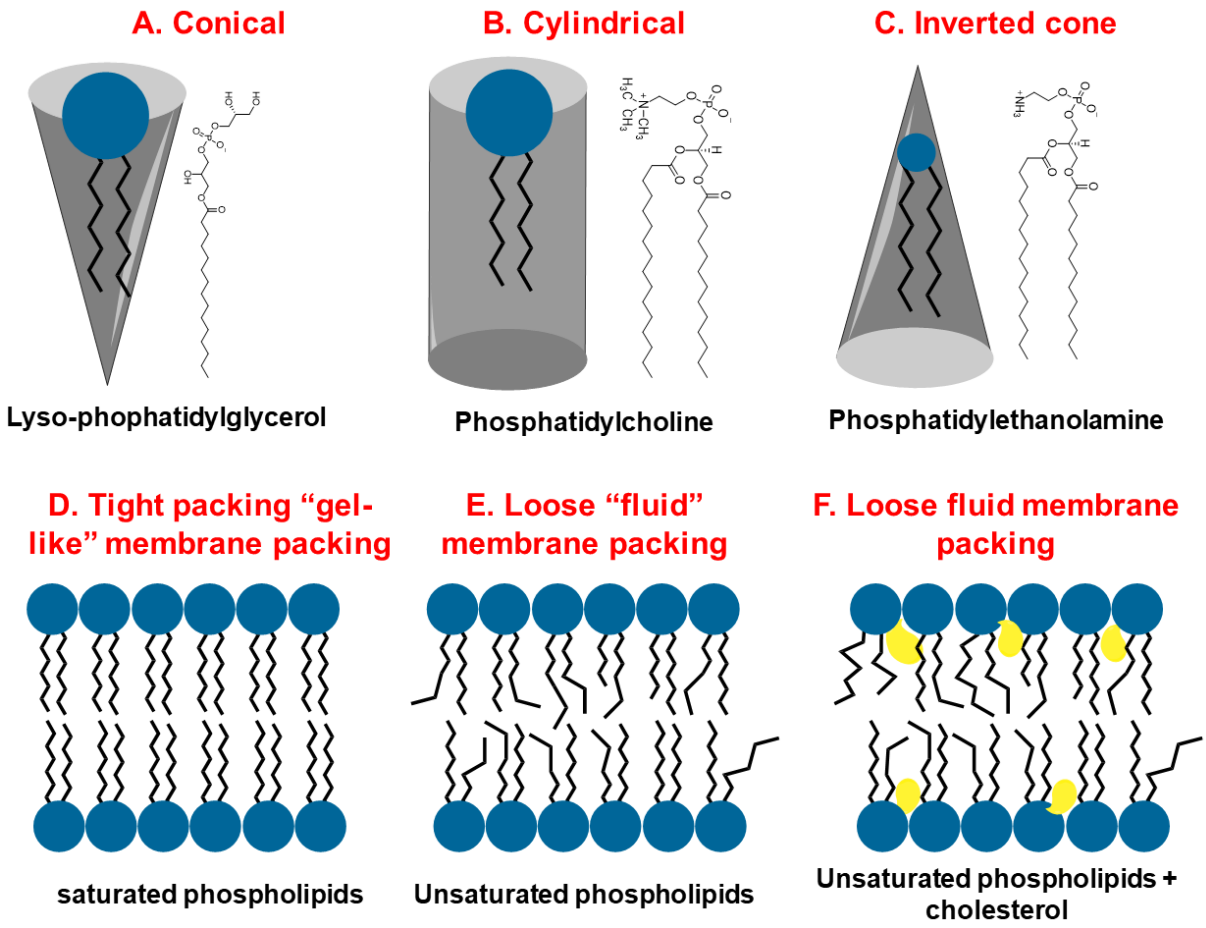


**Figure 1-2: Phospholipid composition determines membrane fluidity.** Lysophospholipids generally have conical molecular geometry (A). Phospholipids with large head groups like phosphatidylcholine assume a cylindrical (B) shape, whereas the phospholipids with relatively small headgroups like phosphatidylethanolamine assume inverted conical molecular geometry (C). The fatty acyl chain saturation also contributes to the molecular geometry also determines membrane fluidity. Saturated phospholipids pack tightly together to produce "gel-like" membranes (D), whereas the kinks produced by the double bonds in unsaturated fatty acid chains pack less tightly to produce membranes of higher fluidity (E). Finally, introducing sterol lipids (symbolised by yellow shapes) such a cholesterol also have a "fluidizing" effect that also leads to membranes that tend to be thicker than non-sterol containing membranes (F). Adapted from Ernst et al.[42]

### 1.2.3 How do we study membrane permeation by passive diffusion?

There are different factors to consider when studying membrane permeability. The selection of models for this purpose largely depends on the membrane transport mechanism in question. The evolution of drug discovery towards HTS prompted the complimentary development of high-throughput permeability screening methods. The most popular of these include the use of Caco-2 monolayers and the PAMPA assay, both of which are briefly discussed below. These are contrasted with the use of liposomes that are not necessarily suitable for high-throughput screening but are still an important tool for studying membrane permeability *in vitro*.

#### *1.2.3.1 Caco-2 monolayers*

Caco-2 monolayers are immortalized cell lines derived from human colon adenocarcinoma cells that are grown on Transwell® polycarbonate membranes to be used as a transport model system for the small intestinal epithelium[45,46]. As such, they are most often used to predict the likely rate of absorption of compounds in the intestine. These are popular because the assay can be performed in a high-throughput format, and also because the monolayers are a representation of biological membranes[47–50]. However, they are exclusively used as a mammalian membrane model. The lack of versatility, inability to distinguish between passive and active transport, as well as the high cost of maintaining the cell lines are some of the drawbacks of this method [4748–50].

#### *1.2.3.2 PAMPA assay*

The Parallel Artificial Membrane Permeability Assay (PAMPA)[50–52] is more cost effective than the monolayer assays as it does not require maintenance of cell lines. However, as is the case with the Caco-2 monolayers, PAMPA assays usually model mammalian cell membranes exclusively. Furthermore, PAMPA assays are exclusively prepared from synthetic lipids and the preparation is such that the researcher cannot manipulate the phospholipid composition.

#### *1.2.3.3 Liposomes*

While the characteristics of the Caco-2 monolayer and PAMPA assays make them indispensable as screening tools, these methods are often not useful as investigational tools, especially when the aim is to understand in greater detail how a drug molecule permeates the membrane. For such studies, liposomes often offer the best alternative. Liposomes are microscopic spherical artificial vesicles created from natural phospholipids, with or without cholesterol[53]. Liposomes have traditionally been used to study biological membranes in general, and have several practical applications, the most notable of which is drug delivery studies. The environmental temperature, conditions of the lipid-water mixture as well as the molecular geometry of the lipids all determine the kind of colloidal particle produced (Figure 1-3)[54]. Detergents and lysophospholipids which have conical shapes tend to produce normal micelles (Figure 1-3 A). Phospholipids of cylindrical molecular geometry such as phosphatidylcholine and phosphatidylserine usually promote formation of lamellar vesicles (Figure 1-3 B). These vesicles can have single or multilamellae, and the term “liposome” usually describes single lamellar vesicles. On the other hand, phosphatidylethanolamine and cardiolipin that have a cone-shaped geometry usually form reverse micelles (Figure 1-3 C). [54].

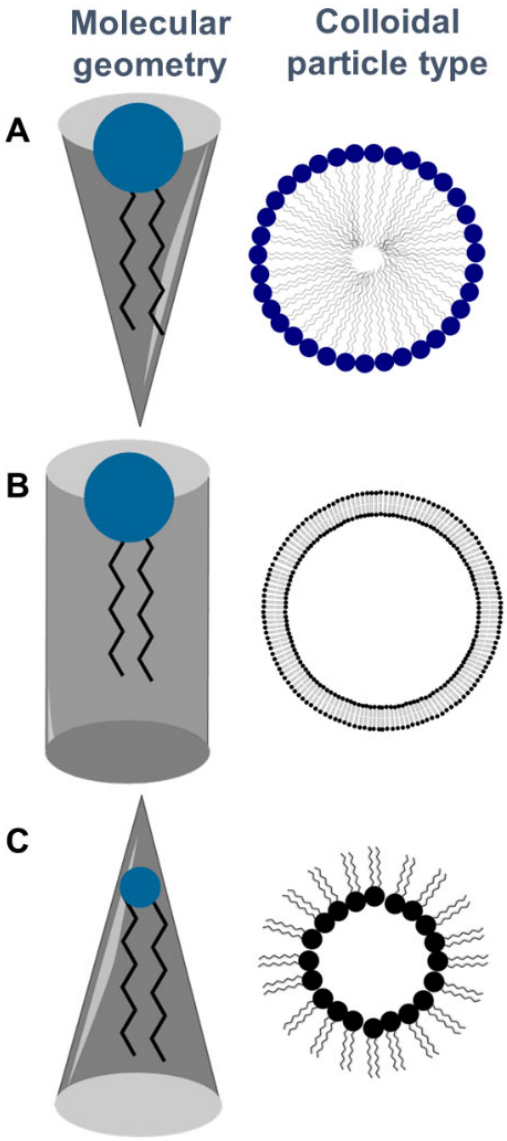


**Figure 1-3: The molecular geometry of phospholipids determines the type of liposomal aggregate.** Phospholipids aggregate spontaneously in aqueous conditions and the colloidal particles formed depend on the properties of the aqueous solution as well as the molecular geometry of the phospholipids used. Phospholipids of conical geometry form micelles (A), cylindrical phospholipids form lamellar vesicles (referred to as liposomes) (B) and inverted conical phospholipids form inverted micelles (C).

Cell-sized liposomes that encapsulate biomolecules provide a versatile mimic of certain aspects of the cell membrane[54,55]. In addition to this, the lipid composition can be manipulated as required, so liposomes can adopt versatile physical characteristics[30,56]. Liposomes also have a low toxicity, and an ability to enclose a wide variety of molecules within its cavity[53,57]. These properties make liposomes attractive as an investigational tool for a large diversity of membrane and membrane permeability studies.

Taken together, these show that despite recent technological advances to improve drug discovery turnover, no new classes of drugs have been identified in the recent years. This can

largely be attributed to a poor understanding of membrane permeability of drug-like molecules. Moreover, whilst guidelines like Ro5 have been useful in predicting – with reasonable accuracy, the probability of a drug molecule to be orally available, such guidelines cannot continue to substitute a fundamental understanding of drug permeability. This is particularly since a substantial amount of recently FDA approved drugs do not obey Ro5, whilst many of the Ro5 obeying molecule go into attrition. This shows that without a fundamental understanding of the molecular determinants of small molecule permeability we cannot hope to make any meaningful progress as far as it relates to drug discovery. Therefore, we use CoA focused drug development to illustrate how poor permeability continues to stunt progress in this field, and how we could benefit from a systematic investigation of small molecule permeability. We make a case for the pantothenamides, which are structural analogues of the CoA precursor pantetheine, as good candidates to help us understand the key structural features that confer permeability (or impermeability) of small molecules, and how insight gained from such an investigation can help us improve (without compromising potency towards the target) membrane permeability of potential drug molecules.

## 1.3 Coenzyme A metabolism and CoA-focused drug discovery: a case study in the biological relevance of the membrane permeability of small molecules

In the early days following its discovery, CoA (**1**, Figure 1-4) was viewed as an “acetate activator”, hence the name coenzyme A (the “A” referring to acetate)[58]. This coenzyme is required by a substantial amount of enzymes for catalytic activity. As such, it is implicated in a number of essential biological processes like energy metabolism, protein acetylation and fatty acid metabolism, to name a few[59–62]. CoA also acts by serving as the source of the phosphopantetheine modification that is found in most acyl- and peptidyl carrier proteins (Figure 1-4). Whether in such proteins or in CoA itself, the functionally relevant component is the terminal –SH on the phosphopantetheine moiety, as it forms thioesters with the –COOH groups of other biomolecules, thereby activating them for catalysis[63].

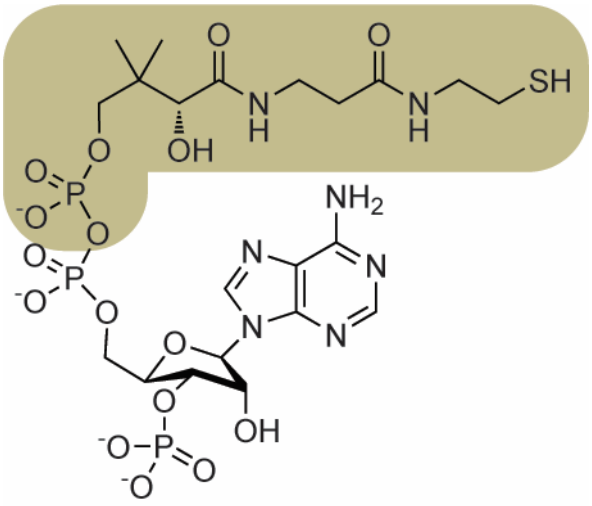

**Figure 1-4: The structure of coenzyme A (CoA), with its 4'-phosphopantetheine (P-PantSH) moiety highlighted.**

We have highlighted the potential benefits of investigating membrane permeation of drug molecules form the standpoint of maximising drug discovery output. However, such investigations can additionally lead to the discovery of novel targets for drug development. For instance, there are many so-called “orphan” transporters, so named because the molecules they transport are yet to be identified – which indicates the extent to which small molecule transport remains unexplored. To make a case for this, we use pantothenate to show that uptake mechanisms of essential molecules can be a viable target for drug development.

Most organisms can synthesise CoA *de novo* from vitamin $B_5$, which is also known as pantothenic acid (PanCOOH, **2**)[63] (Figure 1-5). In addition to this, some fungi, bacteria and plants can also synthesise PanCOOH *de novo* from β-alanine and α-ketoisovalerate[63]. Most organisms also have membrane transport proteins which enable uptake of this molecule from the external environment. Such transporters have been characterized in both prokaryotic and eukaryotic organisms[64–69]. Some functional divergence in these transporters has been established, especially in protozoans which suggests possibility for selective targeting of pantothenate uptake in these organisms for drug discovery purposes[65,70,71] .

### 1.3.1 Pantothenate uptake mechanisms

Some plants, fungi and bacteria (including *Escherichia coli*) can synthesise CoA *de novo* from PanCOOH[72]. However, gene knockout studies performed in *E. coli* show that it remains viable even after the genes encoding the PanCOOH biosynthetic enzymes were silenced. This served to show that *de novo* PanCOOH biosynthesis is not required for survival of the organism, and that it also has mechanisms for direct uptake of this molecule from the environment. The uptake is mediated by a membrane transport protein called pantothenate permease (PanF)[68]. It is a sodium-associated (symporter) transporter that is highly specific for

the vitamin (transport constant of 0.4 μM)[73]. Homologues of this transport protein have also been identified in other bacteria such as *Haemophilus influenza* and *Salmonella typhi*[74–76].

Most mammals are incapable of synthesizing PanCOOH *de novo* and must assimilate it from their environment. Uptake of PanCOOH in these organisms is facilitated by SLC5A6, a sodium-dependent multivitamin transporter (SMVT)[66,77–79]. This transporter accepts PanCOOH, biotin and lipoate as substrates, hence its name. This symporter has a relatively low affinity towards PanCOOH with a $K_m$ ≈1.5–4.9 μM. A homologue of this transporter (FEN2) is also expressed in *Saccharomyces cerevisiae*[64]. However, the yeast transporter differs from the SMVT in that it transports PanCOOH in a proton gradient-dependent manner. Furthermore, its PanCOOH uptake is stimulated by glucose, which also happens to be an activator of the proton-ATPase[64].

*Plasmodium falciparum*, the causative agent of malaria, has an absolute requirement for PanCOOH[80,81]. The intra-erythrocytic stage of this parasite is easy to reproduce *in vitro* and for this reason is also the best studied. Since erythrocytes are metabolically inert these cells have no mechanisms for PanCOOH uptake. Upon infection, the parasite induces new permeability pathways (NPPs) in the erythrocyte membrane to facilitate PanCOOH uptake into the erythrocyte[82]. However, the NPPs are not only specific for PanCOOH, but have the ability to take up various compounds and solutes[83]. The uptake of PanCOOH by the parasites itself is very rapid. PanCOOH is presumed to be present in the parasitophorous vacuole. This vacuole forms as soon as the parasites invade the erythrocyte and occurs via an endocytosis-like mechanism. During this process, the parasite remains enclosed. It is believed that PanCOOH diffuses over the vacuole membrane via low selectivity channels[81]. *P. falciparum* expresses a pantothenate transporter as is the case for its mammalian host and bacteria[65,70]. Therefore, once the PanCOOH is present in the parasitophorous vacuole, it can then be taken up by the parasite via its pantothenate transporter. However, this transporter is divergent from both the bacterial and mammalian transporters in regards to both its sequence and its characteristics. It is a symporter that requires a proton gradient rather than a sodium gradient, and it has lower affinity for PanCOOH relative to the mammalian transporter, with a $K_m$ of 23 mM[80].

### 1.3.2 Efflux pumps reduce efficacy of PanCOOH analogues in Gram-negative bacteria

The chemical synthesis of libraries of PanCOOH analogues to be tested as potential antibacterial agents also led to discoveries regarding other transporter-based processes[81]. For example, specific pantothenamides (PanAms, a class of PanCOOH analogues in which the carboxyl is replaced with *N*-substituted amides) such as *N*-pentylpantothenamide (N5-Pan, **6**)

and *N*-heptylpantothenamide (N7-Pan, **7**), respectively (Figure 1-5) have been shown to be metabolically activated through the CoA biosynthetic pathway to ethyldethia-CoA and butyldethia-CoA[84,85]. These elicit bacteriostatic activity by producing crypto-ACPs which inhibit fatty acid biosynthesis[86,87]. N5-Pan has moderate potency towards *E. coli* and *S. aureus*, but N7-Pan is exclusively potent towards *S. aureus*. Importantly, the low efficacy of N7-Pan towards *E. coli* was found to be due to rapid efflux by TolC proteins found on the outer membrane of Gram-negative bacteria.

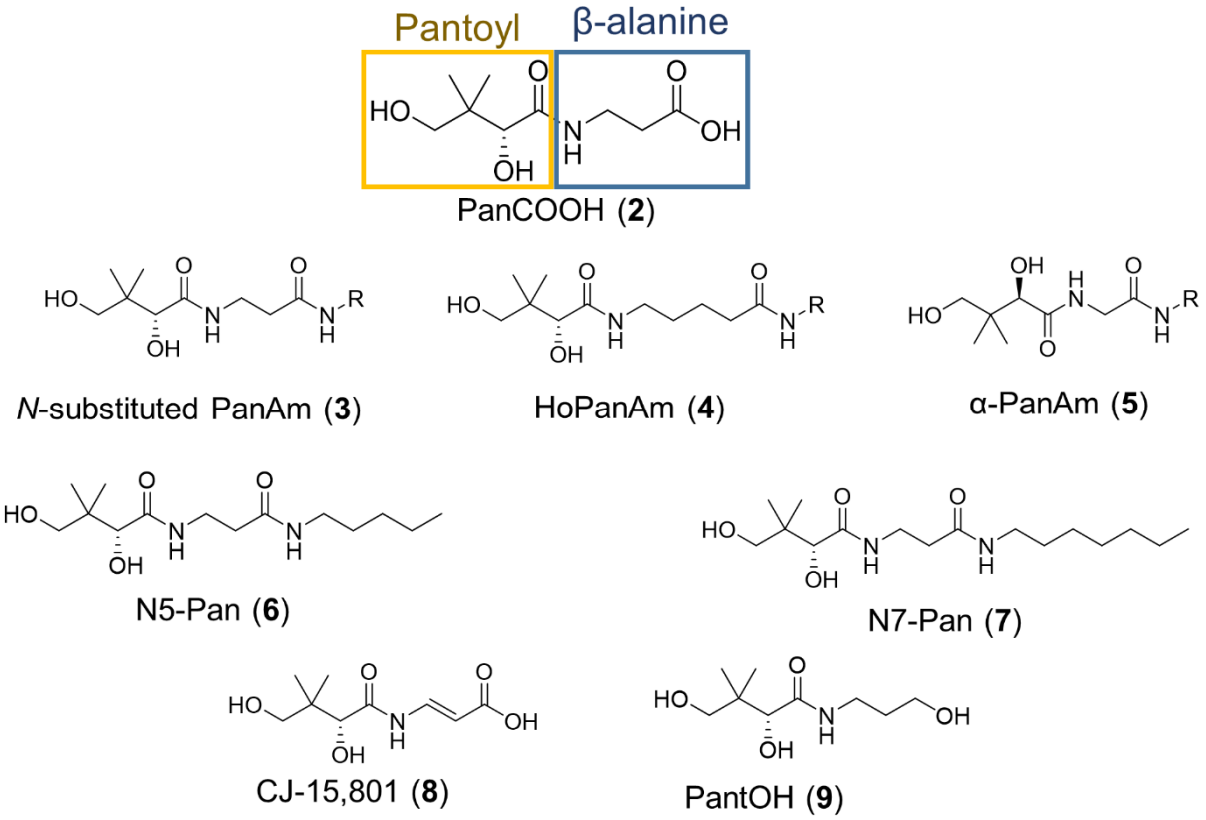


**Figure 1-5: Chemical structures of Pantothenate analogues with promising antibacterial activity.** PanCOOH is made up of pantoyl and β-alanine moieties (**2**). The β-alanine moiety is modified with an *N*-substituted amide (**8**), or is replaced with either a γ-aminobutyric acid or glycine to produce α- and HoPanAms, respectively. The most potent PanAms to date include N5-Pan, N7-Pan and CJ-15,801 (**11**, **12** and **13,** respectively), but **12** and **13** the latter loose potency due to efflux by TolC pumps.

### 1.3.3 Targeting PanCOOH uptake mechanisms for antimicrobial drug discovery

Since PanCOOH can be synthesized *de novo* by bacteria, it is not a viable strategy to target its uptake for antibacterial drug development in most cases. However, the lack of PanCOOH transport mechanism in erythrocytes, together with the low sequence and functional homology of the parasite and host transporters suggest possible selective targeting of the uptake of PanCOOH by the malaria parasite *P. falciparum* for antimalarial drug development. But, the PanCOOH analogues tested on blood stage parasite that do show antiplasmodial activity to

date, do not seem to act by interfering with PanCOOH uptake. These include pantothenol (PantOH, the reduced version of PanCOOH) (**9**), CJ-15,801 (a fungal natural product that only differs from the vitamin in having a single bond exchanged for a double bond) (**8**), and the PanAms (Figure 1-5)[88]. In the case of the latter, a range of analogues were tested in which other features of the molecule were changed as well. Specifically, the β-alanine moiety of PanCOOH was replaced with either a glycine or γ-aminobutyric acid, giving rise to three sets of PanAms: the *n*-PanAms (**3**), with the usual β-alanine moiety, the α-PanAms (**5**), which are substituted pantoylglycyl amides and the HoPanAms (**4**), which are amides of pantoyl γ-aminobutyric acid[89]. Investigation of mode action of these molecules showed that the α-PanAms indeed compete with PanCOOH for transporter-mediated uptake but do not show potency towards the parasite. On the other hand, the *n*-PanAms and HoPanAms that did elicit some antiplasmodial activity *in vitro*, were shown to permeate these organisms by passive diffusion[90]. These findings were the first to provide evidence that a) small changes in the structures of PanCOOH analogues have a large impact on their recognition by transporters, and b) that these changes may also affect the membrane permeability of the compounds. This, in turn, suggested that the PanAms (and other PanCOOH analogues) can be used to study membrane permeability in the context of drug discovery.

### 1.3.4 Diverse modes of CoA formation *in* vivo provide evidence of the importance of membrane permeability to CoA biology

#### *1.3.4.1 Canonical CoA biosynthesis pathway*

In organisms that do not make their own PanCOOH, CoA (**1**) is synthesised *de novo* from PanCOOH that is obtained from the diet or the external environment (Figure 1-6 A). The biosynthesis occurs through a five step pathway mediated by the enzymes pantothenate kinase (PanK)[91,92], phosphopantothenoylcysteine synthetase (PPCS)[93], phosphopanto-thenoylcysteine decarboxylase (PPCDC)[94], phosphopantetheine adenylyltransferase (PPAT)[95] and dephospho-coenzyme A kinase (DPCK)[94].

PanK catalyzes the ATP-dependent phosphorylation of PanCOOH (**2**) to form 4'-phosphopantothenate (P-Pan, **10**), the first step of the pathway. There are at least three known PanK types that can be distinguished based on sequence, structure, active site architecture and specificity towards PanCOOH[96]. A type I PanK ($PanK_I$) was first isolated from *E. coli*, and has relaxed substrate specificity and can accept pantetheine (PantSH) as an alternative substrate. Consequently, it is involved in both *de novo* biosynthesis of CoA, and in the CoA salvage pathway. $PanK_I$ is also subject to feedback inhibition by CoA and to a lesser extent by the CoA thioesters which competitively inhibit ATP binding[97–99]. Type II PanK ($PanK_{II}$) enzymes are predominantly found in eukaryotes.

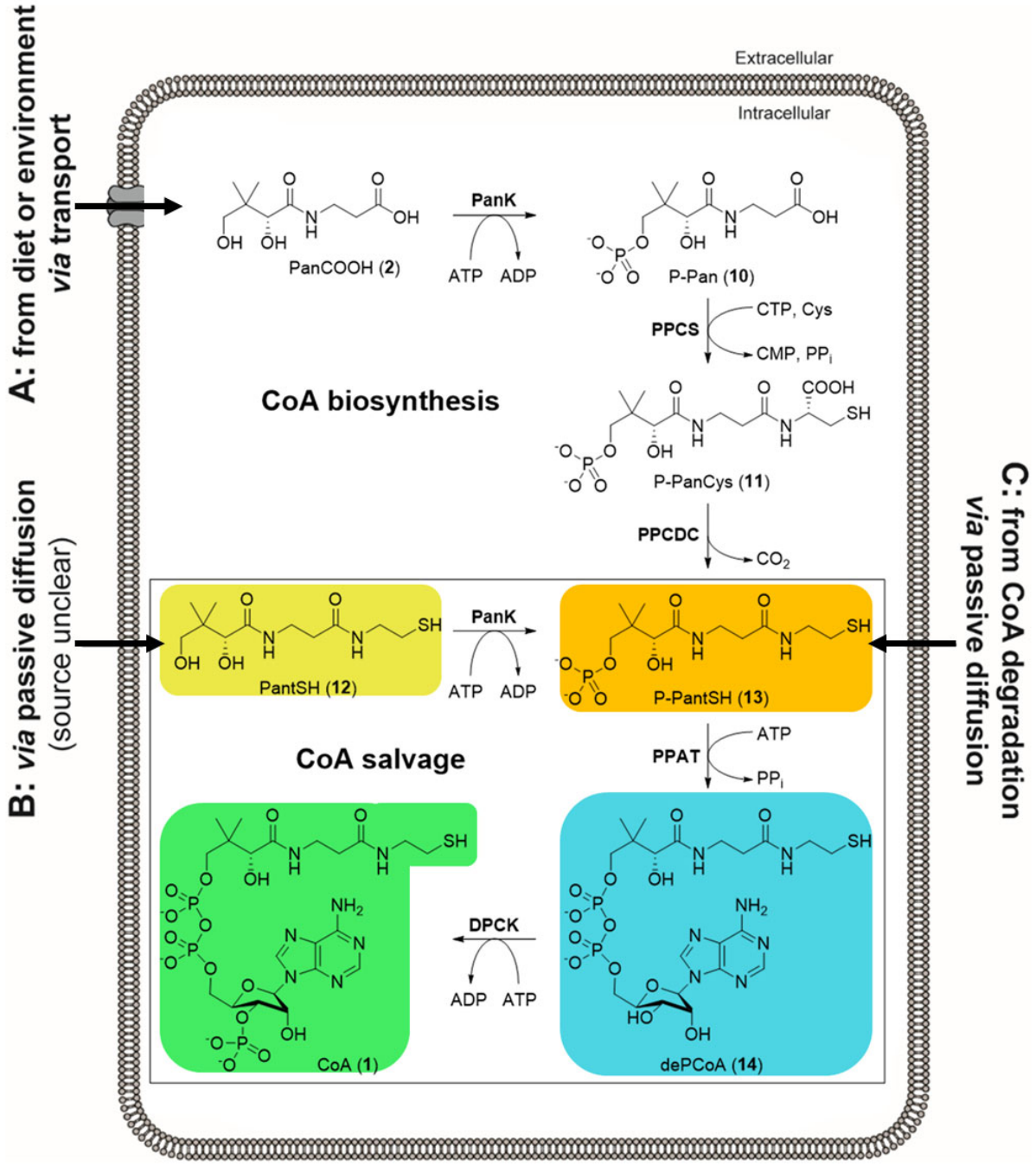


**Figure 1-6: Various routes for formation of CoA.** CoA (**1**) is biosynthesised *de novo* from PanCOOH (**2**) that is taken up from the external environment by dedicated transporters (in the case of organisms that cannot synthesise their own PanCOOH) **(A).** This process in involves the five enzymes: PanK, PPCS, PPCDC, PPAT and DPCK, the last two of which are fused in a bifunctional enzyme complex in most mammals, called CoA synthase (CoASy). In addition, PantSH (**12**) can serve as also serve as substrate for the formation of CoA through a truncated form of the pathway called the CoA salvage pathway **(B)**. This pathway becomes possible in cases where PantSH is taken up (most likely through passive diffusion, i.e. bypassing the need for membrane transporters) and subsequently acted on by PanK, PPAT and DPCK. Finally, when P-PantSH (**6**) is formed by rapid degradation of exogenous CoA it can also serve as a precursor for the formation of CoA through the action of only PPAT and DPCK **(C)**. Importantly, P-PantSH has been shown to be taken up through passive diffusion by some cells, indicating that this pathway is not dependent on any transporters either.

Unlike the bacterial PanKs which are encoded by a single gene, the mammalian $PanK_{II}$s exhibit heterogeneity with three genes encoding four distinct isoforms: PANK1α, PANK1β, PANK2 and PANK3. Like $PanK_{I}$s, $PanK_{II}$ enzymes also have relaxed substrate specificity and are subject to feedback inhibition by CoA and its thioesters with the latter being more potent feedback regulators than free CoA[100,101]. There is an atypical $PanK_{II}$ found in some bacteria such as *Staphylococcus aureus*.

This protein is homologous to the eukaryotic $PanK_{II}$ and, although it also accepts PantSH as an alternative substrate, the turnover rate is so slow that in practice it actually acts as a competitive inhibitor of the enzyme[74,102]. This could possible form part of an alternative regulation mechanism, as a major distinguishing factor of this enzyme is that it does not experienced feedback inhibition by CoA and its thioesters[101]. The type III PanKs ($PanK_{III}$s) are the most recently discovered of the PanK types and is exemplified by the enzyme from *Helicobacter pylori*[99] Like $PanK_{I}$ enzymes, this type is predominantly found in prokaryotic organisms—in fact, more bacterial species have $PanK_{III}$ enzymes than $PanK_{I}$s. $PanK_{III}$s exclusively accept PanCOOH as a substrate (i.e. it is not able to partake in the CoA salvage pathway), and is also not subject to feedback inhibition by any known metabolite[96,99].

The second step is the $Mg^{2+}$-dependent formation of 4'-phosphopantothenoylcysteine (P-PanCys, **11**) from 4'-phosphopantothenate, ATP (CTP in the case of bacteria) and L-cysteine as catalyzed by PPCS. The third step of the pathway involves PPCDC, which catalyzes the decarboxylation of the cysteine moiety of P-PanCys to form 4'-phosphopantetheine (P-PantSH, **13**). The two enzymes are fused as part of a bifunctional enzyme complex called CoaBC in most bacteria[93,103]. However, there are some bacterial species—mainly the streptococci and enterococci—in which the two enzymes are expressed as separate enzymes. Some bacterial species also exhibit heterogeneity characterized by the presence of both the bifunctional complex, as well as monofunctional enzymes[104]. PPCS and PPCDC exist as separate monofunctional enzymes in most eukaryotic organisms[105].

The penultimate step of the pathway is the reversible $Mg^{2+}$-dependent adenylylation of 4'-phosphopantetheine to form dephospho-CoA (dePCoA, **14**) and pyrophosphate ($PP_i$) catalyzed by PPAT[95]. And finally, DPCK catalyzes the selective MgATP-dependent phosphorylation of the 3'-hydroxyl of the ribose moiety of dePCoA to form the final product of the biosynthetic pathway, CoA (Figure 1-6). In mammals, PPAT and DPCK exist as a bifunctional enzyme complex called CoA synthase (CoASy)[106], but are separate monofunctional enzymes in most bacteria[107]. In addition to CoASy, mammalian cells express an additional monofunctional DPCK. This heterogeneity may be important for homeostasis of

organellar CoA pools, since current evidence suggests that the monofunctional enzyme localizes to the cytoplasm, while CoASy localises to the mitochondria[108].

The biosynthesis of CoA from PanCOOH by this “canonical pathway” has long been thought to be only way in which cells can obtain this cofactor. As such, the phosphorylation of PanCOOH by PanK has long been considered a key regulatory step, and that the PanK reaction commits the cell to CoA biosynthesis[86]. However, as outlined below, recent findings have suggested that the reality is more complex, and that the membrane permeability of the CoA biosynthetic intermediates is an important component of this complexity.

#### 1.3.4.2 CoA salvage pathway

Pantetheine (PantSH, **12**) is the amide formed from cysteamine and PanCOOH (Figure 1-6 B). This molecule may serve as an alternative precursor for the formation of CoA since its phosphorylation by PanK produces 4'-phosphopantetheine (P-PantSH, **13**)—the third intermediate of CoA biosynthesis—directly. This means that, apart from PanK, only the last two enzymes of the pathway are required to produce CoA. This truncated form of the pathway is known as the CoA salvage pathway.

PantSH is usually derived from pantethine (disulfide of PantSH) which is often used as a dietary supplement[109,110]. It is also likely produced by dephosphorylation of P-PantSH by selective phosphatases that control the levels of certain metabolites[111]. Importantly, nutrient complementation studies in *Pseudomonas aeruginosa* mutant strains that are auxotrophic for pantothenate, and in which the *panF* and *coaBC* genes (the latter encoding the bifunctional PPCS/PPCDC protein in this organism) have been down regulated, show that PantSH can support its growth when it is complemented with a PanK enzyme capable of phosphorylating PantSH. This suggests membrane permeation of this molecule in a PanF-independent manner (Figure 1-6 B)[112]. Moreover, it also provided the first clear basis for the apparent membrane permeability of certain PanAms, as this class of compounds is clearly closely related structurally to PantSH.

#### *1.3.4.3 Alternative CoA biosynthetic routes*

A long-standing interest in CoA biosynthesis is related to the discovery of pantothenate kinase-associated neurodegeneration (PKAN), one of a group of neurodegenerative diseases collectively called neurodegeneration by brain iron accumulation (NBIA). A hallmark of PKAN is a mutation in the gene that encodes the mitochondrial human PanK isoform. This mutation renders the enzyme catalytically inactive, leading to CoA depleted phenotypes[113]. Results from a nutrient complementation study with *Drosophila melanogaster* PKAN models show that exogenous CoA can rescue the intracellular CoA depletion and so alleviate some of the symptoms of the disease[114,115] Further investigation revealed that the exogenous CoA is

degraded into P-PantSH by ectonucleo-pyrophosphatases (ENPPs), that P-PantSH is biologically stable and that it can enter certain cells by passive diffusion[115,116]. As it is an advanced CoA biosynthesis metabolite, once inside the cell it can be transformed into CoA only by the action of PPAT and DPCK, as a precursor for CoA biosynthesis through an alternative route that bypasses PanK (Figure 1-6 C).

This finding was especially surprising as it indicated that a phosphorylated metabolite, P-PantSH, was able to cross cell membranes—contrary to the standard permeability paradigm that charged molecules are membrane impermeable. However, as outlined in more detail below, the findings also indicated that the permeability of P-PantSH permeability was not general. Elucidating the basis for its ability to cross membranes, as well as the characteristics of the kind of membranes that allows this, is therefore clearly an important goal to be achieved,

### 1.3.5 CoA homeostasis and its implications for drug development

#### *1.3.5.1 There are distinct subcellular CoA pools in mammals*

Eukaryotic cells have distinct cytosolic, mitochondrial, peroxisomal and intrareticular CoA pools[86,108]. However, the mechanisms by which these pools are established or regulated remains largely unknown. The heterogeneity and specific localization of PanK isoforms in mammals suggest that they might play an important role in this regard, as knockout studies show that the loss of one PanK isoform is not always compensated for by another. This may be attributed to the differences in their N-terminal domains that are presumed to direct their subcellular localization[117,118].

Immunocytochemistry and co-localization studies show that PANK1α localizes to the nucleus, that PANK1β is associated with vesicles, PANK3 localizes to the cytosol, and finally PANK2 is exported from the nucleus to the mitochondrion in a cell-cycle dependent manner[118–121]. There is further evidence to suggest specific localisation of PANK2 to the inner mitochondrial space. It is hypothesized that this organellar localisation occurs to allow export of 4'-phosphopantothenate—the product of the PanK-catalyzed reaction—into the cytoplasm where the rest of the biosynthetic enzymes are presumed localized. This hypothesis was formulated on the basis that CoA biosynthesis does not take place in the subcellular compartments to which the individual PanK isoforms localize. It is further postulated that the subcellular localisation allow PanKs to act as sensors for CoA homeostasis in the respective organelles[118]. This in turn is based on the dogmatic view of PanK experiencing feedback inhibition by CoA and its thioesters which in turn translates to its involvement in the maintenance of homeostatic levels of CoA through their production of 4'-phosphopantothenate. Such a perspective requires not only the transport of 4'-phosphopantothenate, but also that CoA is exported from the cytoplasm into the specific

organelles. Since charged molecules generally do not cross membranes, it is presumed that CoA is membrane impermeable[108]. It consequently follows that free CoA must be transported between subcellular compartments by dedicated transporters located on the membranes of the different organelles. While transporters which seem to have such activity have been identified, no evidence of their direct transport of CoA has been obtained as yet.

The current hypothesis may be flawed for the following additional reasons: it overlooks experimental evidence that suggests the localisation of CoASy to the mitochondrion[122], and it also disregards the proposed localisation of PANK3 to the cytoplasm[118]. Taken together, this highlights the importance for an improved understanding of the membrane permeability of CoA and its biosynthetic intermediates, and the various factors that may impact on it.

#### *1.3.5.2 Defects in mammalian PANK 2 and CoASY are associated with mitochondrial dysfunction*

The highest concentration of CoA is found in the mitochondrion and the peroxisome, which suggests that regulation of CoA levels in these organelles is independent of that of the cytoplasmic pool[123–125]. The organellar CoA pools appear to be tightly regulated especially in the case of the mitochondria where defects in CoA metabolism is linked to pathological conditions such as PKAN[114,115,120]. Another variation of the neurodegenerative condition is CoASy associated neurodegeneration (CoPAN) which is associated with defects in CoASy activity[109,126].

The identification of transporters with apparent activity for exchanging CoA and dePCoA for other nucleotides in the mitochondrion and peroxisome provides further evidence to support the suggestion that CoA regulation in these organelles occurs independently[123–125]. This is further illustrated by findings from knockout studies on the gene encoding SLC25A16, an inner mitochondrial transporter associated with CoA transport. Silencing of this gene resulted in the reversal of the CoA concentration between the mitochondrion and the cytosol. However, direct evidence of the transport of CoA or a CoA biosynthetic intermediate by this transporter still needs to be obtained.

#### *1.3.5.3 P-PantSH may play a role in the regulation of subcellular CoA pools in mammals*

As alluded to previously, there is evidence pointing towards an alternative route for obtaining CoA in eukaryotes (Figure 1-6). Disruption of *de novo* CoA biosynthesis by silencing genes that encode selected CoA biosynthetic enzymes led to low intracellular CoA levels and decreased protein acetylation in *D. melanogaster* S2 cell knockout models. However, the protein acetylation could be recovered by adding CoA to the culture medium. Therefore, the findings of this study suggest that exogenous CoA could supply intracellular CoA pools[115]. Further investigation went on to reveal that exogenous CoA is degraded into P-PantSH and

3',5'-ADP by ENPPs[115]. P-PantSH is not susceptible to degradation by pantetheinases and is therefore stable in culture media as well as in circulation *in vivo*[115,127]. Membrane permeability screens of this molecule using the PAMPA assay also suggested that this molecule can enter cells by passive diffusion[115].

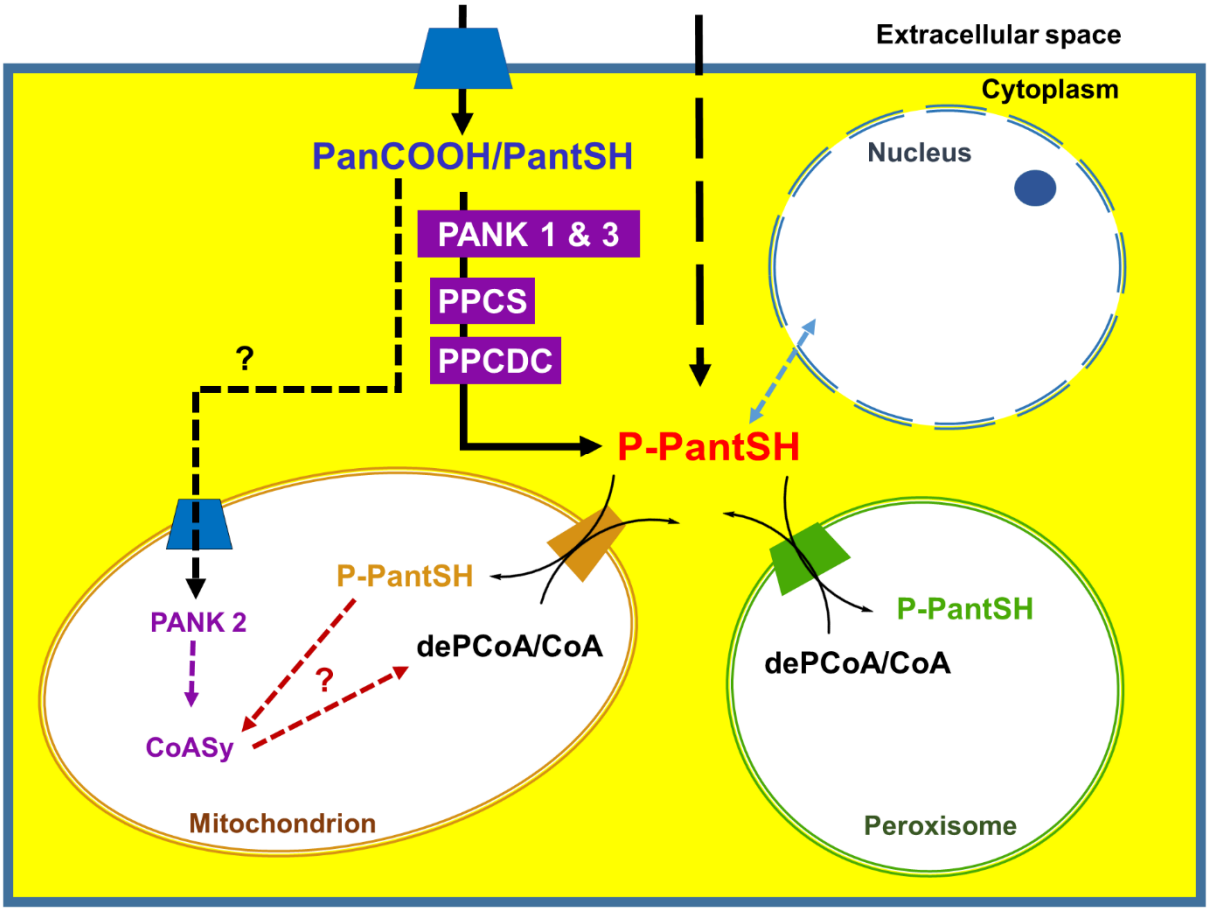


**Figure 1-7: P-PantSH may play a role in homeostasis of subcellular CoA pools in mammalian cells.** The apparent heterogeneity of CoA biosynthetic enzymes is linked to maintenance of subcellular CoA pools in these organisms. For instance: PanK 1 and 3, PPCS as well as PPCDC localise to the cytosol implying biosynthesis of P-PantSH in the cytosol. This molecule should then be exported to the mitochondrion where CoASy is localised for the final steps of CoA biosynthesis. Since transporters with affinity towards dePCoA and CoA have been identified on this organelle, it follows that P-PantSH may enter the organelle by counter exchange with these molecules. Furthermore, localisation of PanK 2 to the mitochondrion implies CoA biosynthesis by salvage with further suggests existence of uptake mechanisms of PantSH in this organelle. On the other hand, a transporter with affinity towards dePCoA and CoA has been identified on the peroxisome as well. This transporter may also have affinity for P-PantSH, since in addition to its unaided membrane permeation, this molecule is synthesised in the cytosol. Taken together, these suggest possibility of involvement of P-PantSH in homeostatic regulation of subcellular CoA pools.

Since subcellular transporters are believed to transport either CoA or one of its intermediate for maintenance of the various organellar CoA pools, it is tempting to speculate that this may occur by means of P-PantSH, based on its demonstrated biological stability and membrane

permeability (Figure 1-7). This would especially be the case in mitochondria, as this is where current evidence indicates that CoASy localizes, and as such P-PantSH would be able to serve as the precursor for CoA formation in the mitochondria through the action of CoASy.

#### *1.3.5.4 P-PantSH is irreversibly removed from E. coli for homeostatic regulation of CoA and ACP*

In an important foundational study, CoA intermediates were quantified in an effort to try and understand the flux through the CoA biosynthetic pathway in *E. coli*. PanCOOH and P-PantSH were found to be the most abundant intermediates in the cell[128]. The same study went on to suggest that P-PantSH is irreversibly removed from the cell for homeostatic regulation of CoA and the biosynthesis of active acyl carrier proteins (ACPs) (Figure 1-8)[128]. ACP is required for fatty acid biosynthesis in bacteria. It exists as an inactive *apo* form that is activated to the *holo* form by covalent attachment of the P-PantSH moiety of CoA in a post-translational modification of the protein. Intracellular *holo*-ACP is recycled to its *apo* form and P-PantSH through hydrolysis mediated by the enzyme ACP hydrolase (AcpH)[129]. As such, free P-PantSH in the *E. coli* cell can be attributed to both CoA and ACP recycling, As well as the slow reaction rate of PPAT (the enzyme that transforms P-PantSH into dePCoA), relative to the other enzymes in the pathway[128,129].

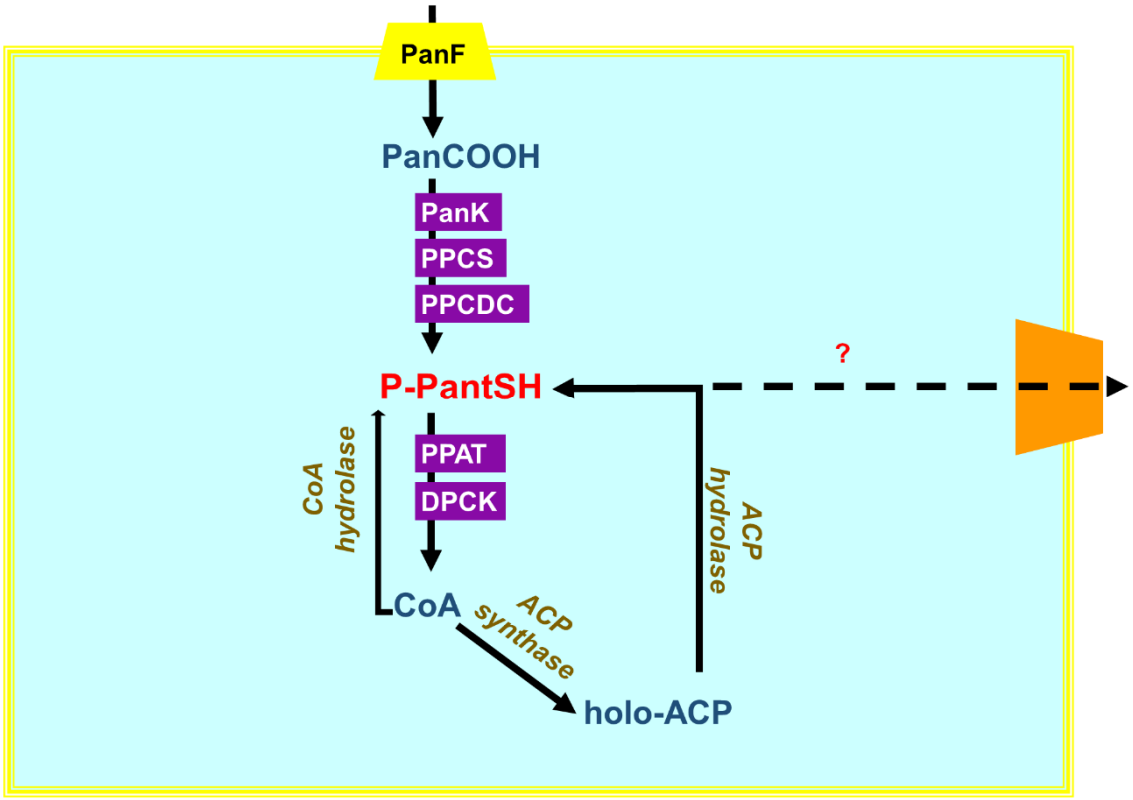


**Figure 1-8: P-PantSH is proposed to play a role in the homeostatic regulation of CoA and ACP levels in *E.coli*.** CoA is biosynthesised through the canonical pathway from PanCOOH actively taken up by PanF. The produced CoA activates ACP from the apo- to the holo-ACP form in a process mediated by ACP synthesis. ACP

and CoA are recycled by hydrolysis to yield P-PantSH in a process mediated by ACP and CoA hydrolase respectively. P-PantSH is the irreversibly removed from the cell to maintain homeostatic levels of both CoA and ACP.

#### *1.3.5.5 CoA related interplay between microbiota and the eukaryotic host may be mediated by P-PantSH*

The apparent irreversible removal of P-PantSH from *E. coli* suggest that this organism, together with other members of the gut microbiota, can provide excess P-PantSH to the eukaryotic host[108]. Studies on *D. melanogaster* models in which PanK was inactivated to prevent *de novo* biosynthesis of CoA, show that these organisms could still survive the early embryonal and larval stages because basal levels of CoA persisted[108]. It is probable that this was due to CoA being formed by the conversion of P-PantSH obtained from the *D. melanogaster* gut flora.

This postulation is further reinforced by findings from a study on murine models which were fed a PanCOOH depleted diet[114]. Despite this depletion, these animals did not experience any symptoms unless antibiotics were also administered with the diet. It is possible that when the animals were deprived of PanCOOH, the required CoA biosynthesis occurred through P-PantSH obtained from the microbiota[108,115] .

This interplay of P-PantSH between host and bacterium can also apply in the reverse direction when organisms such as *Treponema pallidum* are considered (Figure 1-9). *T. pallidum* is the causative agent of syphilis[108]. Comparative genomic data suggests that it has an unusual CoA biosynthetic machinery ensemble consisting of a $PanK_{III}$, PPAT and DPCK, but no PPCS or PPCDC enzymes[115]. These organisms cannot use PantSH as a CoA precursor for the CoA salvage pathway since $PanK_{III}$ exclusively accepts PanCOOH as a substrate. Moreover, the organism does not have PPCS and PPCDC enzymes, which in turn suggests that the phosphorylation of PanCOOH would be futile, as the produced 4′-phosphopantothenate cannot be biotransformed any further. Early nutrient complementation studies performed on the *Treponema* spp. also suggested a preference for P-PantSH over PanCOOH and PantSH as a starting material for CoA biosynthesis[115]. This suggests that these organisms are obtaining the P-PantSH required for CoA biosynthesis from the circulation of its eukaryotic host (Figure 1-9). Comparative genomic data suggests that other intracellular parasitic organisms such as *Mycoplasma* spp. may follow a similar approach for CoA biosynthesis[108] Taken together, these point towards P-PantSH as a nexus metabolite of CoA biosynthesis and degradation. Moreover, uptake mechanisms in organisms like *T. pallidum* may be a viable target for drug development.

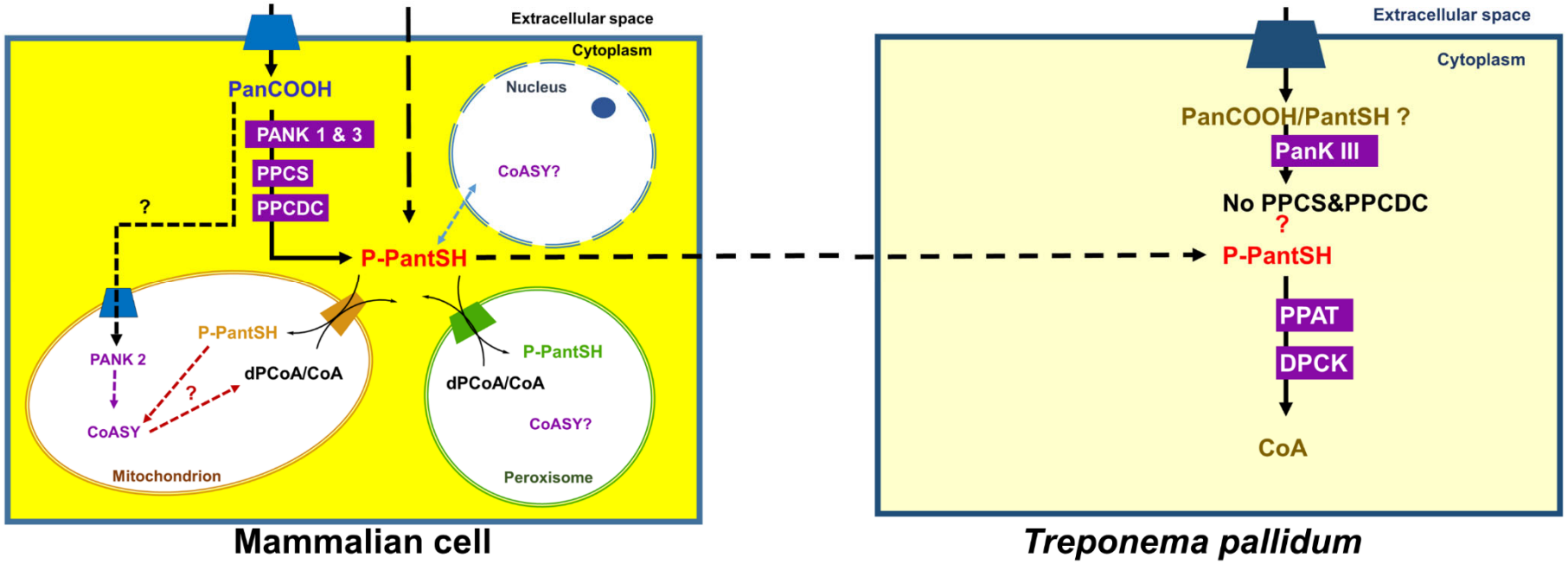


**Figure 1-9: P-PantSH abundance provides an alternative route for CoA biosynthesis**. P-PantSH is biologically stable and can therefore stay in host circulation for prolonged periods. This in turn implies that P-PantSH can serve as a CoA precursor for organisms with unusual biosynthetic machinery such as *T. pallidum* which demonstrates preference for this molecule over traditional precursors.

### 1.3.6 Problem statement

A vast amount of knowledge has been acquired in the past two decades regarding pantothenate analogues and their potential use as therapeutics. It is known that the uptake of these analogues differs between organisms, however, the exact mechanism of uptake is not well studied between analogues and thus unclear. This is compounded by the complexity of CoA homeostasis and the poor understanding thereof. While numerous PanCOOH transporters have been characterized, the uptake mechanisms of this molecule or how it is regulated is still vague. This is best illustrated by the intra-erythrocytic stage of *P. falciparum*, where there is an interplay between host and pathogen cells to ensure PanCOOH uptake by the parasite. The permeability of PantSH and PanAms has also been speculated on, but there is still no experimental data that can definitively confirm the mechanism by which these molecules enter the cell.

Another factor that contributes to the lack of knowledge of pantothenate analogue uptake is the poor understanding of CoA homeostasis between a eukaryotic host and members of its microbiome. This process may involve exchange of CoA intermediates between the host and bacteria. Subcellular CoA pools are maintained by tight regulation of the transmembrane transport of CoA and/or its intermediates in eukaryotic cells. Existing experimental evidence points towards P-PantSH as the key intermediate in this process. There is also evidence to suggest the role of this molecule in homeostatic regulation of CoA and ACP in *E. coli* cells. This together with the apparent biological stability of P-PantSH, suggests an interplay between the eukaryotic host and its microbiome in regards to CoA metabolism.

Existing experimental evidence suggests that some pantothenate analogues, like PantSH and PantOH, may permeate cell membranes by methods independent of protein transporters. This is presumed to occur by passive diffusion, based on the observation that P-PantSH can rescue CoA-depleted phenotypes in *Drosophila* S2 cells in a non-saturable manner[115]. Therefore, we would like to investigate the molecular determinants of membrane permeability of these molecules by addressing the following questions: Is it the pantoyl, cysteamine or phosphate moiety that confers permeability, or does the membrane composition have a greater role to play in this regard? Insight gained from such a study will not only help us understand how these molecules cross membranes but will also inform strategies for mitigating poor permeability of certain PanAms, some of which are potent inhibitors of their targets *in vitro* but fail to elicit antibacterial activity.

The study also seeks to characterize the SLC25A16, a mitochondrial carrier implicated in the regulation of CoA levels in the mitochondria. Understanding the mechanism by which this transporter works will help us understand the link between mitochondrial CoA dysfunction and

pathological states like PKAN. We propose that P-PantSH may be a substrate for this carrier protein, and experimental demonstration of this may provide direct evidence linking this molecule to homeostatic regulation of subcellular CoA pools in is. Insight gained from characterizing this mitochondrial solute carrier may aid in identifying similar carriers which may be vulnerable targets for drug development in pathogenic organisms.

Therefore, the following study aims were set out:

1. *Aim 1: To design and validate a liposomal fluorescence-based assay for measuring membrane permeability of CoA-related small molecules.*
   The studies towards this aim is described in chapter 2 of this dissertation.

2. *Aim 2: To investigate the molecular determinants which confer membrane permeability of pantothenate analogues.*
   This was achieved by performing membrane permeability measurements and membrane interaction studies of P-PantSH and other pantothenate analogues, as described in chapter 3.

3. *Aim 3: To characterize the mitochondrial solute carrier SLC25A16 associated with regulation of CoA levels in the mitochondrion.*
   This work is described in chapter 4.

The dissertation concludes with a short chapter summarizing the findings of the study, and a description of future work that would contribute to the results already achieved, with all the references used in the study listed thereafter.

# 2 Development and validation of a discontinuous assay for measuring membrane permeability of P-PantSH and other CoA-related small molecules

## 2.1 Introduction

The current study seeks to investigate the membrane permeability of P-PantSH in order to find out if this molecule is unique in its ability to cross membranes unaided, if the permeability extends to different kinds of membranes, as well as to determine the membrane constituents that enable permeation by passive diffusion. This is in an effort to understand CoA homeostasis especially as it pertains to the interplay of CoA intermediates between eukaryotes and their microbiome.

Membrane permeability of P-PantSH by passive diffusion has been inferred by findings from a nutrient complementation study of *Drosophila melanogaster* S2 cells as well as from results of a PAMPA assay[115]. It is important to highlight that the PAMPA assay does not distinguish between passive and membrane transporter mediated membrane translocation, and that it is an exclusively mammalian-based membrane model[51,52]. In contrast, the current study seeks to compare permeability of molecules between different membrane systems, including a bacterial model, and do so in such a manner that distinguishes passive diffusion from active transport. The PAMPA assay does not have the versatility required to achieve these objectives and we therefore elected to use a liposome-based assay for these studies. Liposomes do possess the versatility needed for this study as these particles can be functionalized as required by the investigator. It is therefore possible to prepare liposomes with lipid compositions that mimic either eukaryotic or bacterial membranes[56,130–133]. The liposomes can also be prepared with solutes loaded in the intraliposomal cavity, a feature that is useful for performing permeability measurements.

Besides selecting a suitable membrane model, another important aspect to consider is the method used to perform permeability measurements. There are numerous published methods for measuring membrane permeability, many of which are based on radioactivity or fluorescence emission[32,134–138]. Whilst these methods have all generated useful data, a major drawback is that in most cases the measurements in transport exchange experiments are only directly made for one of the compounds being investigated, while transport of the other is being inferred. For instance, a study that characterizes a symport membrane transporter measured radioactivity exchange to determine the transporter kinetics of two target molecules transported in opposite directions of the membrane[123]. The radiolabeled version of one molecule was placed in the intraliposomal cavity, and the other in the external environment.

The change in radioactivity over time was subsequently monitored in the external environment. While this experiment can show the movement of the radiolabeled compound out of the liposome, the exchange with the unlabeled compound is inferred, as its transport into the liposome cannot be determined.

Nevertheless, there are some assays that directly monitor the membrane translocation of a molecule of interest. One such assay was described by Eyer et al[139]. It monitors the change in fluorescence of 8-hydroxypyrene-1, 3, 6-trisulfonate trisodium salt (pyranine), a pH sensitive dye to determine membrane permeability of the molecule of interest. Pyranine has high fluorescence emission at pH levels higher than 5.9 and is quenched at pH levels below this value. Pyranine-loaded liposomes were prepared according to the desired phospholipid composition. The pH of the extraliposomal environment was kept at pH 5.9 using the membrane-impermeable zwitterion 2-ethanesulfonic acid (MES). The intraliposomal cavity where pyranine was located was not buffered. This means the pH of the intraliposomal cavity was subject to pH fluctuations by dissociation of permeating molecules.

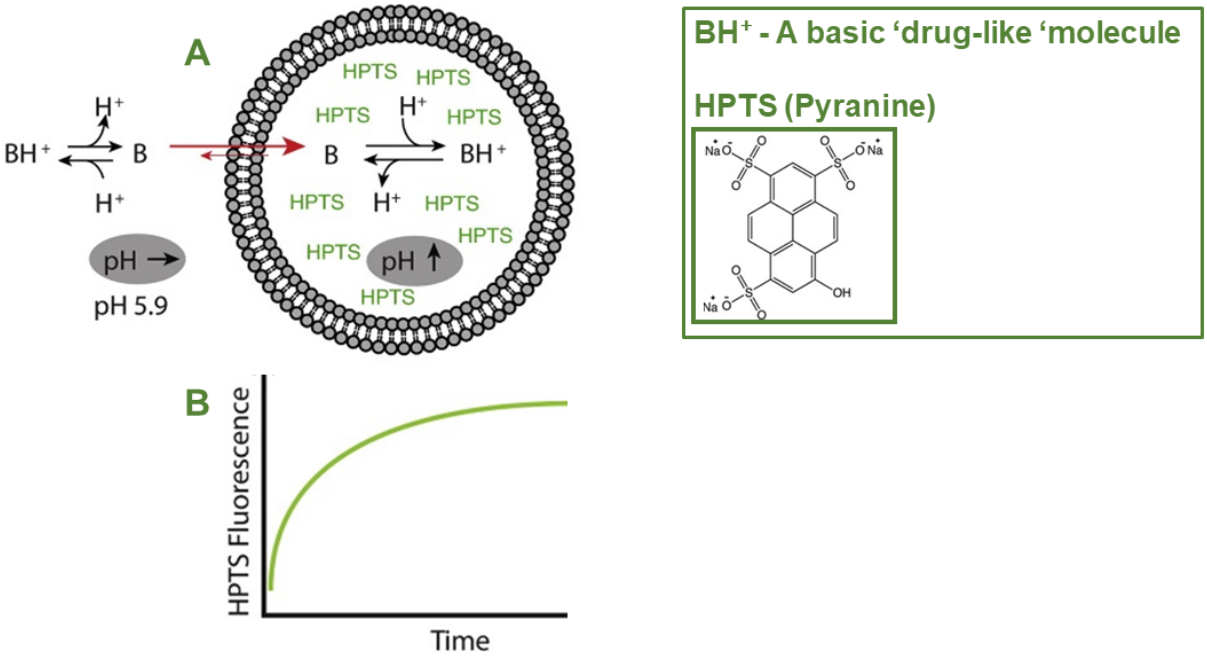


**Figure 2-1: Principle of the HTPS (pyranine)-based liposomal assay for measuring membrane permeability.** The extraliposomal (*outer*) compartment is buffered (MES/NaCl, pH 5.9), whereas the liposomal lumen (*inner*) is unbuffered (A). After the addition of a weak base ($B/BH^+$), permeation results in a net proton ($H^+$) release at the outer membrane surface and a net proton capture at the inner surface, according to the Henderson–Hasselbalch equation, to reach equilibrium. This results in fluorescence changes of a pH-sensitive fluorescent dye (indicated by "pH ↑") in the liposomal lumen or at the inner membrane surface while the proton at the outer membrane surface is neutralized by the buffer system (indicated by "pH →"). This is such that the membrane permeability of the molecule of interest can be determined by change in fluorescence over time. Adapted from Eyer *et al*. [139].

The drug molecules used in the assay have weak acid/based-like properties and could cause pH fluctuations in the liposomal cavity. This in turn, resulted in changes in pyranine fluorescence emission. The permeability of these drug molecules could hence be determined by changes in fluorescence intensity as a function of time (Figure 2-1).

This is a good example of a liposome-based assay used to measure the permeability of small drug molecules. The value of this method lies in the principle that the assay measures changes in the liposomal environment due to exposure to the molecule of interest, and uses these changes to give measurable output about the permeability of the molecule. The assay uses an inexpensive, non-toxic fluorophore that is easy to dispose with the added advantage that the measurements are continuous with the potential for high-throughput method development.

However, the assay does have some drawbacks. The use of pyranine suggests that only molecules that have weak acid/base properties can be profiled using this assay. The assay was also designed without a positive or negative control as a point of reference. This makes it difficult to distinguish true outcomes from false positives. In turn, this suggests a probability of observed outcomes not translating to an actual biological event.

In this study we were particularly interested in studying the transport of CoA and its biosynthetic intermediates PantSH and P-PantSH, all of which are thiolated molecules. Therefore, we set out to devise a liposome-based membrane permeability assay specific to these molecules but with the versatility to measure membrane permeation by passive or protein-mediated modes on *in vitro* membrane models. The result was a fluorescence-based assay that uses a fluorophore that is complimentary to the properties of P-PantSH and other CoA intermediates. The assay is set up in such a manner that it is amenable and can be used to measure permeability of molecules with structural diversity.

## 2.2 Results and Discussion

As previously stated, the main aim of this part of the study was to perform membrane permeability studies on P-PantSH and other CoA-related compounds that have structural similarity to P-PantSH. Liposomes were selected as an *in vitro* membrane model for investigating the membrane permeability of these molecules. Liposomes can exist in different forms like micelles, which exclude all hydrophilic molecules including water, and multilamellar or single lamellar vesicles of different sizes (Figure 2-2).

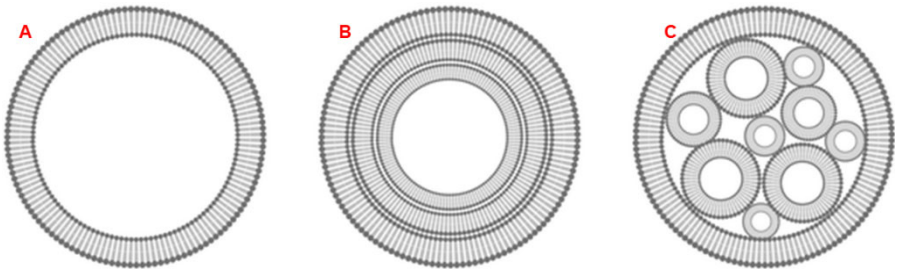


**Figure 2-2: Different types of liposomal vesicles can form.** Examples of vesicles that can spontaneously form include single lamellar (unilamellar) (A), multilamellar (B) or multivesicular (C) liposomal vesicles.

It is important that the liposomes be single lamellar vesicles of uniform size when investigating membrane permeability by passive diffusion[39,40,44]. Furthermore, the membrane permeability assay described in the current study requires that solutes be encapsulated in the intraliposomal cavity thereby making intraliposomal encapsulation efficiency an important factor to consider as well. The assay described by Eyer *et al*.[139] involved preparation of pyranine-loaded liposomes. These were single lamellar vesicles with a molecule loaded in the intraliposomal cavity as is required for the current study. Furthermore, since pyranine is a fluorescent molecule, the formation of the vesicle could be confirmed by confocal microscopy. The pyranine loaded liposomes could thereby serve as a useful tool for evaluating liposome preparation as demonstrated below.

### 2.2.1 Evaluation of liposome purification

The pyranine-loaded liposomes were prepared by hydration of a lipid film with a solution containing pyranine, followed by extrusion to promote formation of unilamellar vesicles. The excess pyranine was removed by size exclusion chromatography on a Sephadex G50 column prepared in house. This was done to ensure that only intraliposomal pyranine was present in the preparation. The pyranine-loaded liposomes (without the excess pyranine) were then harvested by elution with gravitational force and collected in 500 µL fractions from the Sephadex-G50 column. Fractions containing a green opaque suspension were then collected and evaluated by confocal microscopy to confirm the presence of the pyranine-loaded liposomes. The collected fractions had relatively high background fluorescence with no definite liposomal particles (Figure 2-3). This is with the exception of Figure 2-3 B which had a few distinct spherical green fluorescence emitting particles presumed to be liposomes.

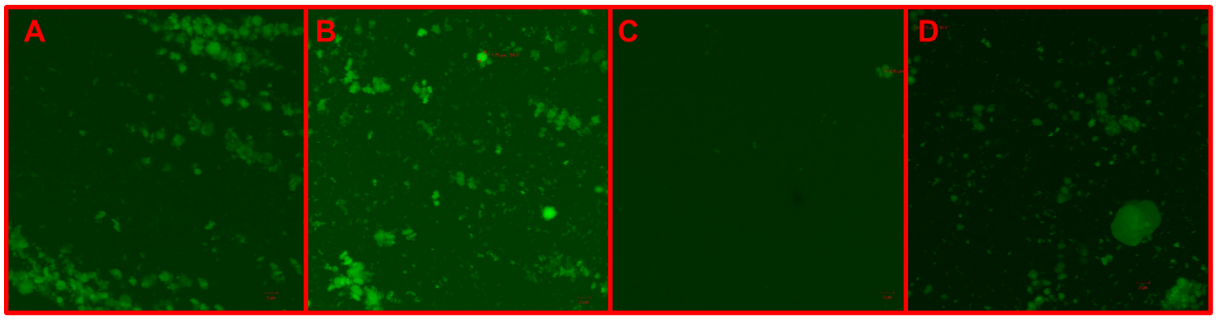


**Figure 2-3: Liposomes prepared by 11 extrusion passages and purified with Sephadex-G50 column chromatography.** "Pure" liposomal preparations were collected in 500 µL fractions indicated in panels A-D. Fraction B contained some particles presumed to be pyranine-loaded liposomes, however the background fluorescence signal was relatively high for all four fractions. This indicates the presence of extraliposomal pyranine.

Since the background fluorescence signal was high, indicating an abundance of extraliposomal pyranine, all fractions were discarded. The liposomal preparation was attempted again, but the volume of fractions collected was increased to 1 mL for each fraction. Evaluation of two of these fractions showed more promising results than the previous preparation. Spherical particles that emit green fluorescence were observed. Furthermore, these had relatively low background signal which indicates successful removal of excess pyranine from the liposomal preparation (Figure 2-4).

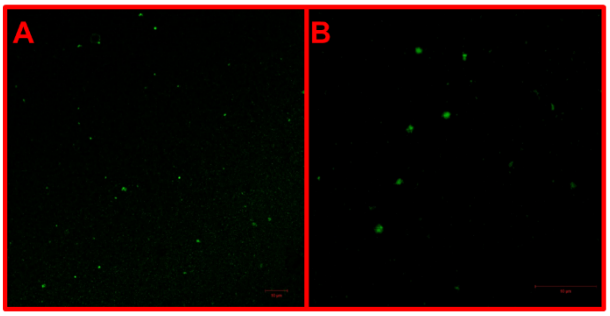


**Figure 2-4: Liposomal preparation harvested by collecting 1 mL fractions the Sephadex-G50 column.** The first two fractions collected are represented by the images in Panel A and B, respectively. Both images show spherical particles presumed to be pyranine-loaded liposomes. The relatively low background fluorescence signal suggests absence of extraliposomal pyranine.

### 2.2.2 Comparison of extrusion and sonication

Though the liposomal preparation and purification was successful as indicated by Figure 2-4 the number of liposomes formed was relatively low and the fluorescence signal emitted by these liposomes was not strong. Consequently, the next objective was to investigate sonication as a technique to prepare single lamellar pyranine-loaded liposomes. This was done to determine the most efficient method for preparing large populations of solute-loaded liposomes.

Liposomes were once again prepared as described above, except that the lipid suspension was subjected to 5 minutes of sonication in an sonication bath (rather than to extrusion passages) to promote formation of single lamellar vesicles. The excess pyranine was removed by size exclusion chromatography and the liposomes were harvested by collecting 1 mL fractions from the Sephadex G50 column as described above. These were evaluated by confocal microscopy to confirm successful formation of pyranine-loaded liposomes. Imaging was performed in fluorescent (Figure 2-5A) and normal light (Figure 2-5B) modes, as well as the overlay of the two modes for comparison (Figure 2-5C). The images confirmed the presence of liposomes, however these appear to exclude pyranine since there is no fluorescence signal emitted by the particles presumed to be liposomes.

Nonetheless, this method appeared to promote formation of greater populations of liposomes relative to extrusion. A liposomal preparation involving a combination of both extrusion and sonication to promote formation of single lamellar liposomes was attempted next. This was done to determine if it was possible to combine the benefit of solute encapsulation efficiency exhibited by extrusion with the benefit of greater liposome populations exhibited by sonication.

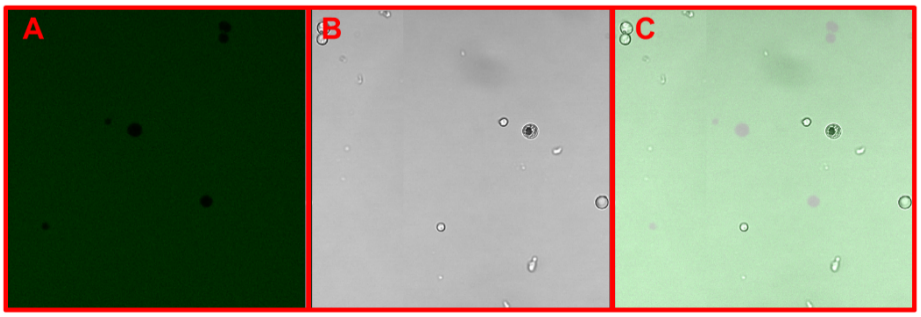


**Figure 2-5: Pyranine-loaded liposomes prepared by sonication.** The lipid suspension was subjected to sonication for 5 minutes to promote formation of unilamellar vesicles. Excess pyranine was removed by sonication on a Sephadex G-50 column and the “pure” liposomes were harvested by elution with gravitational force and collection of 1 mL fractions. The fractions were imaged in fluorescent (A) and normal light (B) modes, as well as an overlay of the two (C).

Excess pyranine was removed and pyranine-loaded liposomes harvested as described above. The collected fractions were once again evaluated for successful liposome formation by confocal microscopy and images were acquired in fluorescence and normal light modes as well as an overlay of the two modes (Figure 2-6). The images show more liposomes per area than in previous liposomal preparations. This in turn, suggests that the combination of extrusion and sonication does promote formation of more liposomes relative to individual application of these techniques. Unfortunately, these liposomes still appear to exclude the pyranine. This may be attributed to formation of micelles rather than unilamellar vesicles which may occur when a lipid suspension is subjected sonication. Since there is no way of ensuring

that unilamellar vesicles rather than micelles are produced by sonication, this technique was deemed suboptimal for preparation of solute-loaded liposomes.

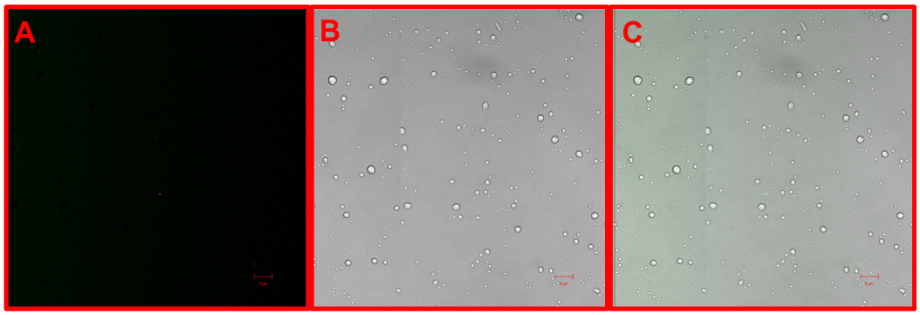


**Figure 2-6: Preparation of pyranine-loaded liposomes by combination of extrusion and sonication.** Lipid suspension was subjected to sonication, followed by 11 extrusion passages to promote formation of single lamellar vesicles. The resultant pyranine-loaded liposomes were collected by elution with gravitational force from Sephadex-G50 to remove excess pyranine. Imaging was performed in green fluorescent (Panel A) and normal light (Panel B) modes as well as an overlay of both (Panel C).

Nevertheless, as the combination of extrusion and sonication produced more liposomes, which in turn implies that longer processing time was key to producing liposomes from each preparation, the number of extrusion passages was increased from the 11 (manufacturer recommendation) to 20 passages to improve liposome formation efficiency.

Once again, the excess pyranine was removed by size exclusion chromatography and the liposomes were harvested in 1 mL fractions by elution with gravitational force from the Sephadex-G50 column. Evaluation of these fractions by confocal microscopy reveals spherical particles that emit green fluorescence from both fractions (Figure 2-7). However, the first fraction had a relatively high background fluorescence signal which was subtracted to improve the contrast in the image (Figure 2-7 A&B). In contrast, the second fraction contained more liposomal particles and had a low background fluorescence signal relative to the first (Figure 2-7 C). No further processing was required for the image of this fraction, and the image was then re-captured in a zoomed position in an effort to obtain more detail about the size distribution of the liposomes (Figure 2-7 D). This image represents the upper magnification limit of the confocal microscope and demonstrates the small size of the liposomal particles. This made it challenging to obtain more detail.

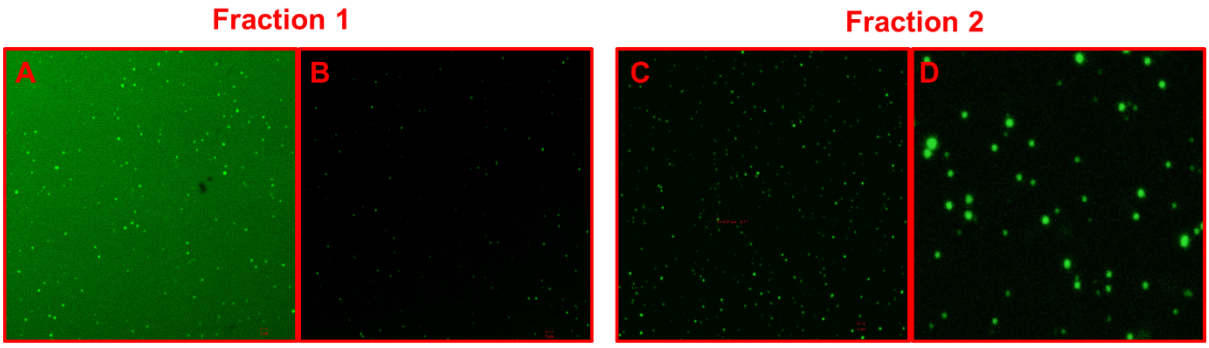


**Figure 2-7: Pyranine-loaded liposomes prepared after 20 extrusion passages.** The lipid suspension was subjected to 20 extrusion passages to promote formation of pyranine-loaded single lamellar vesicles. Excess pyranine was removed by size exclusion chromatography on a Sephadex G-50 column. The first two 1 mL fractions collected (Panels A, B and C, D, respectively) were imaged to confirm the presence of "pure" liposomes. This first fraction contained spherical particles presumed to be the liposomes (A), however the background fluorescence had to be subtracted to improve contrast (B). The second fraction also contained these spherical particles presumed to be pyranine-loaded liposomes (C). The re-captured image in a zoomed position was produced in an attempt to obtain more detail about liposomal size distribution (D).

The average diameter of the liposomes was expected to be close to 100 nm[140], because the extruder was fitted with 2 × 100 nm polycarbonate filters. This is about 20 times smaller than an average bacterial cell[141], which is also much smaller than the smallest mammalian cell, the erythrocyte[141]. In addition to this, it was challenging to obtain a good image of the liposomes in solution as the particles moved around a lot due to the aqueous environment. This could have been resolved by fixing the liposomes to the microscope slide. However, this is additional processing that would also require further optimization and deviated from the objectives of the study and was therefore not performed.

### 2.2.3 Determination of size distribution by scanning electron microscopy (SEM)

The challenges outlined above and instrument limitations encountered necessitated switching to a more sensitive technique like scanning electron microscopy (SEM). As the name suggests; SEM is a form of electron microscopy that provides topographic detail about the particles in question. It has higher resolution than confocal microscopy because it uses high energy electrons rather than light to generate images[142,143]. This technique requires that the sample be dry during imaging which eliminates the particle movement issues observed with confocal microscopy.

The liposomal preparation imaged in Figure 2-7 by confocal microscopy was also evaluated by SEM. The image was initially acquired in dark field mode which creates a contrast between light emitting and non-light emitting particles (Figure 2-8 A). This was done to identify the fluorescent particles presumed to be the pyranine-loaded liposomes. Subsequently, imaging was performed in bright field mode (Figure 2-8 B). Both images show the presence of spherical

particles presumed to the pyranine-loaded liposomes. The average size distribution was determined by measuring the diameters of some of the particles observed (Figure 2-9). The particles ranged in size between 50 and 100 nm which is within the expected range since the extruder was fitted with polycarbonate filters of 100 nm pore size.

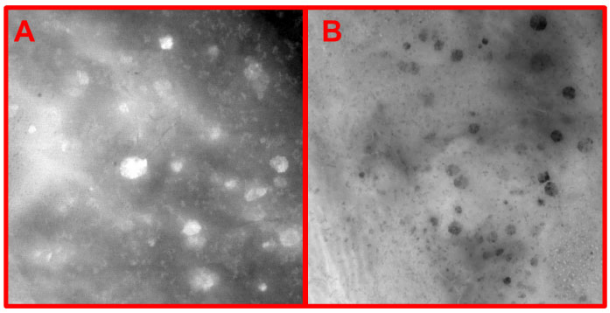


**Figure 2-8: Pyranine-loaded liposomes imaged by scanning electron microscopy (SEM).** The fractions were captured in dark field (A) and in bright field (B) modes, respectively.

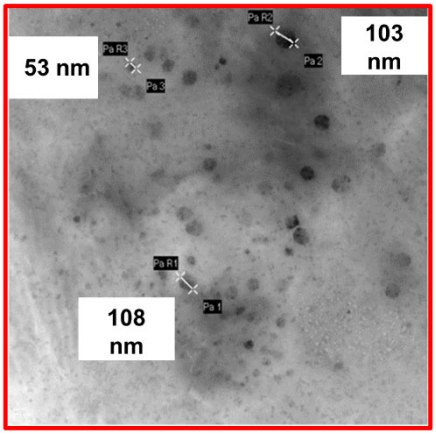


**Figure 2-9: Size distribution of pyranine-loaded liposomes prepared by extrusion followed by size exclusion chromatography.** The image was captured in bright field modes using SEM.

Taken together, the observations demonstrate the feasibility of SEM for qualitative determination of liposome size distribution. The observations show that extrusion is useful for preparation of liposomes of a predetermined size. Nonetheless, there were still challenges encountered when imaging liposomes with this technique. A major challenge was that the phospholipids in the liposomes oxidized as a result to exposure to the electron beam. This led to darkening in the exposed areas which in turn made it difficult to obtain a good quality image. Imaging with Cryo-electron microscopy in which samples are imaged in a frozen state would have been ideal for this kind of sample[142]. Unfortunately, such an instrument was not readily available at the time of performing this study.

### 2.2.4 Harvesting the liposomes by centrifugation improves the size dispersion

The relatively small size of the liposomes made it difficult to obtain good quality images with confocal microscopy. It also made it necessary to use a higher resolution technique (SEM) to obtain the detail that was required to determine size distribution of the particles, at least from a qualitative perspective. However, due to the inability to obtain good quality images it was decided to revert back to confocal microscopy. However, to circumvent some of the previous challenges liposomes of a greater diameter were prepared by fitting the extruder with polycarbonate filters of 800 nm pore size, which should result in liposomes with an average diameter of up to 800 nm[140]. This is relatively close to the diameter (1 000 nm) of an average bacterium. The liposomes were prepared as previously described, except this time the “pure” pyranine-loaded liposomes were harvested by low speed centrifugation in a swing bucket rotor instead of using size exclusion chromatography. The flow-through was collected and imaged in fluorescent and normal light (as well as a combination of the two) to evaluate this method (Figure 2-10 A-C).

The image confirms the presence of spherical green light emitting particles presumed to be pyranine-loaded liposomes. It also shows more particles per area imaged relative to the previous preparation. This can be attributed to the method used to harvest the liposomes, since it is the only factor that was varied in addition to the liposomal size.

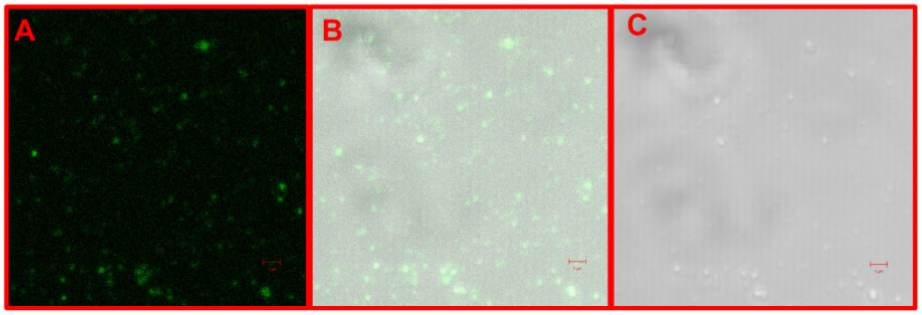


**Figure 2-10: Pyranine-loaded liposomes of 800 nm diameter prepared by 20 extrusion passages and imaged using confocal microscopy.** Imaging was performed in green fluorescent light (Panel A), normal light (Panel B), as well as the overlay of fluorescent and normal light (Panel C).

### 2.2.5 Determining size dispersion by dynamic light scattering

The size dispersion of the bigger liposomes preparation was determined by dynamic light scattering (DLS) (Figure 2-11). DLS measures the single scattering events to provide information on the dynamic properties of a particle[144]. It assumes that each detected photon has been scattered by the sample only once. The diameter size is indicated in nm on the x-axis, and the relative abundance is indicated by peak intensity which is expressed as a percentage on the y-axis (Figure 2-11). The peak close to 100% intensity indicates that most

of the particles in the sample are between 500 and 800 nm diameter, suggesting that the majority of the particles in the sample are within the expected range. There is also a small shoulder at 20% intensity with a 100 nm diameter, indicating the presence of some smaller particles. Extrusion performed with membrane filters of a pore size greater than 200 nm tend to produce liposomes of a slightly smaller diameter than the membrane pore size, hence the observed polydispersity[140]. Since the majority of the population was made of liposomes within the expected size range, this was considered to be a reasonable size dispersion and no further optimisation was done.

Taken together, these observations suggest that solute-loaded unilamellar liposomes of 800 nm diameter can be prepared by 20 extrusion passages in a hand-held extruder fitted with 2 polycarbonate filters of 800 nm pore size. The results also suggest that excess solute can be adequately removed by size-exclusion chromatography on a Sephadex G50 column prepared in house. Following this, the pure solute loaded liposomes can be harvested by low speed centrifugation to obtain liposomes of reasonable sample concentration and uniform size dispersion.

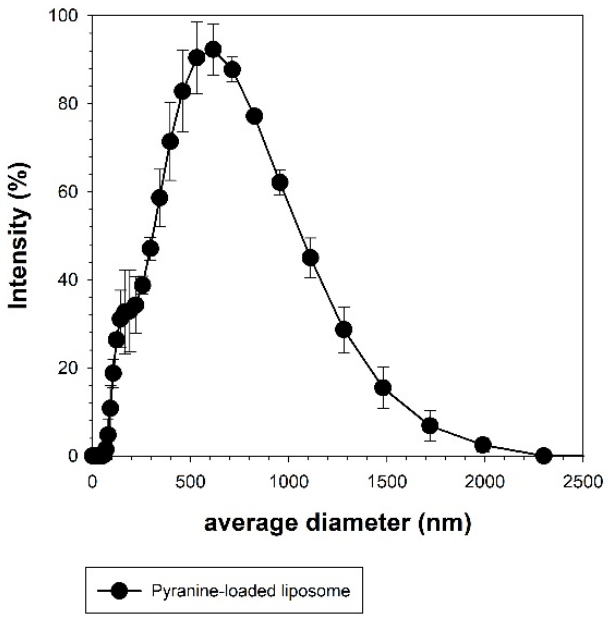


**Figure 2-11: The size distribution of pyranine-loaded liposomes as determined by dynamic light scattering (DLS).** The particle size is indicated as average diameter in nanometres (nm), and the intensity weighted distribution of particles is indicated as percentage. The symbols represent the average of value obtained from triplicate determination, with the error bars representing ± standard deviation.

### 2.2.6 CPM-loaded liposomes are not suitable for performing permeability measurements

Following the validation of the liposome preparation method, the next objective was to identify a suitable fluorophore for performing permeability measurements of the compounds of interest

in this particular study, i.e. CoA and its biosynthetic intermediates. The fluorophore selected for this purpose is 7-diethylamino-3-(4-maleimidophenyl)-4-methylcoumarin (CPM) (Figure 2-12). This molecule has a low fluorescence emission—unless it forms adducts with a thiolated molecules. Moreover, it was also an attractive option because its sensitivity towards P-PantSH and CoA intermediates has already been demonstrated[145].

In addition, a reference compound also needed to be identified to be used as negative control. This compound should not be able to efficiently cross the membrane, but should also contain a free thiol to allow for its reaction with CPM. While considering compounds that would possibly fit this profile, we noted that a transport protein dedicated to the membrane translocation of glutathione (GSH) has been determined[146]. This suggests that GSH is incapable of crossing biological membranes by passive diffusion. This molecule is also a low molecular weight thiol similar to CoA and its intermediates (including P-PantSH, which is the subject of the current study). For these reasons, GSH was selected as a reference.

CPM-loaded liposomes were prepared on the principle that no fluorescence signal would be observed unless the molecule interest can permeate the membrane and react with CPM to form fluorescent adducts inside the liposome. Since GSH is expected to be membrane impermeable, a control experiment was set-up by treating a fraction of the CPM-loaded liposomes with 0.1% Triton X-100 to “permeabilize” the liposomal membrane. GSH was expected to permeate the Triton-treated membrane. However, the observed outcomes show no distinction between intact and permeabilized liposomes (Figure 2-13). This was attributed to CPM apparently being membrane permeable, which implies that the observed fluorescence signal is due to CPM- efflux from the liposome[147].

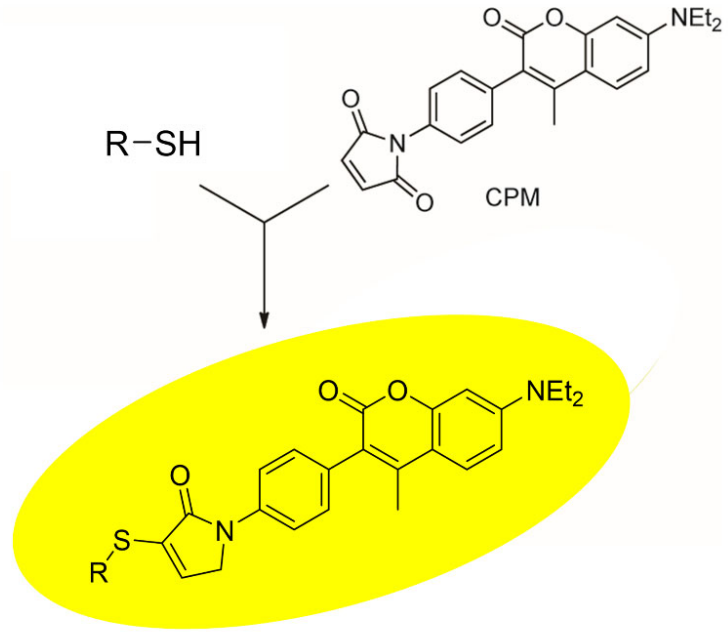


**Figure 2-12: The principle behind CPM fluorescence**. CPM is a coumarin-based fluorophore that does not produce fluorescence unless it forms adducts with thiol molecules like PantSH or P-PantSH.

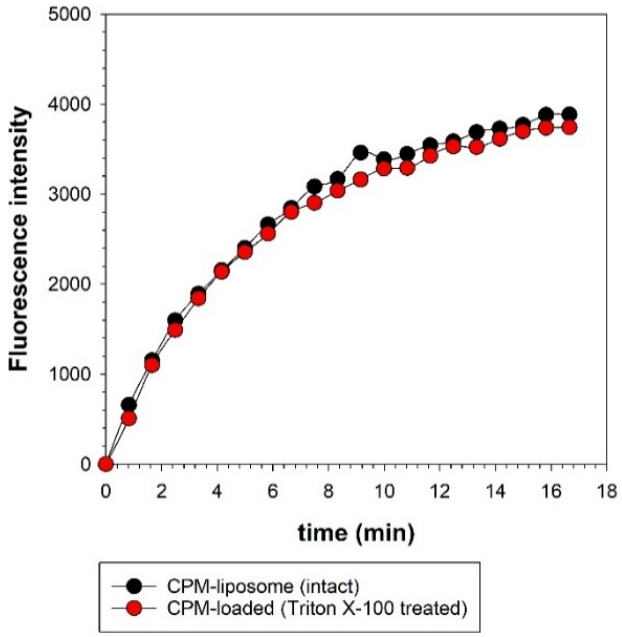


**Figure 2-13: Membrane permeability measurements of GSH using CPM-loaded liposomes.** A fraction of the liposomes was treated with Triton X-100 to “permeabilize” the liposomal membrane (red). The influx of GSH into the liposomes was monitored by measuring change in fluorescence intensity over time. Intact CPM-loaded liposomes were used as a control (black) since GSH is expected to be membrane impermeable.

### 2.2.7 A discontinuous assay for determining the membrane permeability of thiolated molecules

The unexpected result that CPM is permeating the liposome prompted an adjustment in the experimental set-up in such a way that would circumvent this property. First, the reverse experimental set-up was performed by preparing liposomes with the molecule of interest, instead of CPM, being encapsulated in the intraliposomal cavity. Liposomes were prepared as described earlier for the pyranine-loaded liposomes 800 nm in diameter (2.2.4). Next, membrane permeability measurements were performed in a discontinuous manner. This was achieved by using a dialysis membrane as a barrier between the molecule-encapsulated liposomal suspension and a solute-free dialysate (Figure 2-14). The liposome suspension was placed in the dialysis unit, and then a solution devoid of the molecule of interest was used as a dialysate.

In principle, if the molecule of interest is membrane permeable, it would diffuse out of the liposome through liposomal membrane, then through dialysis membrane and into the dialysate. The diffusion would continue in that direction until there are equimolar amounts of the molecule on either side of the dialysis membrane. The rate of diffusion can then be monitored by collecting aliquots of the dialysate at different time points, and adding CPM to determine the amount of thiolated molecule in each aliquot. The diffusion rate can then be reported as a change (increase) in fluorescence intensity over time. On the other hand, if the molecule of interest is membrane impermeable, it would not be able to escape from the liposome and would be absent from the dialysate aliquots. This in turn would translate to low or no fluorescence signal being observed upon analysis of the aliquots (since CPM has to form thiol-adducts with the molecule of interest in order to produce a fluorescence signal).

The dialysis membrane is also a semipermeable membrane, which implies that the diffusion rate across this membrane is subject to molecular geometry and size of the molecule in question. For this application, the size of the molecules is not of concern as the molecular weight of the compounds of interest is smaller than the dialysis membrane molecular weight cut off (MWCO) by several orders of magnitude. However, these molecules do differ in geometry and polarity, and will therefore have distinct diffusion rates. These differences are then accounted for by determining the diffusion rate of the “free” molecule (i.e. the diffusion of the molecule across the dialysis membrane when it is not encapsulated in a liposome) in a similar manner to what is described above. The ratio of the liposomal diffusion rate described above, and “free” diffusion rate, is then considered as the relative liposomal diffusion ratio. This, in turn, is used to establish whether or not a molecule is membrane permeable. More specifically, the more similar the two rates are (i.e. the closer the ratio is to one), the more likely the molecule of interest is to be membrane permeable.

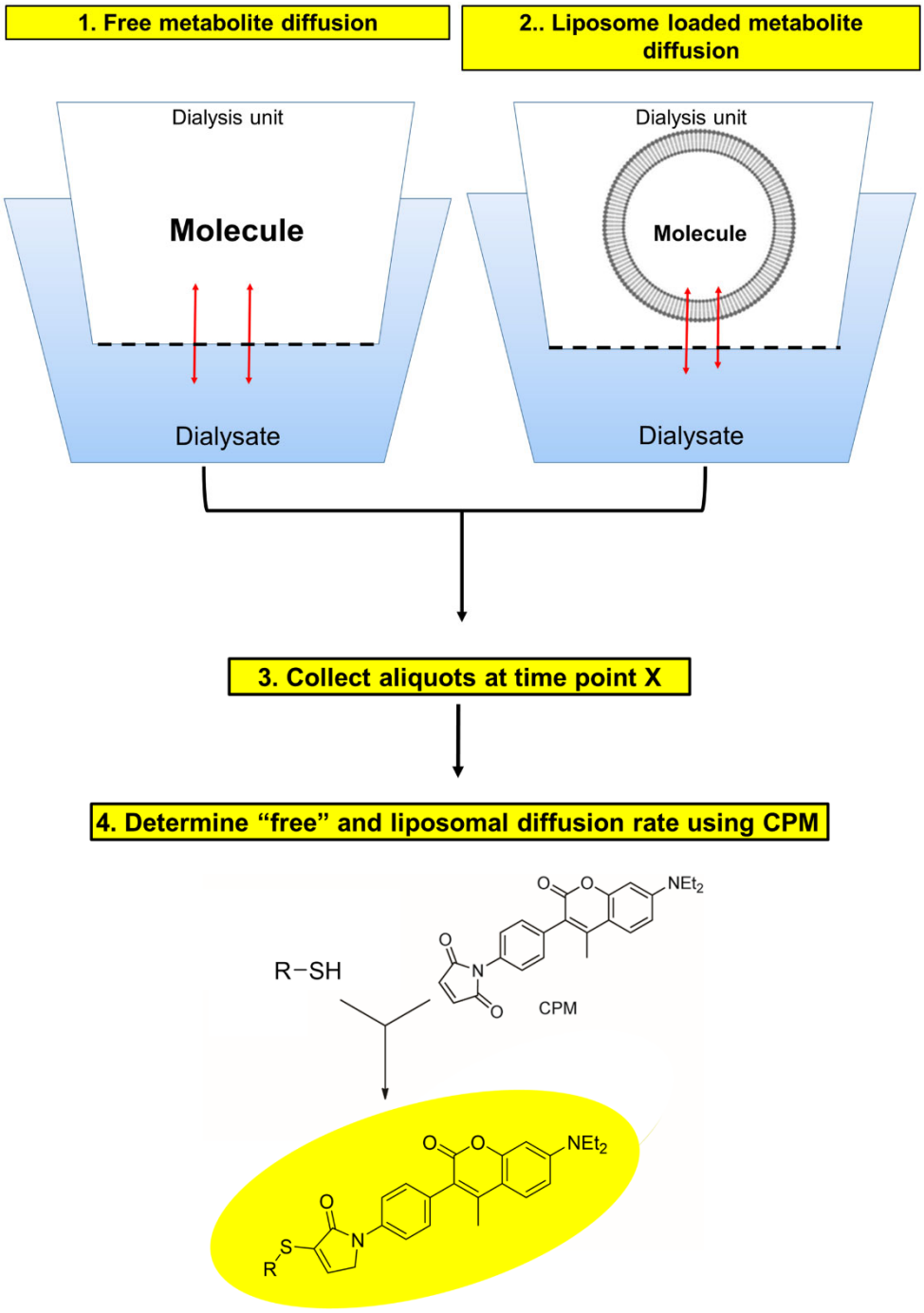


**Figure 2-14: The principle behind the discontinuous assay for measuring membrane permeability of P-PantSH and other CoA-related thiolated small molecules.** Liposomes are prepared with the solute of interest loaded in the lumen. The solute-loaded liposomes are placed inside the dialysis device, which is suspended in a solution devoid of the solute of interest (the dialysate). The diffusion rate of free metabolite (A) is measured concurrently with the liposomal diffusion rate (B) by taking aliquots of the dialysate at different time points. CPM is then added to the aliquots to determine the diffusion rate. The liposomal diffusion rate is then normalised relative to the free metabolite’s diffusion rate in order to describe the relative permeability of the molecule in question.

### 2.2.8 Permeability measurements of GSH using a CPM-fluorescence based detection method: A control experiment

GSH was expected to have low relative liposomal diffusion since it is has a dedicated transporter and is therefore presumed to inefficiently permeate membranes by passive diffusion[148–150]. For this reason, GSH was selected as a reference molecule for determining the membrane permeability of the molecules of interest. However, its suitability for this purpose had to first be validated using the membrane permeability assay described above.

GSH-loaded liposomes were prepared as described earlier for the pyranine-loaded liposomes 800 nm in size (section 2.2.4). In addition, 1 mM GSH and 1.5 mM TCEP (non-thiol containing reducing agent) was added to the liposomal suspension prior to performing extrusion. This was done so that GSH-loaded unilamellar vesicles could be prepared. An aliquot of the same solution was also used to determine the diffusion rate of "free" GSH. The liposomal diffusion of this molecule was then monitored as described in the work-flow depicted in Figure 2-15. The diffusion rate of free GSH was also monitored concurrently. CPM was then added to all aliquots collected and the fluorescence intensities were plotted against time to show the progression of the diffusion.

A continual increase in fluorescence intensity was observed for free GSH (Figure 2-16). This was expected since as the MWCO of the dialysis membrane was 7 kDa which exceeds the size of GSH and would therefore allow free diffusion of the dialysis membrane. On the other hand, very low fluorescence signals were observed for the diffusion of liposomal-encapsulated GSH relative to the diffusion of the free metabolite. These observations suggest that the liposomal membrane is a physical barrier that GSH cannot overcome, and in turn that it cannot diffuse over the dialysis membrane. To confirm this, a fraction of the GSH-loaded liposomes was treated with Triton X-100 to permeabilize the liposomal membrane. The GSH diffusion from these permeabilized liposomes was also monitored and then plotted as fluorescence intensity as a function of time. The results show that GSH could diffuse over this compromised liposome membrane, though not to the same extent as free GSH.

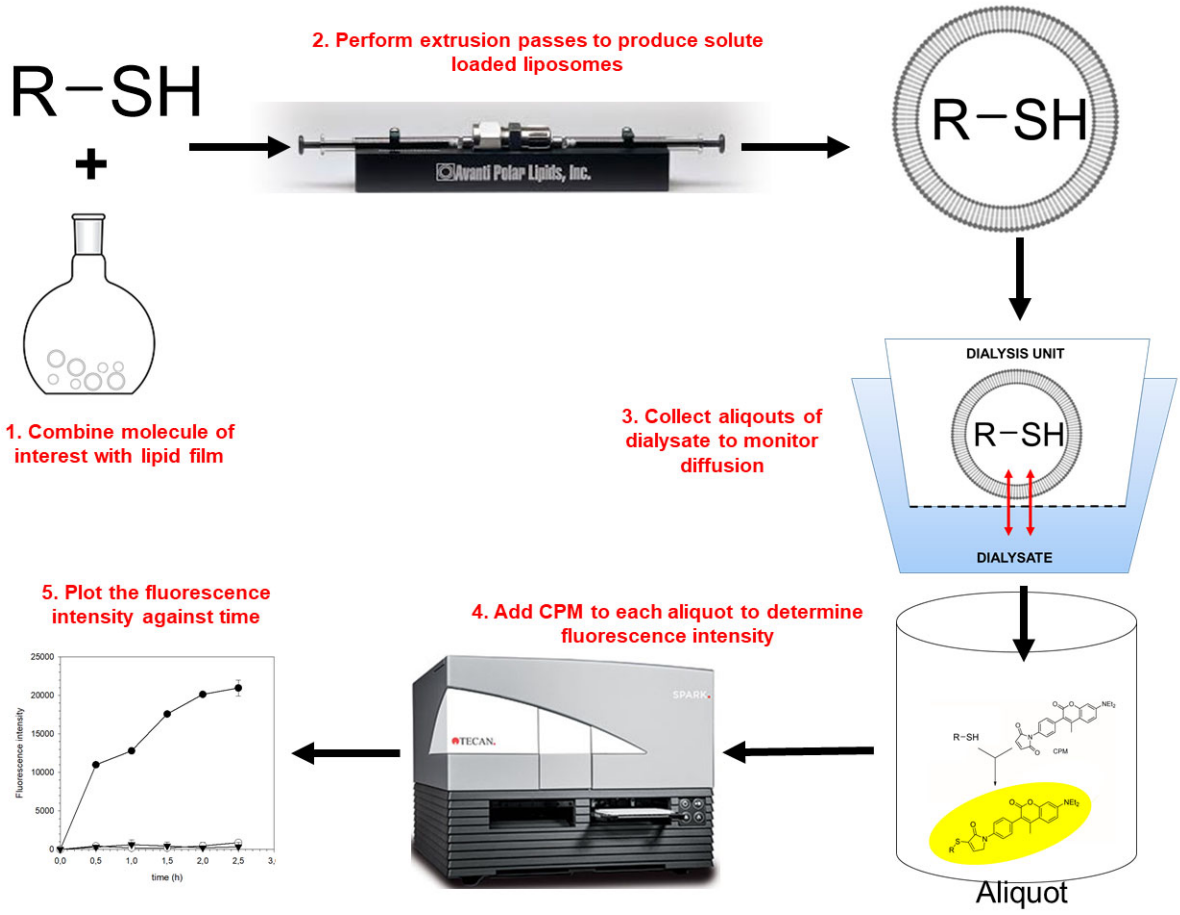


**Figure 2-15: Work-flow for the discontinuous assay for measuring the membrane permeability of thiolated small molecules.** A solution containing the molecule of interest is used to hydrate the lipid film **(1),** the resultant lipid suspension is the subjected to 20 extrusion passages to promote formation of unilamellar vesicles loaded with the molecule of interest **(2),** the diffusion of the molecule from the liposome is then measured discontinuously by placing the liposomal preparation inside a dialysis unit then collecting aliquots at different time points **(3),** CPM is then added to each aliquot to determine the fluorescence intensity **(4),** from which the diffusion rate is calculated **(5).**

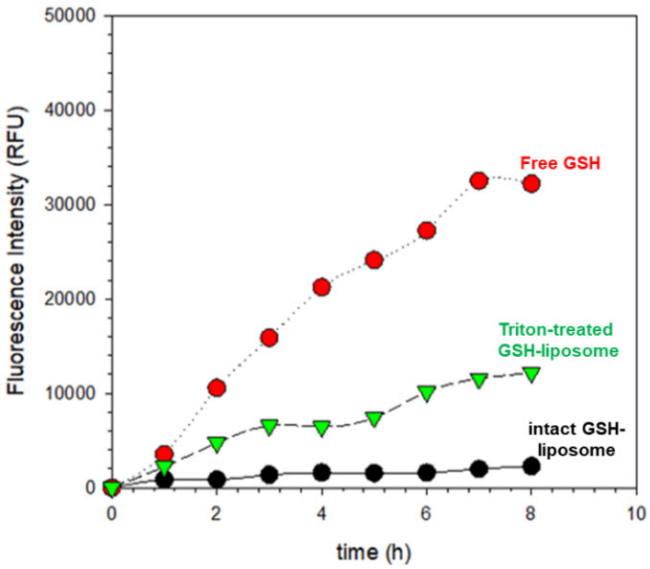


**Figure 2-16: Membrane permeability measurements of glutathione (GSH).** The diffusion rates of free GSH (red), and liposome-loaded GSH (black), were determined in a discontinuous manner by collecting aliquots at different time points. The diffusion rate of GSH from liposomes treated with 0.1 % Triton X-100 (Green) was also determined. The diffusion rate is depicted as an increase in fluorescence intensity of CPM-GSH adducts over time.

Taken together, these observations suggest that the liposome is a physical barrier that mimics biological membranes in its ability to exclude molecules that are inherently membrane impermeable. The observations further confirm the suitability of GSH as a reference molecule for permeability measurements of thiolated metabolites (such as P-PantSH and other related molecules) and validates the adjusted experimental set-up as a viable method to optimize for further permeability studies.

### 2.2.9 The detection method can be changed to accommodate a diverse selection of molecules

As previously mentioned, the reactivity of CPM towards P-PantSH and other CoA intermediates has been demonstrated and further confirmation is therefore not required[145]. However, to optimize the permeability assay further, the “free” diffusion rates of the molecules of interest had to be determined using CPM-based fluorescence as a detection method (Figure 2-17). In addition to GSH and P-PantSH, the diffusion rates of PantSH, dePCoA, *N*-acetylcysteamine (H-SNAC), and CoA were be determined using a CPM-based fluorescence detection method. This further demonstrates the suitability of this fluorophore for use in measuring the membrane permeability of a variety of thiolated molecules.

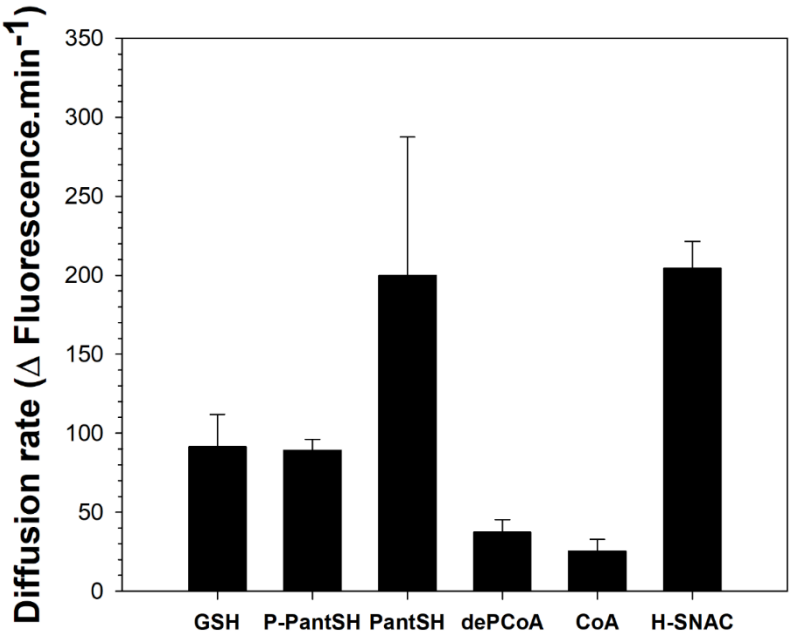


**Figure 2-17: The diffusion rates of 1 mM GSH, P-PantSH, and other thiolated CoA intermediates through the Slide-A-Lyzer® mini-dialysis membrane (MWCO = 7 kDa, Thermo scientific, U.S.A).** The diffusion rates were the determined using the CPM-based fluorescence assay to determine the suitability thereof for application as a detection method in a membrane permeability assay. The experiment was performed twice (n = 2), each in triplicate. The bar indicates the average of the two experiments, and the error indicates the range/2 (i.e., the upper and lower limits of the range as determined).

As CPM is only suitable for thiol molecules and thereby not applicable to other kinds of molecules, the permeability assay is set up in such a manner that it is possible to change the detection method without changing the fundamental principles on which the assay is based. This implies that the fluorophore can be replaced as required to accommodate molecules with a variety of structural features or different structural diversities. However, the important requirements to consider is a suitable molecule to use a reference, as well the sensitivity of the detection method towards all molecules in question. The latter can be confirmed by measuring the “free” diffusion of the molecules using the detection method in question to find out if all the molecules are detectable.

The molecules of interest in the current study could be divided into three classes: thiolated CoA intermediates for which CPM was used as part of the detection method; structural analogues of PanCOOH that can act as substrates for a PanK-coupled enzyme assay utilizing NADH consumption as detection method, and finally phosphorylated PanCOOH analogues that are substrates for alkaline phosphatase (ALP) coupled to a malachite green assay that could be used as a detection method.

### *2.2.9.1* PanK-coupled enzyme assay as a detection method

The PanCOOH analogues selected for the current study are all substrates for PanK – the enzyme that catalyzes the first reaction of CoA biosynthesis[105]. A pyruvate kinase-lactate dehydrogenase (PK-LDH)-coupled enzyme assay for determining catalytic activity of PanK has been previously described and used routinely for mechanistic studies of PanK (Figure 2-18)[151]. Therefore, this assay was selected as a detection method in the current study since it required no further optimization and PanCOOH analogues selected for the current study are all substrates for PanK. In this assay PanK-mediated phosphorylation of PanCOOH analogues takes place in the presence of ATP-hydrolysis to ADP. This reaction is then coupled to the production of lactate from phosphoenolpyruvate (PEP) via pyruvate as catalyzed by PK and LDH. The latter requires NADH as a cofactor and its consumption can be monitored spectrophotometrically at 340 nm.

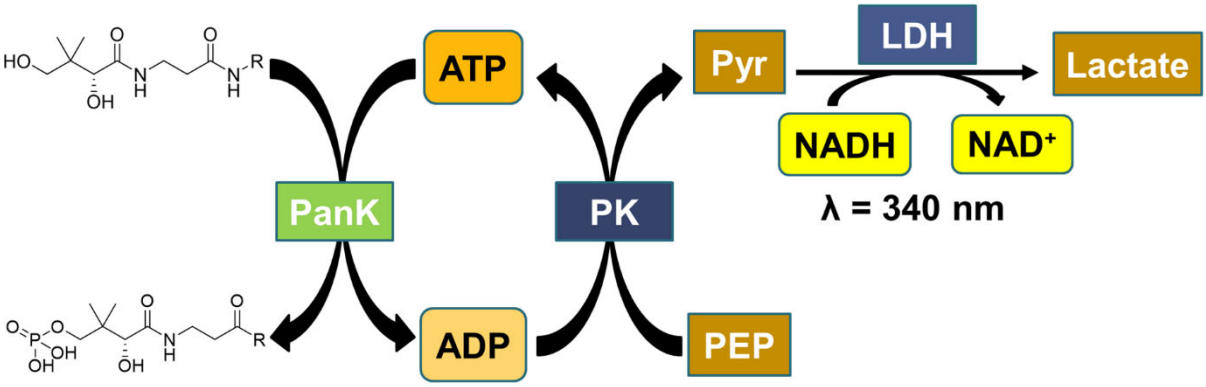


**Figure 2-18: Principle behind the PK-LDH coupled enzyme assay for determining PanK activity.** The phosphorylation of PanCOOH to P-PanCOOH is mediated by PanK. This reaction is coupled to ATP hydrolysis and the resultant ADP is used as cofactor for the conversion of PEP to pyruvate (Pyr) which is mediated by pyruvate kinase (PK). The pyruvate is reduced to lactate by lactate dehydrogenase (LDH), and this is coupled to NADH oxidation. NADH is chromogenic and the oxidation can be monitored at 340 nm on a spectrophotometer.

If the molecule of interest is present in the aliquots collected to monitor the rate of diffusion, PanK can be used to determine the concentration of PanCOOH and most compounds retaining the pantoyl moiety (Figure 2-19). In this manner, the rate of NADH consumption corresponds to the amount of “substrate” in each aliquot. The diffusion rates can then be determined by plotting the NADH consumption rates in each aliquot against time.

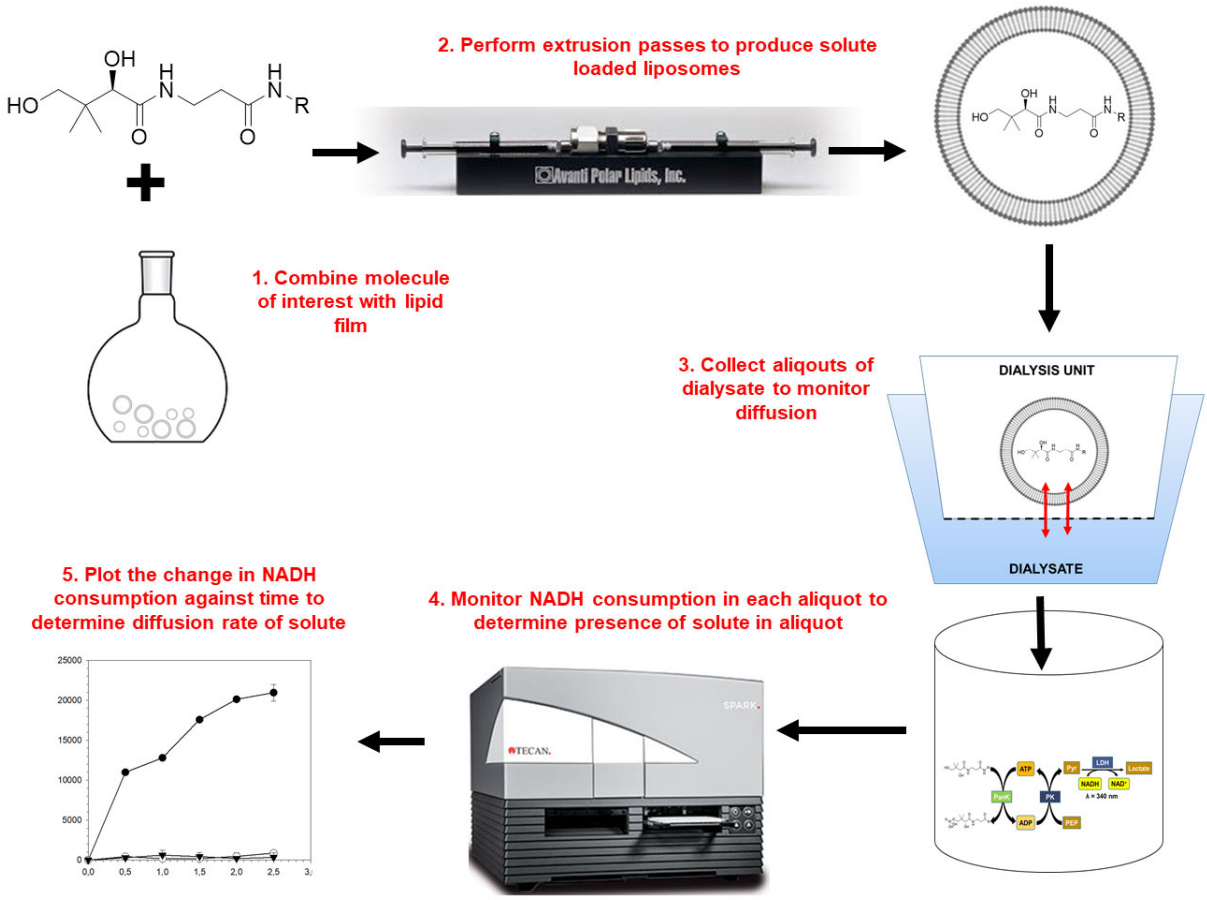


**Figure 2-19: Detection method can be changed without changing the experimental set-up for the discontinuous assay for measuring membrane permeability.** The detection assay can be changed to accommodate diverse chemical and structural diversities, which in turn makes the assay versatile: For determination of diffusion rates of pantothenate and its selected structural analogues, instead of using CPM (step 4) the detection method is changed to a PanK-coupled enzyme assay which monitors NADH consumption.

PanCOOH is the natural substrate for PanK and since a dedicated transporter has been characterized for this molecule[73,152], it is also presumed to be incapable of membrane permeation by passive diffusions similar to GSH. For these reasons, it was selected as a negative control for molecules studied by the PanK coupled enzyme assay. The diffusion rates of free PanCOOH and pantothenate analogues of interest in the current study were determined by the described discontinuous assay (Figure 2-20). The figure shows the diffusion rates of PantSH, PantOH, N5-Pan and *N*-phenethylpantothenamide *(N*-PE-Pan) in addition to that of PanCOOH, this in turn confirms suitability of the coupled enzyme assay as a detection method in the discontinuous membrane permeability assay.

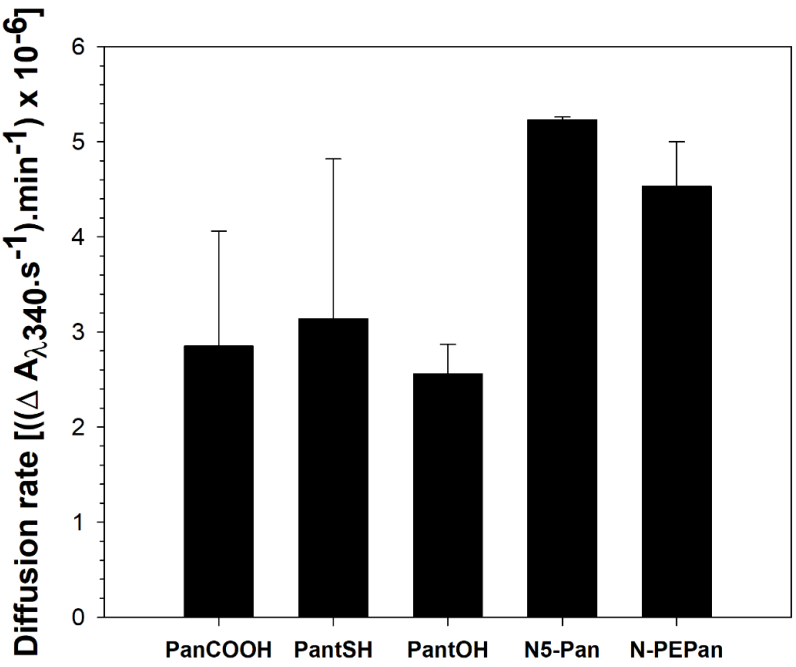


**Figure 2-20: The diffusion rates of 1 mM PanCOOH, PantSH, PantOH, N5-Pan and *N*-PE-Pan through the Slide-A-Lyzer® mini-dialysis membrane (MWCO = 7 kDa, Thermo scientific, U.S.A).** The diffusion rates were the determined using the PanK-coupled enzyme assay which monitors NADH consumption to determine the suitability thereof for application as a detection method in a membrane permeability assay. The experiment was performed twice (n = 2), each performed in triplicate. The bar indicates the average of the two experiments, and the error indicates the range/2.

### *2.2.9.2* Alkaline phosphatase-malachite green coupled assay as a detection method

ALP is an enzyme that cleaves phosphate esters to liberate inorganic phosphate groups[153]. The cleavage reaction can be monitored spectrophotometrically using the malachite green dye which undergoes a color change in the presence phosphates and is detected at 620 nm (Figure 2-21)[154,155].

Similar to the two assays a negative control had to be identified for this assay. Glucose-6-phosphate (G6P) is a small molecule for which a dedicated transporter has been characterized in eukaryotes and prokaryotes[156,157]. Therefore, this molecule should also be unable to cross membranes by passive diffusion. Furthermore, this molecule may be a substrate for ALP, and for these reasons it was selected as reference molecule for the membrane permeability measurements of phosphorylated PanCOOH analogues which are related to P-PantSH.

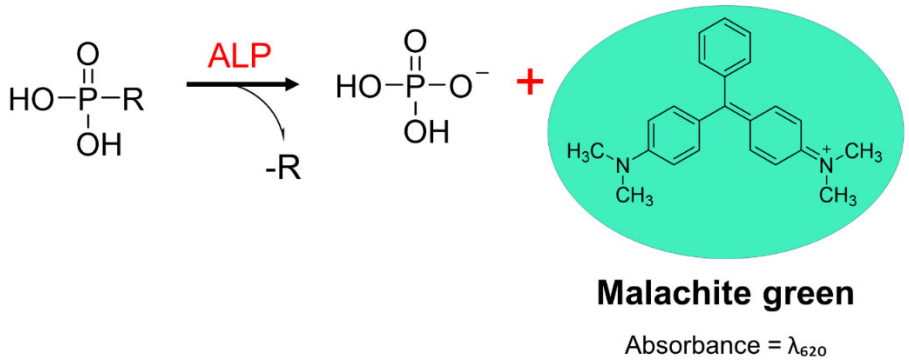


**Figure 2-21: The principle behind the ALP-malachite green coupled assay.** ALP cleaves the phosphorylated substrate and the amount of phosphate that is liberated is determined spectrophotometrically through its interaction with malachite green dye which undergoes a colour change in the presence of phosphates. The observed changes can be attributed to their rate of diffusion across the dialysis membrane.

G6P is structurally unrelated to the P-PanCOOH analogues that are of interest in this assay, and the activity of ALP towards G6P and the molecules of interest had to be determined to confirm compatibility with the assay conditions (Figure 2-22). In addition, a chromogenic molecule, *p*-nitrophenyl phosphate (pNPP), is commonly applied as a positive control for ALP-based assays and was included for this purpose.

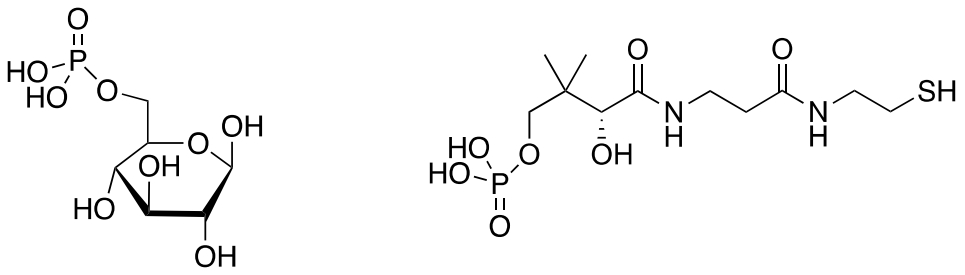

Glucose-6-phosphate (G6P) 4'-Phosphopantetheine (P-PantSH)

**Figure 2-22: Chemical structures of G6P and P-PantSH to illustrate the difference in composition.**

The activity of ALP towards pNPP was used as a reference to compare relative activity towards G6P and P-PantSH (Figure 2-23). The figure shows that the ALP could cleave both G6P and P-PantSH with similar efficiency to pNPP cleavage. This shows that the enzyme has relaxed substrate specificity and is therefore suitable for application in the context of this study.

Once ALP activity was confirmed, selected analogues including phospho-*N*-pentylpantothenamide (P-N5-Pan), phospho-N-phenethylpantothenamide (P-*N*-PE-Pan), and 4′-phosphopantothenate (P-PanCOOH) as well as 4′-phosphopantothenol (P-PantOH) were used to evaluate the suitability of the ALP-malachite green assay for application as a detection method in the membrane permeability assay using liposomes. The diffusion rates were reported as a change in absorbance as a function of time in minutes (Figure 2-24). The rates

for all six molecules could be determined which indicates the suitability of the ALP-malachite green coupled assay as a detection method for discontinuous measurement of the membrane permeability of P-PantSH and selected phosphorylated pantothenate analogues.

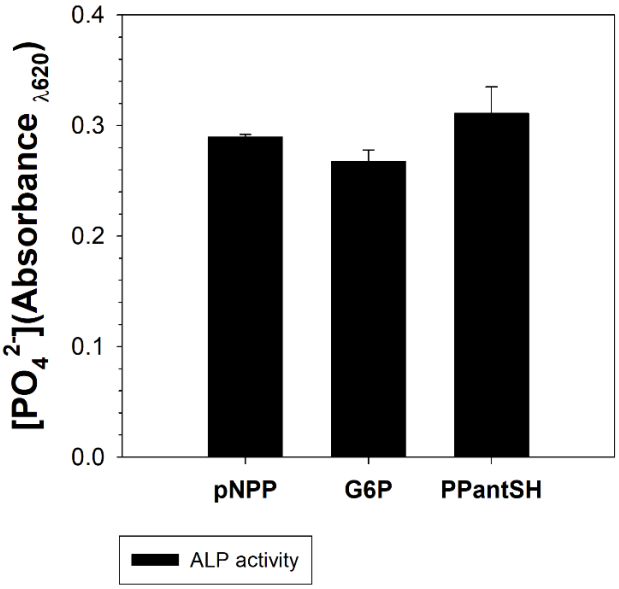


**Figure 2-23: ALP has relaxed substrate specificity and can cleave G6P and P-PantSH with similar efficiency to pNPP.** The activity of ALP towards G6P and P-PantSH was evaluated using activity towards pNPP as a control. The experiment was performed twice (n = 2), each in triplicate. The bar indicates the average of the two experiments, and the error indicates the range/2.

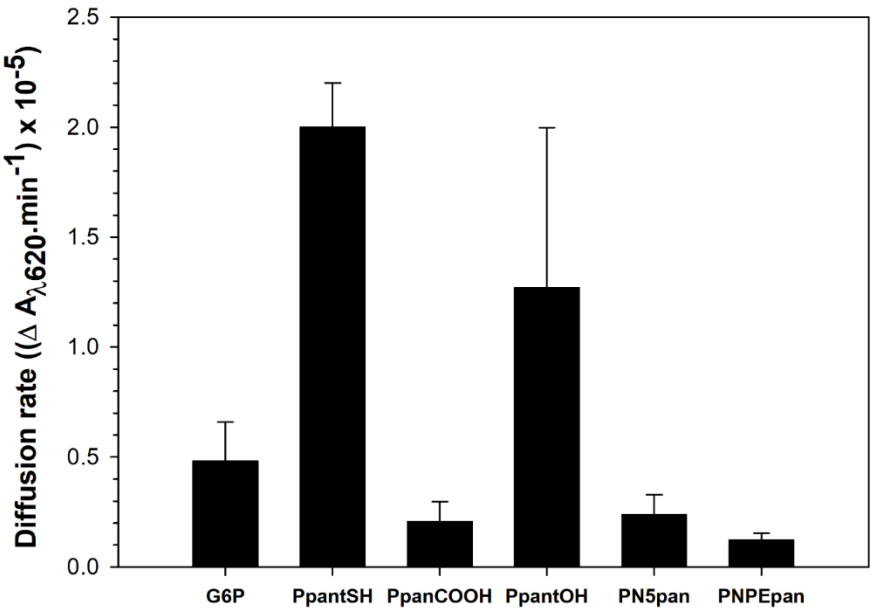


**Figure 2-24: The diffusion rates of 1 mM G6P, P-pantSH, P-N5-pan, P-*N*-PE-pan, P-panCOOH and P-pantOH through the Slide-A-Lyzer® mini-dialysis membrane (Thermo scientific, U.S.A).** The diffusion rates were the determined using the ALP-malachite green coupled assay to determine its suitability thereof for application as a detection method in a membrane permeability assay. The experiment was performed twice (n = 2), each in triplicate. The bar indicates the average of the two experiments, and the error indicates the range/2.

## 2.3 Conclusion

Small molecule permeability is an important but often neglected aspect of drug discovery. The lack of fundamental understanding of the molecular determinants of membrane permeability in small molecules is brought about in part by the scarcity of adequate investigatory tools. This challenge is further compounded by the overwhelming diversity chemical compounds that could serve as potential drug candidates. In an effort to address this issue we have described a liposome-based discontinuous assay for measuring membrane permeability of small molecules – with particular focus on CoA related molecules. The assay is set up in such a manner that the detection methods used to identify the molecules of interest can be changed as required to accommodate chemically and structurally diverse molecules. The use of liposomes as a membrane model also means the assay in amenable and can be used to study membrane permeation by passive diffusion as well as by protein mediated transport.

## 2.4 Materials and methods

The following reagents purchased from Sigma-Aldrich, Germany were all buffer grade, at purity of 95% or higher pantothenic acid (PanCOOH), pantethine, dephospho-CoA (dePCoA), coenzyme A (CoA), MES (2-(*N*-morpholino)ethanesulfonic acid), sodium chloride (NaCl), tris(2-carboxyethyl) phosphine (TCEP), potassium chloride (KCl), Tris, magnesium chloride ($MgCl_2$), calcium chloride ($CaCl_2$), ammonium molybdate and Triton X-100. This is with the exception of the following: pyranine and malachite green* (microscopy grade, *1% stock solution), 7-diethylamino-3-(4-maleimidophenyl)-4-methylcoumarin (CPM), adenosine-3',5'-triphosphate (ATP) and glutathione (GSH) which were HPLC grade, *p*-nitrophenyl phosphate (pNPP), glucose-6-phosphate (G6P) and (phospho-enol pyruvate) PEP which were enzyme assay grade. Cholesterol and 1-palmitoyl-2-oleoyl-sn-glycero-3-phosphocholine (POPC) were Sigma grade. Chloroform and ethanol were HPLC grade with 99% purity and were both purchased from Merck Germany. HCl was also purchased from Merck, Germany. PK from rabbit muscle (10 mg/ml), LDH from pig heart (10 mg/ml), ALP from calf intensitine (10 mg/ml), BSA as well as NADH (Laboratory grade at 98% purity) were all from Roche, Germany. PanK from *Escherichia coli* (*Ec*PanK) was obtained by heterologous expression with a histidine tag followed by Immobilized metal affinity chromatography (IMAC) purification according to previously published methods[99]. Polycarbonate membrane filters were from Whatmann. The hand-held mini-extruder was from Avanti Polar Lipids®, U.S.A. Sephadex-G50 were from Amerscham, UK. 96-well black and clear plates used for fluorometry and spectrophotometry, respectively, were from Thermo Scientific, U.S.A. The Haereus benchtop swing bucket centrifuge is manufactured by Thermo Scientific, U.S.A. The Power sonic 405 sonication bath is manufactured GT sonic, U.S.A. The Slide-A-Lyzer® mini-dialysis membrane units were from

Thermo scientific, U.S.A. The rest of the phosphorylated and non-phosphorylated pantothenate analogues were chemically synthesised in-house by Dr. Leanne Barnard.

### 2.4.1 Lipid stock preparation

Lipid stocks of cholesterol and POPC were prepared by weighing out the dry lipid powder and dissolving it in chloroform to a concentration of 10 mg/mL for each compound. From each stock, a 1 mL aliquot was transferred to a round bottom flask after which the organic solvent was removed *in vacuo*. Residual solvent was removed under high vacuum for a period of 12 hours.

### 2.4.2 Preparation of pyranine-loaded liposomes by extrusion

A solution of 100 µM Pyranine in 20 mM MES (pH 5.9) and 180 mM NaCl was used to hydrate the dry lipid film. The resultant liposome suspension was subjected to 10 cycles of freezing at -80 ˚C (in liquid nitrogen) and thawing at room temperature to promote formation of unilamellar vesicles. Following this, the suspension was subjected to 11 or 20 extrusion passes on the mini-extruder fitted with 2 × 0.1 µm diameter polycarbonate membrane filters. Filter membranes were included to promote formation pyranine-loaded liposomes. Excess pyranine was removed by size exclusion chromatography using a Sephadex-G50 column prepared in-house. To prepare the column, 2 g of Sephadex-G50 beads was weighed out and hydrated with 20 mM MES (pH 5.9) and 180 mM NaCl. The slurry was allowed to stand at room temperature for 1 hour for full hydration of the beads. The excess buffer was decanted out and the slurry was transferred to a 5 mL syringe column sealed with cotton wool. The column was then placed in a 15 mL centrifugal tube and the beads were packed by centrifugation at 3 000 g for 5 minutes in a benchtop swing bucket centrifuge. The residual buffer collected in the flow through and was discarded. The extruded lipid suspension was then placed on the column bed. The pyranine-loaded liposomes were then eluted and collected in 0.5 mL or 1 mL fractions with 20 mM MES (pH 5.9) buffer containing 180 mM NaCl (from here on called "MES-NaCl").

### 2.4.3 Preparation of pyranine-loaded liposomes by sonication

The liposome suspension was subjected to freeze-thaw cycles as described in 2.4.2. However, instead of promoting liposomal formation with extrusion, the suspension was electrosonicated for 5 minutes, in a sonication bath at 10 °C. The excess pyranine was then removed as described in 2.4.2.

### 2.4.4 Preparation of pyranine-loaded liposomes of 800 nm diameter

The liposomes were prepared as described 2.4.2 except that the extruder was fitted with 2 × polycarbonate filters of 800 nm diameter. Furthermore, the liposomes were harvested from

the Sephadex-G50 column by centrifugation at 1000 g for 5 minutes in the benchtop swing bucket centrifuge. The pure liposomes were then collected in the flow-through.

### 2.4.5 Preparation of the GSH-loaded liposomes

The lipid film was prepared as described in **Error! Reference source not found.**. However, the film was hydrated with a solution of 1 mM GSH containing 1.5 mM TCEP. The resultant lipid suspension was subjected to freeze-thaw cycles as described for 2.4.2. Following this, the suspension was subjected to 20 extrusion passes on the mini-extruder fitted with 2 × 800 nm diameter polycarbonate membrane filters. This was done to promote formation of GSH loaded liposomes. Excess GSH was removed by size exclusion chromatography in a Sephadex-G50 column prepared in-house as described in 2.4.2, except the slurry was hydrated with MilliQ water instead of the MES-NaCl buffer. The GSH-loaded liposomes were then harvested by centrifugation as described in 2.4.4.

### 2.4.6 Confocal microscopy

Liposome imaging was performed on the Carl Zeiss LSM 780 confocal microscope housed in the cell imaging unit of the Central Analytical Facility (CAF) available at Stellenbosch University. The objective used was Alpha Plan-Apochromat 100x/1.46 Oil DIC M27. The light source used was an argon multiline laser 25 mW and the ~400/~480 nm emission filter was used to acquire the image.

### 2.4.7 Scanning Electron Microscopy (SEM)

Liposome imaging was performed on the Zeiss MERLIN SEM microscope housed at the Electron beam unit of CAF, Stellenbosch University. The following parameters were set for imaging: probe I = 250 pA, EHT = 200 keV and WD = 3.4 mm.

### 2.4.8 Dynamic light scattering

The size distribution of the unilamellar vesicles was determined by dynamic light scattering on the Malvern Zetasizer version 7.11 housed at Kansai Plascon in the Department of Chemistry and Polymer Science of Stellenbosch University. A 12 µL aliquot of the pyranine-loaded liposomal preparation was used to determine the size distribution. Water was used as a dispersant. Thus, 12 µL of the liposomal preparation was dissolved in water to a final concentration of 1 mL. The measurements were performed in a disposable sizing cuvette of 1 cm path length. The instrument temperature was set to 25 °C. The measurements were acquired at a count rate of 364.3 counts.$s^{-1}$ with an average acquisition time of 60 s. The attenuator index was set at 7 such that 1% of the laser light could penetrate the cuvette.

### 2.4.9 Membrane permeability measurements of GSH using the CPM-based continuous liposomal assay

The lipid film was prepared as described in 2.4.1 However, the film was hydrated with a solution of 50 µM CPM to a final lipid concentration of 10 mg/ml. The resultant lipid suspension was subjected to freeze-thaw cycles as described for 2.4.2. Following this, the suspension was subjected to 20 extrusion passes on the mini-extruder fitted with 2 × 800 nm diameter polycarbonate membrane filters. This was done to promote formation of CPM loaded liposomes of 800 nm diameter. Excess CPM was removed by size exclusion chromatography in a Sephadex-G50 column prepared in-house as described in 2.4.2, except the slurry was hydrated with MilliQ water instead of the MES-NaCl buffer. The CPM loaded liposomes were then harvested by centrifugation as described in 2.4.4.

A 200 µL aliquot of CPM-loaded liposomes was then treated with 0.1 % Triton X-100. This aliquot, together with an aliquot of the intact CPM loaded liposomes were transferred to a 96-well plate. The GSH solution (stock solution 10 mM) was added to a final concentration of 1 mM in both the intact and the permeabilized CPM-loaded liposomes. The GSH influx into the liposome was then determined by monitoring the change in fluorescence intensity of CPM at 1 minute intervals for about 20 minutes. This experiment was performed on a TECAN spark 10M fluorimeter (Switzerland) where fluorescence emission was monitored at $\lambda_{ex}$ = 387 nm and $\lambda_{em}$ = 465 nm. The fluorescence signal was optimised for 1 mM GSH.

### 2.4.10 Membrane permeability measurements of GSH using the discontinuous membrane permeability assay

A 1 mM GSH solution was prepared to represent the “free” GSH. Three dialysis membrane units were hydrated for 10 minutes in 3 × 10 mL beakers filled with 900 µL of MilliQ water each. Following hydration, 200 µL of the GSH-loaded liposomes were placed inside the first dialysis unit and 200 µL 1 mM GSH solution was added the second dialysis unit to measure liposomal diffusion of “free” GSH. For the “permeabilized” liposome experiment a 500 µL aliquot of the liposomal suspension was treated with 0.1% Triton X-100 (this 5 µL of 10% Stock solution. Following this, 200 µL of this detergent-treated liposomal preparation was placed in the last dialysis unit. The respective diffusion rates were then monitored by collecting 20 µL aliquots of the dialysate at 1 hour intervals for 8 hours. The aliquot was then transferred to a black 96-well plate to which 160 µL MilliQ water and 20 µL of CPM (10 µM) were added. The plate was then incubated at room temperature for 30 minutes to allow formation of CPM-adducts. Following this, the fluorescence intensity of each aliquot was measured on the TECAN spark 10M fluorimeter (Switzerland) at $\lambda_{ex}$ = 387 nm and $\lambda_{em}$ = 465 nm. The signal was again optimised to 1 mM GSH. The fluorescence intensity values were then plotted

against time intervals to illustrate GSH diffusion. The diffusion rates were then determined by calculating the slopes of respective plots.

### 2.4.11 Determination of small molecule diffusion rates using PanK-PK-LDH based discontinuous liposomal assay

Solutions of PanCOOH and selected PanCOOH analogues (N5-Pan, *N*-PE-Pan, PantSH and PantOH) were prepared to a final concentration of 5 mM each. Following this, 900 µL of water was placed in 3 × 10 mL beakers. Dialysis membranes were placed in each beaker and allowed to hydrate for 10 minutes. Following this, 200 µL of 1 mM PanCOOH solution was placed in the respective dialysis membrane unit such that there were three replicates. Aliquots of 20 µL dialysate were collected at 1 hour intervals for 5 hours and transferred to a 96-well plate. This process was repeated for each pantothenate analogue. A reaction mixture of 1.5 mM ATP, 2 mM PEP, 0.5 mM NADH, *Ec*PanK (2 µg/200 µL reaction), 2 U PK, 2 U LDH was prepared in a 50 mM Tris-HCl (pH 7.4) buffer containing 20 mM KCl and 20 mM $MgCl_2$. The presence of PanCOOH (or other analogues of interest) in each aliquot was determined by adding 180 µL of the reaction mixture and monitoring change in absorbance at 340 nm to determine NADH consumption from each aliquot. Each experiment for each of the analogues of interest was performed twice.

The coupled enzyme assay is set up in such a manner that the NADH consumption rate corresponds to the amount of PanCOOH (or other pantothenate analogues) used as a substrate for the PanK reaction. For this reason, the resultant NADH rates obtained for each aliquot were plotted against the time interval at which the aliquot was collected to represent the diffusion of the metabolite of interest over time. The slopes of these time courses were then used to calculate the diffusion rate of each of the metabolites investigated.

### 2.4.12 Determination of small molecule diffusion rates using the ALP-malachite green based discontinuous liposomal assay

Solutions of G6P, P-PantSH, and the selected phosphorylated PanCOOH analogues were prepared to a final concentration of 5 mM each. Following this, 900 µL of water was placed in 3 × 10 mL beakers. Dialysis membranes were placed in each beaker and allowed to hydrate for 10 minutes. Following this, 200 µL of 1 mM G6P solution was placed in each dialysis unit such that these were replicates. Aliquots of 20 µL dialysate were collected at 1 hour intervals for 5 hours and transferred to a 96-well plate. The experiment was performed twice for each molecule of interest. To determine the diffusion rate, a phosphate cleavage reaction was prepared by adding 4 mM $NiCl_2$, 50 mM Tris-HCl (pH 7.6), 0.1 mM $CaCl_2$, BSA (2 mg/mL) and 5 U ALP to each 20 µL aliquot to a final volume of 100 µL. Each reaction mixture was incubated at 37 °C for 2.5 h to allow cleavage of the phosphorylated compound by ALP.

Following this, the enzyme was heat-inactivated at 65 °C for 15 minutes. The reaction components were then removed by centrifugation at 13 000 g for 5 minutes. The supernatant from each aliquot was transferred to a 96-well plate. To determine the amount of phosphate in each aliquot, 50 µL of a malachite green solution (0.034 (v/v) % malachite green, 3.4 (v/v) % ethanol, 10 mM ammonium molybdate dissolved in 1 M HCl) was added to each well. The plate was allowed to stand at room temperature for 10 minutes for color development. The absorbance for each aliquot was measured at 625 nm and plotted against time to show the diffusion of each molecule of interest over time. The slopes of the resultant plots were then used to calculate the diffusion rate for each molecule of interest.

# 3 Membrane permeability studies of 4'-phospho-pantetheine (P-PantSH) and selected pantothenate analogues

## 3.1 Introduction

Observations from a nutrient complementation study in *Drosophila* S2 cells as well as PAMPA permeability screens suggested that P-PantSH has the ability to enter membranes unaided[158]. In this context, this part of the study seeks to identify the molecular determinants that confer permeability by passive diffusion by attempting to answer the following questions: What are the specific structural components that enable P-PantSH to cross membranes? And, are there specific membrane constituents that enable permeation by passive diffusion? Two approaches were used to attempt to answer these questions. The first investigated the structure-permeability relationship with a view of understanding the importance and relevance of particular aspects of the chemical structure of P-PantSH and its analogues that promote permeability. The second investigated the membrane fluidity-permeability relationship and focused on how differences in membrane composition influence the permeability of these membranes to P-PantSH. Together, these investigations attempted to improve our understanding of the interplay of molecular structure, membrane composition and permeability.

### 3.1.1 Structure-permeability relationship

The structure of P-PantSH has three distinct components that may play a role in the ability of this molecule to translocate membranes. These are a 4'-phosphate group, a pantoyl moiety and a cysteamine moiety (Figure 3-1 **1**). Analogues that differ from P-PantSH in at least one of these moieties were selected for membrane permeability studies. This was done to determine if there was any correlation between a specific structural component and the ability of the molecule to permeate a specific membrane. The membrane impermeability of CoA is always assumed based on the view that charged molecules cannot cross membrane unaided, but is yet to be demonstrated experimentally[108]. For that reason, CoA as well as its immediate biosynthetic precursor, dePCoA, were also included in the study.

### 3.1.2 Membrane fluidity-permeability relationship

There are various techniques that can be used to determine membrane fluidity. These include:

- spectroscopic techniques such as nuclear magnetic resonance (NMR) and Fourier transform infrared spectroscopy (FTIR)[159,160],

- small angle scattering of X-rays and neutrons (SAXS and SANS, respectively) which is based on the deflection of parallel rays of radiation away from a straight trajectory following interaction with structures much larger the wavelength of the radiation[161,162],
- differential scanning calorimetry (DSC) in which the difference in the amount of heat required for increasing the temperature of a sample and reference is measured as a function of temperature, with both the sample and reference maintained at a same temperature approximately throughout the experiment[161].
- membrane binding dyes that are sensitive to the polarity of their environment, such as 6-Propionyl-2-Dimethylaminonaphthalene (Prodan) and its variants[163,164].

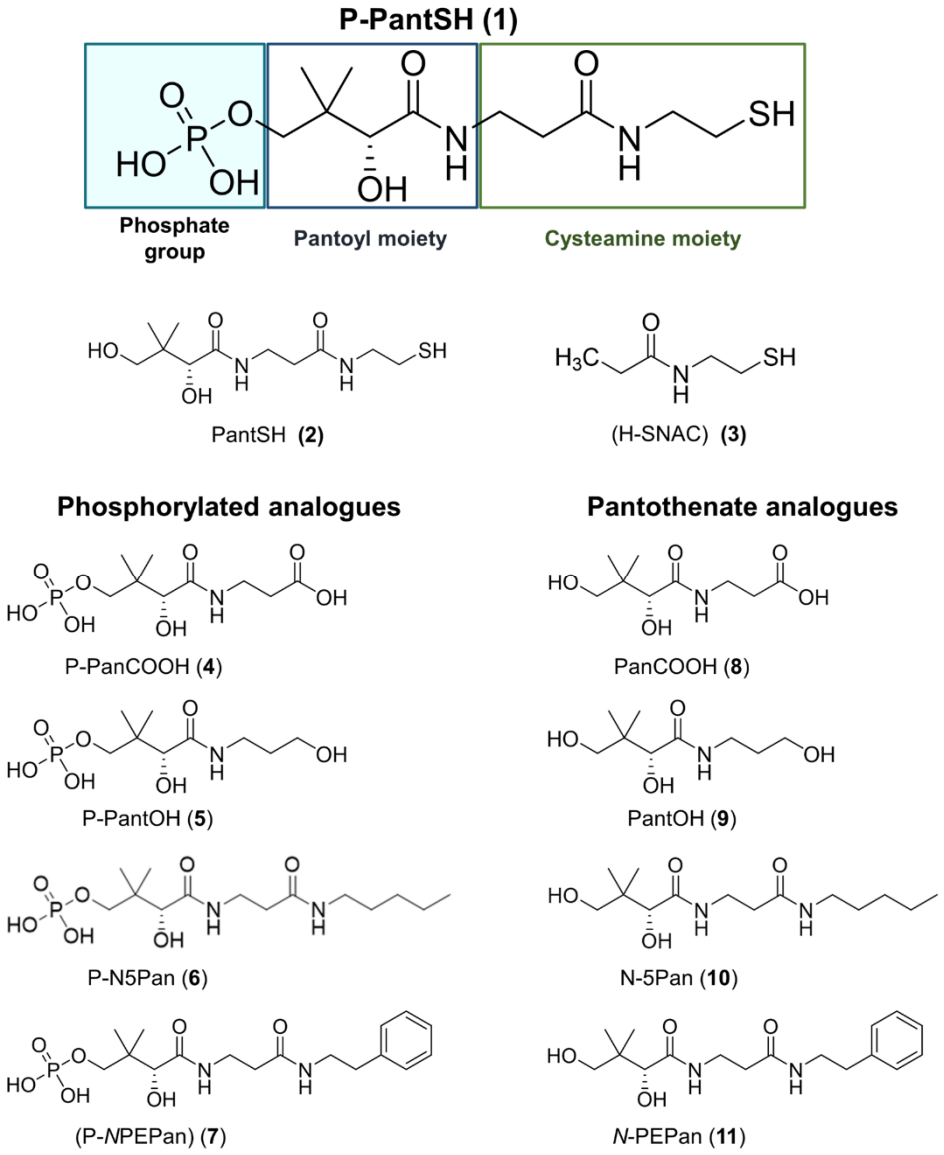


**Figure 3-1: Pantothenate analogues selected to investigate the structure-permeability relationship of P-PantSH.** Compounds **2** and **3** represent non-phosphorylated and cysteamine comparator of **1**. **4** and **5** and pantoyl analogues of **1** and **8** and **9** are their respective non-phosphorylated analogues. **6** and **7** are analogues of **1** that vary in the cysteamine moiety, and **10** and **11** are the respective non-phosphorylated forms thereof.

In this study, membrane fluidity was studied using Prodan based on its availability, ease of use and the ability to easily perform the same analysis on a wide range of different systems. The mechanism of the Prodan-based assay will be explained in more detail in the next section. It was used to investigate the membranes used as models, as well as how the presence of P-PantSH and selected pantothenate analogues impact on membrane fluidity. Solubility-diffusion theory suggests a close relationship between fluidity and membrane permeability by passive diffusion as saturated phospholipids with cylindrical geometry such as phosphatidylcholine tend to produce relatively rigid membranes, while the presence of mono- and poly-unsaturated fatty acyl chains and cholesterol tend to make membrane more fluid. This relationship between phospholipid composition and fluidity in turn implies a relationship between phospholipid composition and permeability.

For this reason, we used a membrane model that mimics the membrane composition of a eukaryotic membrane. We also included a model membrane that mimics the composition of a bacterial membrane since bacterial membranes have distinct phospholipid compositions and therefore are most likely to have membranes with different fluidity from those of eukaryotic membranes. Bacterial membranes also tend to be negatively charged at physiological pH because of the presence of lipid constituents such as cardiolipin (CL). Therefore, comparing P-PantSH permeability across the two types of membrane models may aid in identifying specific molecule-phospholipid interactions that may be of importance. These interactions may in turn be useful for devising strategies to improve permeability of potential drug molecules such as the PanAms that have potential for antimicrobial drug development.

## 3.2 Results

### 3.2.1 Strategy used to perform membrane permeability measurements

The objective of this part of the study was to measure the membrane permeability of P-PantSH, selected pantothenate analogues, dePCoA and CoA across eukaryotic and bacterial membrane models. The eukaryotic membrane is typically asymmetric with sphingomyelin and phosphatidylcholine as the major constituents of the outer leaflet, and phosphatidylserine and phosphatidylethanolamine abundantly observed in the inner leaflet[25]. Furthermore, the presence of sterol lipids in eukaryotic membranes is another factor that distinguishes these membranes from bacterial ones. Cholesterol (Chol) is the typical sterol lipid found in mammalian cell membranes[25,160]. However, the typical distribution of this molecule in the membrane is poorly understood. Nonetheless, these illustrate the complexity of the mammalian cell membrane composition.

In this study we asked fundamental questions regarding the membrane permeability of P-PantSH, and we wanted a simple yet biologically relevant model to help us understand the

manner in which this process occurs. Within this context we selected phosphatidylcholine and cholesterol as a simplified form of the outer leaflet of the eukaryotic cell membrane. The major fatty acyl chains of the phospholipids of eukaryotic membranes are palmitic acid (16:0) and oleic acid (18:1) and therefore 1-palmitoyl-2-oleoyl-*sn*-glycero-3-phosphophatidylcholine (POPC) was selected as the phospholipid component of the membrane, such that the composition of the eukaryotic membrane model was POPC-Chol[25,28].

The phospholipid composition of the bacterial comparator represented the cytoplasmic membrane of *E. coli*. The main component of this membrane model is phosphatidyl-ethanolamine, which is a zwitterion like phosphatidylcholine but carries a slight negative charge at physiological pH[165]. The behaviour of this phospholipid is largely influenced by neighbouring lipids, and homogenous compositions thereof are non-bilayer forming. In the model used in the study the second major constituent of the bacterial membrane model was phosphatidylglycerol which also has a negative charge, and similar conical geometry to phosphatidylethanolamine[166]. The other constituent is CL which is derived from phosphatidylglycerol and may also carry a negative charge at physiological pH[167]. The properties of these lipids in turn give rise to a negative charge on the surface of the bacterial membrane model used in this study.

For the sake of simplicity and ease of comparison, the same fatty acyl chain composition was used for the phospholipids of the bacterial membrane model such that the head groups were the main distinguishing factor between the membranes, apart from the addition of cholesterol in the case of the eukaryotic membrane.Therefore, liposomes made up of POPC-Chol were used as the *in vitro* eukaryotic membrane model, and those made up of 1-palmitoyl-2-oleoyl-*sn*-glycero-3-phosphoethanolamine (POPE),1-palmitoyl-2-oleoyl-*sn*-glycero-phosphoglycerol (POPG) and cardiolipin (i.e. POPE-POPG-CL) were used as the *E. coli* (Gram-negative bacterial) membrane model. The diffusion rates of the molecules of interest were determined by using the discontinuous assays described in chapter 2. Specifically, liposomes loaded with a molecule of interest were prepared and the liposomal diffusion measured for liposomes of both membrane models by taking aliquots at set time points and determining the concentration of the molecule of interest present in the aliquot (Figure 3-2). These measurements were all performed in triplicate. The process was repeated twice for each molecule of interest.

The molecules of interest were divided into thiolated, phosphorylated and non-phosphorylated compounds, and the diffusion rates were in each case determined using the detection method most appropriate to each group. The following assays were performed in each case:

A. For thiolated molecules, the assay used was based on the reaction of CPM, which forms fluorescent adducts with thiol molecules.

B. For phosphorylated compounds, alkaline phosphatase (ALP) was used since the amount of inorganic phosphate produced from cleavage of the phosphates can be determined spectrophotometrically by a malachite green dye.
C. Non-phosphorylated analogues of pantothenate are substrates for PanK-mediated phosphorylation, which can be monitored by a coupled enzyme assay in which NADH consumption is measured spectrophotometrically.

In all cases, the concentrations of the molecule of interest at each time point was used to determine the rate of diffusion from the liposome. This rate was compared to the rate of “free” diffusion, i.e. the rate of diffusion of the molecule of interest from a liposome-free solution across the dialysis membrane. Since both the free diffusion and liposome-loaded diffusion rates were determined twice, the ratios of the lowest and highest values obtained in each case provides upper and lower limits of the relative liposomal diffusion. For reporting purposes, all results in this section will report the average of these two limiting values, with the limits being used to indicate the range of the results (Figure 3-2).

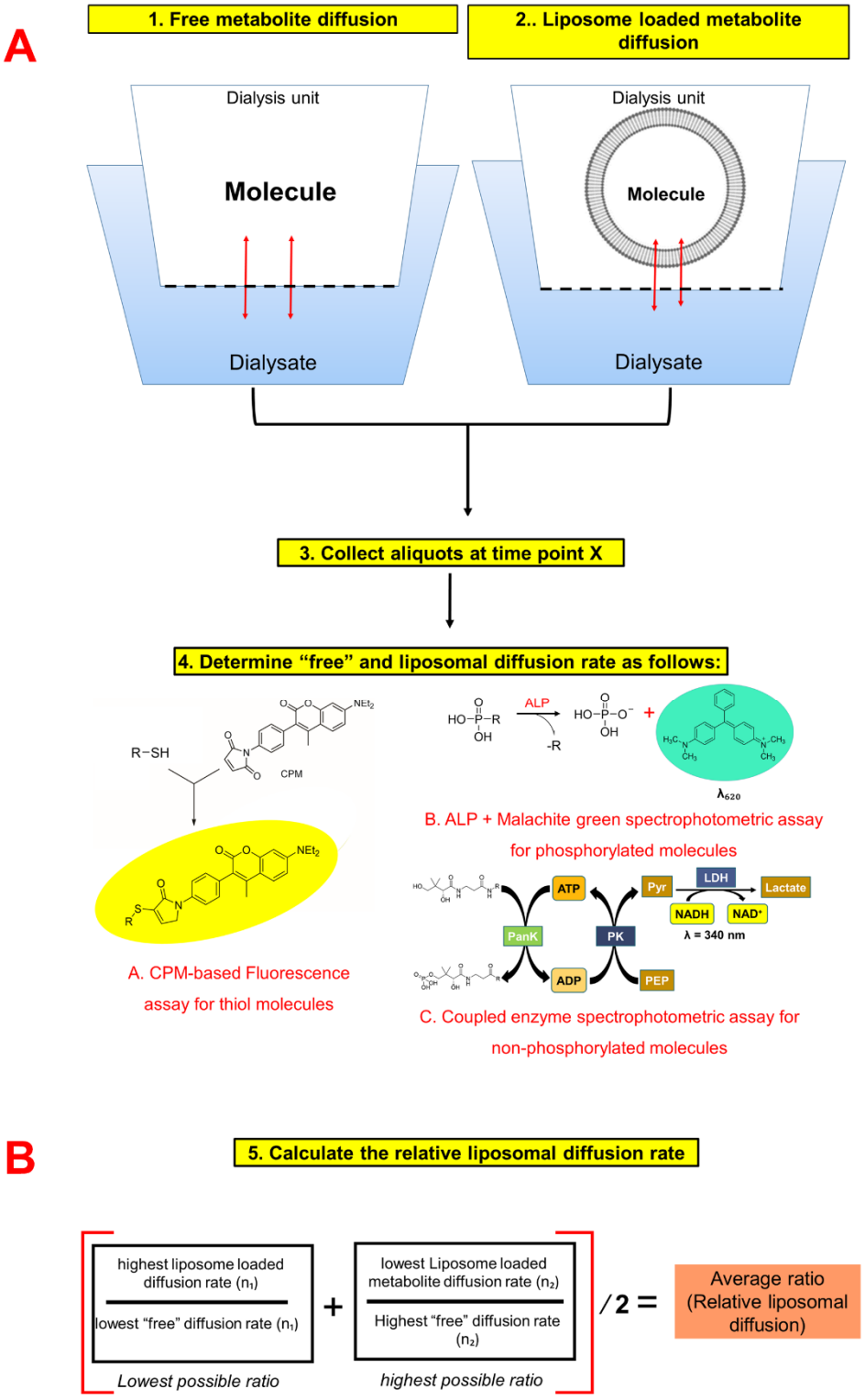


**Figure 3-2: Strategy used to investigate membrane permeability of P-PantSH and selected pantothenate analogues. A:**the free (1) and liposome (2) loaded diffusion across the dialysis membrane was measured by collecting aliquots of the dialysate at different time points (3), based on the identity of the molecule of interest, one of the three detection methods (A-C) was then for the detection of the molecule of interest in each aliquots(4). **B :** the relative liposomal diffusion rate was determined by calculating the lowest and highest possible ratios of the free and liposomal diffusion rates, the average ratio was then calculated from this, such that the relative liposomal diffusion was and an average of range of possible ratios (5).

### 3.2.2 Confirmation of the liposomal encapsulation efficiency

The membrane permeability assay was set up in such a manner that the liposomal diffusion rate had to be reported relative to the free metabolite diffusion rate to factor in the variation brought about by the dialysis membrane. The liposomal encapsulation efficiency was determined to ensure that the concentration of "free" molecule solution as well that of the liposome encapsulated solution were comparable. PantSH is used to illustrate how this was done. First, a standard curve of PantSH was constructed by preparing series of PantSH solutions varying in concentration from 7 to 1000 mM and then measuring the fluorescence intensity of each of these solutions (Figure 3-3). A linear curve fit was performed on the data points using SigmaPlot® 14.0 software and the equation of the line was then used to determine the concentration of PantSH in a given liposomal preparation.

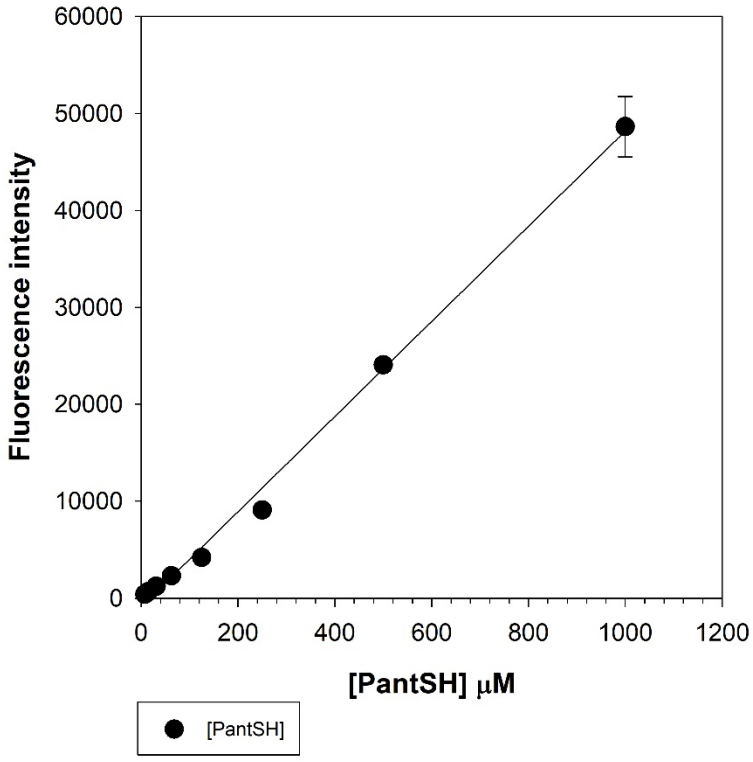


**Figure 3-3: Standard curve of [PantSH] as a function of CPM fluorescence intensity.** Each data point represents the average of three replicates and the error bars indicated the standard deviations (n = 3 ± standard deviations). Linear curve fit gave the equation y= -898.179 + 49.087x ($R^2$ = 0.992).

PantSH-loaded liposomes were prepared as described in Chapter 2. A fresh solution of 1 mM PantSH was also prepared. Equal volumes of the two preparations were transferred to a black 96 well plate, 10 μM CPM was added to each and the fluorescence intensity was measured. Water was used as a reference since all the solutions (as well as the liposomal suspensions) were prepared in water. Comparison of the fluorescence signal of the "free" PantSH and the liposome encapsulated PantSH to the reference solution show that both preparations emit

strong fluorescence signals (Figure 3-4). However, the fluorescence emission of the 1 mM PantSH solution is significantly higher than that of liposome-encapsulated PantSH solution.

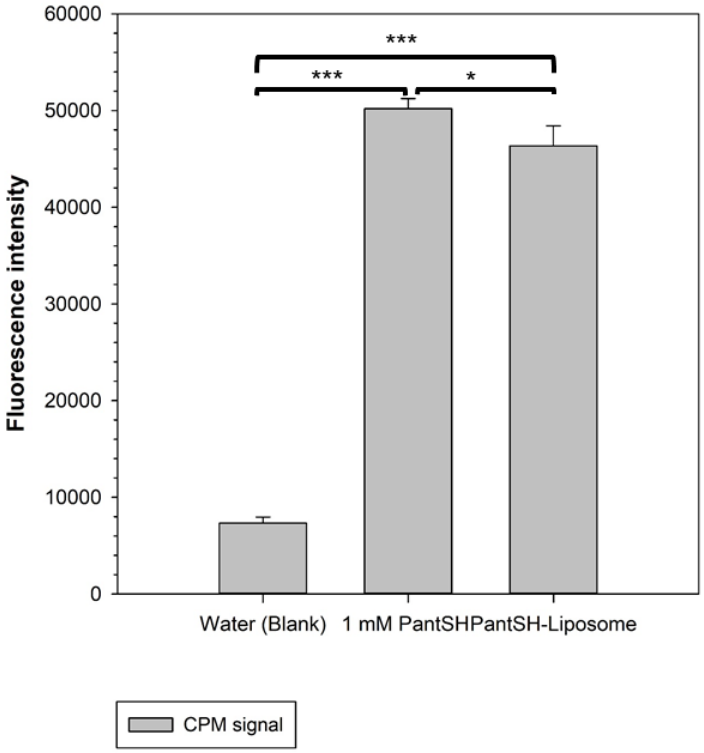


**Figure 3-4: Fluorescence signal of "free" PantSH, as well as liposome-encapsulated PantSH solution.** Water was used as a reference for measuring fluorescence intensity of CPM-PantSH adducts. Each data point represents an average of three technical repeats and the errors represent the standard deviations (i.e.: n = 3 ± standard deviations). Student's t-test (paired distribution, * $p < 0.05$, *** $p < 0.001$).

We proceeded to calculate the PantSH concentration in liposomes using the standard curve shown in Figure 3-3. The calculated concentration estimates the PantSH concentration in the liposomes to be 962.335 ± 60.7 µM (equation 1b). When considering the error this falls within a range close to 1 mM, which is the original concentration used to prepare the liposomes. The PantSH concentration of the 1 mM used to perform the "free" diffusion measurements was recalculated from the standard curve as a quality control measure. The calculation shows that the concentration is slight overestimated which in turn suggests that the accuracy of the standard curve could be improved (equation 2b). Unfortunately, despite several attempts, the standard curve could not be reconstructed to levels of accuracy beyond the one in Figure 3-3 Therefore, we proceeded to calculate the encapsulation efficiency with PantSH concentrations of "free" PantSH and liposome-encapsulated PantSH determined from the standard curve. The encapsulation efficiency was calculated to be 92.43% for PantSH.

#### 3.1.1.1 Liposomal encapsulation efficiency

*Linear curve fit = (y= -898.179 + 49.087x)* … From the standard curve (Figure 3-3)

And,

PantSH-Liposome signal = 46340 ± 2082.411 Fluorescence units……1(a)

Therefore,

[PantSH] in the liposome = (46340 + 898.179)/ 49.087 = 962.335 ± 60.7 µM……..1(b)

And,

1 mM PantSH signal = 50206.33 ± 1037.791 Fluorescence units……...2(a)

"Free" [PantSH] = (50206.33 + 898. 179)/ 49.087 = 1 041.10 ± 39.51 µM……2(b)

**The encapsulation efficiency = (962. 335/ 1041.10) × 100 = 92.43 % ……3**

The encapsulation efficiency was also calculated for the thiol molecules used in the study and found to be above 90% in all cases (results not shown). Since the difference between the encapsulated and "free" molecule solution was consistently below 10 % for the liposomal preparations tested, and the molecule loaded liposomes produced a fluorescence signal with comparable strength to the "free" molecule solution, the difference was considered small enough not to influence the data analysis. We concluded to proceed with the data processing described in Figure 3-2 for reporting the potential membrane permeability of the molecule of interest.

### 3.2.3 P-PantSH permeates the eukaryotic model membrane but not the bacterial membrane model

The membrane permeability measurements of P-PantSH, its non-phosphorylated counterpart PantSH (Figure 3-1, **2**), the representative of its cysteamine moiety H-SNAC (Figure 3-1, **3**), as well as dePCoA and CoA were performed to determine the structure-permeability relationship that may exist for these molecules. Glutathione (GSH) is also a low molecular weight thiol, and protein transporters dedicated to its membrane translocation have been identified[168]. Therefore, this molecule is less likely to permeate cells by passive diffusion and for this reason it was used as a reference in the permeability measurements. The relative liposomal diffusion of GSH was set as a "permeability threshold" (indicated by the dotted lines, Figure 3-5) for both the eukaryotic and bacterial model membranes. Therefore, all molecules for which the liposomal diffusion was above this value was considered to have a membrane permeability exceeding that of GSH (i.e. they are relatively membrane permeable), and those below this value were considered to have a permeability below that of GSH (i.e. they are relatively membrane impermeable).

The “free” and liposomal diffusion rates were determined using the CPM-based fluorescence assay according to the strategy described in Figure 3-2. The results show that PantSH and H-SNAC have the highest free diffusion rates and dePCoA and CoA have the lowest (Figure 3-5 A and B). The molecular weight of CoA and dePCoA is almost six times that of H-SNAC, and these molecules also have an adenylyl group which gives them a “bulky” molecular geometry. Therefore, the observed diffusion rates are consistent with the principle that smaller molecules diffuse over distances relatively faster than larger molecules.

The liposomal diffusion rates were measurably higher in POPC-Chol liposome than in the POPE-POPG-CL liposomes, which suggests that the eukaryotic model membrane is generally more permeable towards these molecules than the bacterial model. Nonetheless, comparison of the relative liposomal diffusion of the molecules to the permeability threshold show that P-PantSH can likely permeate the eukaryotic model but not the bacterial membrane model, and that no other molecule can permeate either membrane model by passive diffusion. However, due to low free diffusion rates, dePCoA and CoA have much larger signal-to-noise- ratio. Therefore, more experimental repeats would be beneficial for confirming that the apparent permeability is indeed a true result. Nonetheless, the observed permeability of P-PantSH in the eukaryotic model is consistent with previous findings and validates our membrane model as a good representation of such biological membranes *in vitro*[115].

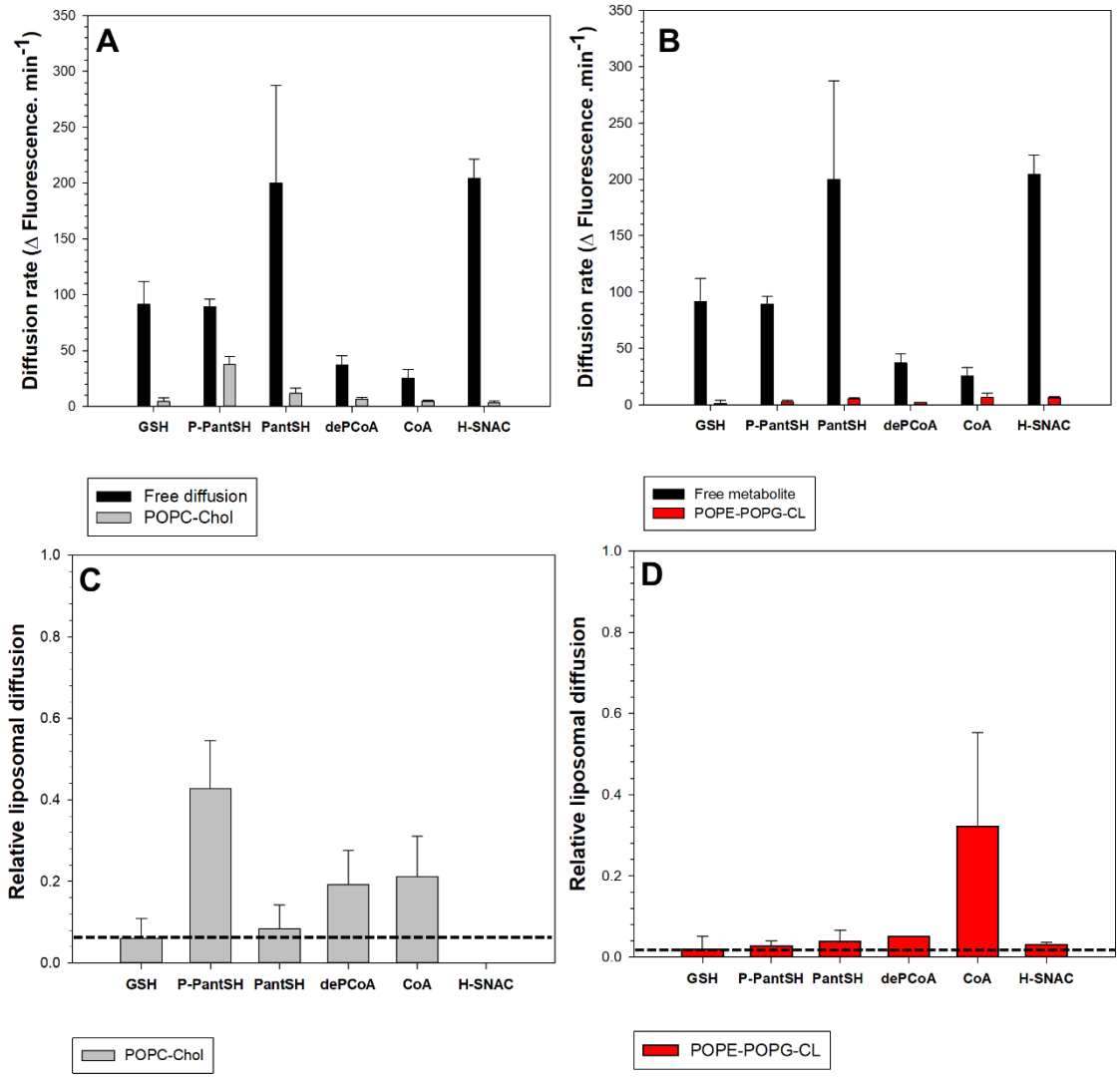


**Figure 3-5: Membrane permeability profiles of P-PantSH, CoA and other thiol intermediates.** "Free" and liposome-loaded diffusion rates (panels A and B) was used to determine the relative permeability (relative liposomal diffusion) of the thiol-containing molecules (panels C and D). This was done for both the eukaryotic (panels A and C) and bacterial (panels B and D) membrane models. GSH was used as a reference and its relative liposomal diffusion was set as a permeability threshold indicated by a dotted line. For panels A and B, bar height indicates the average value from two experiments, with the error indicating the range/2. For panels C and D, bar height indicates the average value from the lowest and highest possible ratios, with the error indicating the upper limit.

We next proceeded to investigate the membrane permeability of analogues of P-PantSH in which the cysteamine moiety was either completely absent (Figure 3-1, **4** & **5**), or modified in such a manner that the terminal thiol was replaced with an alkyl or phenyl group (Figure 3-1, **6** & **7**). These compounds were studied to determine if the cysteamine moiety (and its thiol group in particular) contributes to the permeability of P-PantSH. For these compounds the ALP-Malachite green assay described in section 3.2.1 was used to determine the "free" and liposomal diffusion rates across both membrane models. Glucose-6-phosphate (G6P) was used as a reference because like GSH, protein transporters for its membrane translocation

have been identified and was therefore expected that is would not efficiently cross biological membranes by passive diffusion[156].

The results show that the outcome of the ALP-based assay is dependent on several factors, and therefore likely suffers from low reproducibility. Specifically, P-PantSH and P-PantOH were found to have the highest “free” diffusion rates in the first set of experiments (performed to study the permeability of the eukaryotic membrane model), but interestingly G6P had the highest “free” diffusion in the second set of experiments (for the study of the permeability of the bacterial membrane model) (Figure 3-6 A & B, respectively). Comparing the actual values obtained for the “free” diffusion rate of G6P, it was found to be ~6-fold higher in the second experiment. This large difference is likely because two different batches of ALP were used in each case. Since the amount of inorganic phosphate produced from cleaving a phosphorylated compound with ALP is used to determine the diffusion rate of the molecules of interest, the big difference suggests that variations in ALP activity may affect the observed diffusion rate.

Although we did not see the same large variations in the “free” diffusion rates of the other compounds tested, the variation in the results obtained for G6P raises concerns about the validity of the data obtained for the other compounds. This can further be illustrated by the comparison of the obtained for P-PantSH, which indicate that this molecule cannot permeate POPC-Chol by passive diffusion when using the ALP assay (Figure 3-6 C), while the CPM assay used to obtain the data shown in Figure 3-5 indicated that it can. Overall, the data obtained with the ALP assay—although it seems to indicate that several of the phosphorylated pantothenate analogues can cross the membranes unaided—should be interpreted with caution. It would be ideal to repeat these experiments using a standard ALP substrate such as *p*-nitrophenyl phosphate (pNPP) (Section 2.2.9.2) for comparison, and to confirm the activity of the enzyme.

We next proceeded to investigate the membrane permeability of non-phosphorylated pantothenate analogues to find out if any structure-permeability relationships could be deduced with these molecules (Figure 3-7). The molecules tested were similar to those tested in the previous experiment, except that they the phosphate group (Figure 3-1, **8**-**11**). PanCOOH was used as a reference, because like the previous reference molecules, it has dedicated membrane transporters and is therefore not expected to efficiently cross biological membranes by passive diffusion[66,68,152]. For these assays, the PanK enzyme reaction was used to establish the concentration of the compounds of interest as they moved across the dialysis membrane.

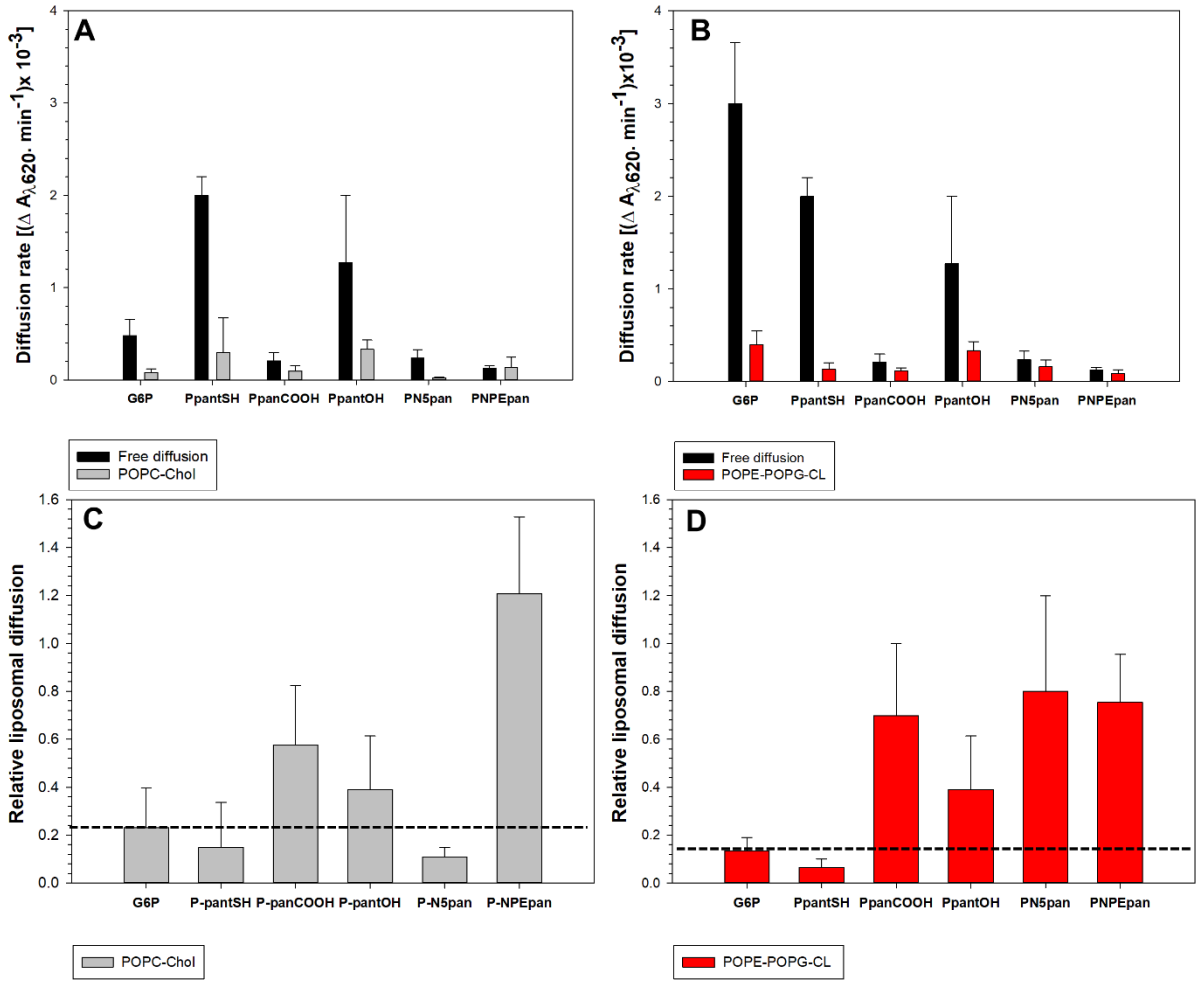


**Figure 3-6: Membrane permeability measurements of phosphorylated pantothenate analogues, including P-PantSH.** "Free" and liposome-loaded diffusion rates (panels A and B) was used to determine the relative permeability (relative liposomal diffusion) of the phosphorylated molecules (panels C and D). This was done for both the eukaryotic (panels A and C) and bacterial (panels B and D) membrane models. G6P was used as a reference and its relative liposomal diffusion was set as a permeability threshold indicated by a dotted line. For panels A and B, bar height indicates the average value from two experiments, with the error indicating the range/2. For panels C and D, bar height indicates the average value from the lowest and highest possible ratios, with the error indicating the upper limit.

Comparison of the free diffusion rate of the pantothenate analogues show that these molecules have similar diffusion rates which is to be expected since they have similar structure and molecular size (Figure 3-7 A & B). In contrast to the thiol-containing molecules, the liposomal diffusion measurements suggest higher permeability of these compounds of the POPE-POPG-CL (bacterial model) membrane than the POPC-Chol (eukaryotic model) membrane. The results seemed to indicate that PantSH and PantOH permeate across the prokaryotic membrane model, and also to some extent the eukaryotic membrane model (Figure 3-7 C and D). However, that data obtained with PantSH again contradicts that obtained with CPM in the first experiment (Figure 3-5), which indicated that PantSH does not permeate

either membrane. This result raised question also about the reproducibility of this assay, and the need to include controls and references to ensure that the activity of the PanK used in the assay remains constant.

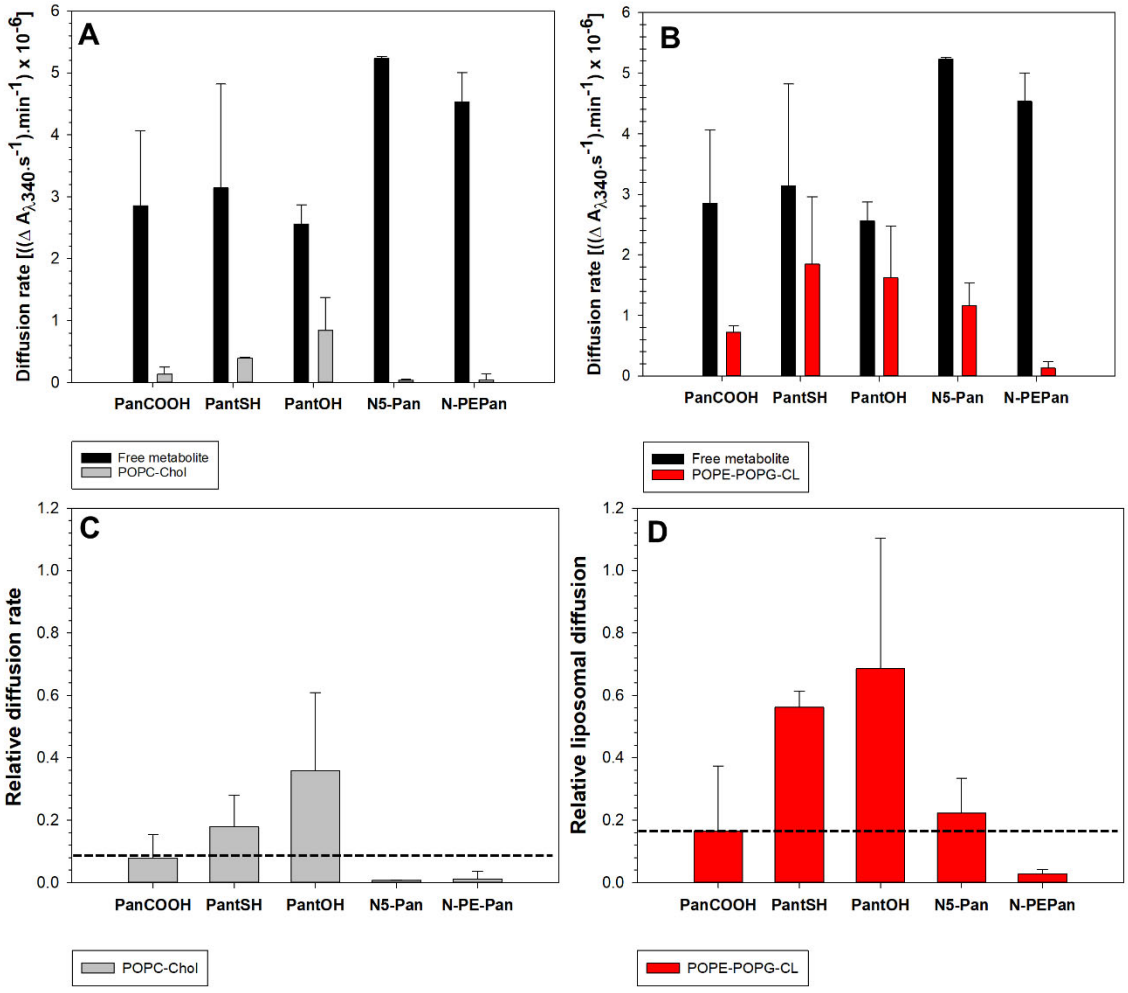


**Figure 3-7: Membrane permeability measurements of non-phosphorylated pantothenate analogues.** "Free" and liposome-loaded diffusion rates (panels A and B) was used to determine the relative permeability (relative liposomal diffusion) of the non-phosphorylated molecules (panels C and D). This was done for both the eukaryotic (panels A and C) and bacterial (panels B and D) membrane models. PanCOOH was used as a reference and its relative liposomal diffusion was set as a permeability threshold indicated by a dotted line. For panels A and B, bar height indicates the average value from two experiments, with the error indicating the range/2. For panels C and D, bar height indicates the average value from the lowest and highest possible ratios, with the error indicating the upper limit.

Taken together, these results obtained with the CPM assay show that P-PantSH can permeate eukaryotic but not bacterial membrane models by passive diffusion. The observed membrane impermeability of PantSH and H-SNAC in turn suggests that the phosphorylated pantoyl moiety is important for membrane translocation of P-PantSH. However, the indirect determination of the diffusion rates by using the ALP-Malachite green assay as well as the PanK-coupled enzyme assay produced data that was not reproducible in comparison to those

obtained with the CPM-based assay, making it difficult to obtain meaningful insight regarding structure-permeability relationships.

In spite of this rather disappointing outcome, the data—when taken together—does seem to indicate that the permeability of a molecule of interest seem to be more dependent on the composition of the membrane, than on its own structure. This conclusion is made based on the large differences in the results obtained for the two membrane models, even when all other variables are expected to be similar between the two systems. Based on this outcome, we decided to investigate the impact that P-PantSH and PantOH has on membrane fluidity under various conditions.

### 3.2.4 Membrane interaction studies

The next objective of the study was to find out whether or not the pantothenate analogues interacted with the membrane, and if there was any correlation between the membrane fluidity and such an interaction. For these studies PantOH was used because the findings from the membrane permeability studies suggested that this molecule most likely permeates both the eukaryotic and bacterial membrane models. In addition, the impact of P-PantSH on a membrane was also investigated, but only in the context of the eukaryotic membrane model, as this was the only system that showed some permeability to this molecule.

An indicator of the interaction of either of these compounds with the membrane would be changes in membrane fluidity in the presence of the analogue. Liposomes were therefore prepared as was done in the previous experiment, except that reference liposomes were also prepared with only water loaded in the intraliposomal cavity. The fluidity was analyzed for liposomes suspended in water, as well as in a buffered environment. The buffered environment was introduced to investigate the effect of the pH on membrane fluidity, specifically as charged lipids like phosphatidylglycerol and cardiolipin are pH-sensitive and may therefore cause changes in fluidity as a response to changes in pH of their immediate environment. Therefore, two different solutions of 10 mM Tris-HCl were prepared at pH 7 and pH 8 to represent neutral and alkaline conditions respectively, and a solution of 10 mM MES-HCl at pH 6 was prepared to represent an acidic environment. The selection of 10 mM ionic strength of the buffers falls within the range generally used for liposomal studies involving investigation of fluidity[159,163].

Artificial membranes like those represented by liposomes can assume three general phases based on the phospholipid composition thereof. These phases can in turn be used to describe membrane fluidity[26]. Membranes made exclusively of saturated phospholipids, especially those of cylindrical geometry like phosphatidylcholine, tend to be “gel-like” and these membranes are described as ordered or rigid. Introducing cholesterol to such membranes has

a fluidizing effect, however since cholesterol binds in an asymmetric manner, the membrane becomes unevenly thick in certain regions and is therefore described as liquid-crystalline or liquid-ordered membrane. Unsaturated fatty acyl chains, especially in phospholipids with conical geometry produces membranes of much higher fluidity than the two described above. Such lipids have low transition temperatures ($T_m$), and produce membranes described as liquid-liquid or liquid-disordered.

Membrane fluidity was analyzed using Prodan – a membrane binding fluorophore that produces has an excitation maximum ($\lambda_{em}$) of 515 nm in water[162]. Prodan is loosely anchored to the bilayer and locates closer to the aqueous phase of the bilayer (Figure 3-8). This molecule experiences dipolar relaxation in a lipidic environment as a result of water molecules located at the level of the glycerol backbone where the fluorophore binds[163,164]. The dipolar relaxation results in a spectral shift which provides useful information about the membrane phase state, which in turn describes fluidity.

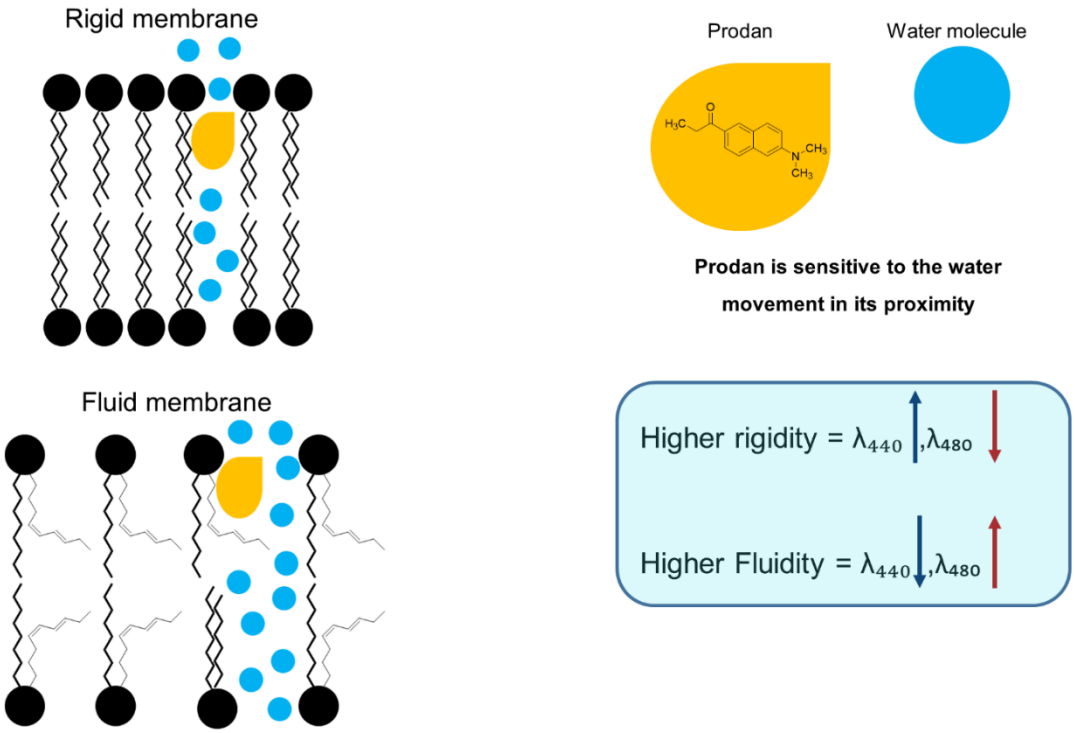


**Figure 3-8: Principle of Prodan-based membrane fluidity determination.** Rigid membranes have less, and more fluid membrane have relatively more, water molecules moving at the aqueous interface and area surrounding the glycerol backbone. Prodan is sensitive to this water movement and its emission spectrum can provide information about the membrane based on this property. A prodan emission peak at 440 nm is characteristic of a "gel-like" ordered membrane phase, and an emission peak at 480 nm is characteristic of a liquid-disordered membrane phase.

Generalized polarization (GP) is a method developed to quantitatively analyze the difference in Prodan emission spectra[169]. It is sensitive to the properties of the membrane and may allow

determination and quantification of these membrane phase states and in so doing describe the degree of fluidity of the membrane.

GP can be defined as follows:

$$\mathbf{GP = I_B – I_R / I_B + I_R} \qquad \text{.....1}$$

Where, $I_B$ = Fluorescence intensity at $\lambda_{440}$ and $I_R$ = Fluorescence intensity at $\lambda_{480}$.

The GP values are restricted between 1 and -1. The higher the membrane associated water movement, the closer the value is to -1, and the lower the water movement the closer the value is to 1. A “gel-like” membrane is indicated by ordered phase, it has restricted water movement and the GP value in that case would be closer to 1. On the other hand, liquid-ordered (liquid-crystalline) as well as liquid-disordered (liquid-liquid) phases have higher membrane associated water movement and would therefore result in GP values close to -1.

#### *3.2.4.1* Both P-PantSH and PantOH interact with the eukaryotic membrane model

Prodan emission spectra were recorded for control liposomes (containing no compound), as well as for POPC-Chol liposomes loaded with either P-PantSH or PantOH. The Prodan emission spectra were recorded in a non-buffered environment, as well as at pH 6, 7 and 8 respectively. All four sets of spectra have a distinct emission peak at 440 nm which suggests the presence of relatively ordered particles for all liposomes tested. This is supported by the negative control sample, which contains no liposomes but only Prodan and water, where no peak at 440 nm is observed (spectrum not shown). Since the emission at 480 nm also gives valuable information about membrane fluidity, the slopes of the change in emission from 440 nm to 480 nm were evaluated to determine the influence that the presence of P-PantSH or PantOH has on membrane fluidity. The results indicate that change is larger in P-PantSH loaded liposomes (Figure 3-9 A) compared to that of the control liposomes and PantOH-loaded liposomes in water. This is indicative of a membrane “ordering” effect by the molecule.

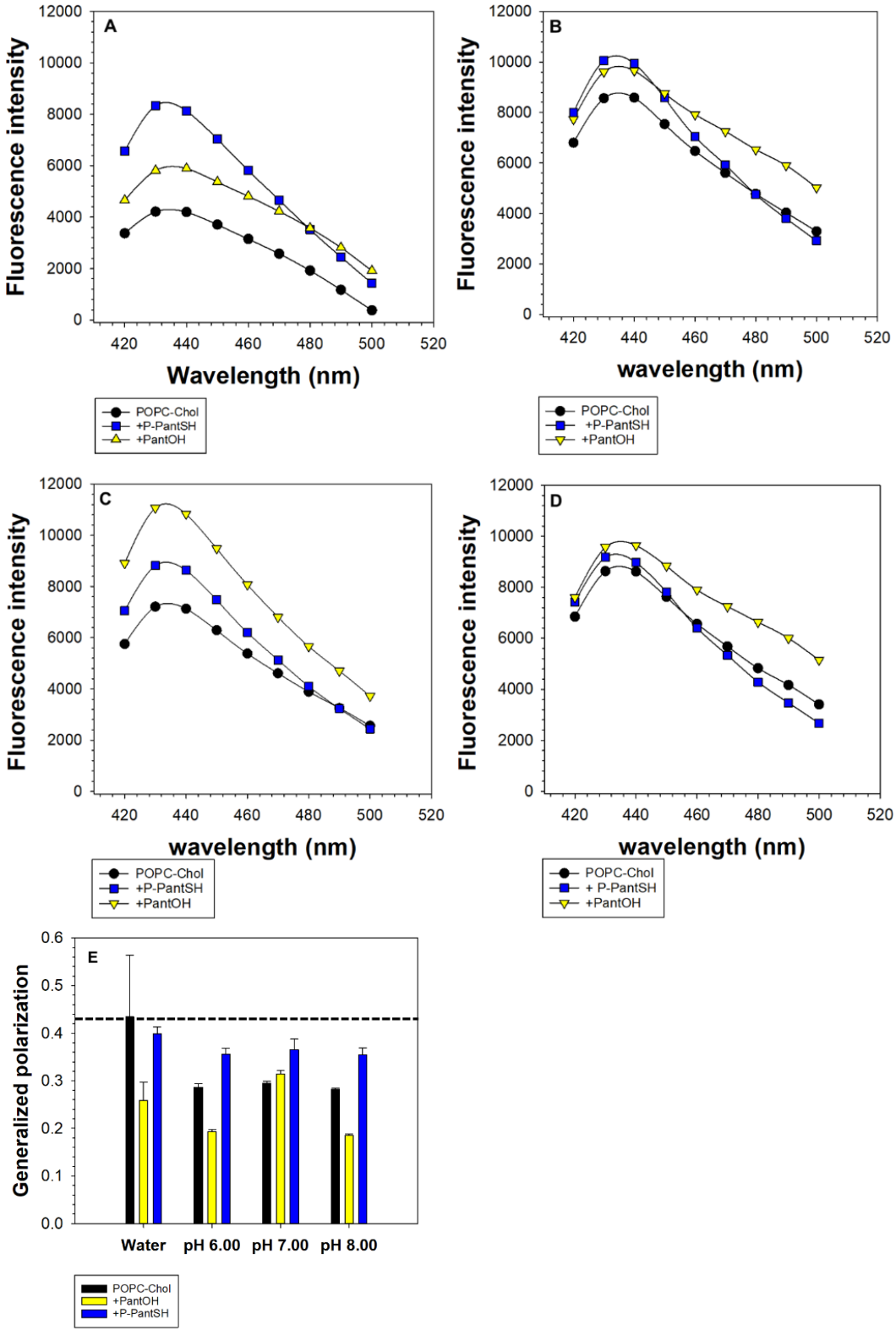


**Figure 3-9: Membrane fluidity of POPC-Chol in the presence of P-PantSH and PantOH.** Prodan emission spectra of control liposome, P-PantSH-, and PantOH-loaded liposomes were recorded in water (A), pH 6 (B), pH 7 (C) and pH 8 (D), respectively. The GP values were calculated from these spectra and used to evaluate the membrane fluidity for the three liposomal preparations under the different conditions (E).The experiment was performed in triplicate; the bars show the average value and the errors show the standard deviation.

On the other hand, the PantOH-loaded liposome has a higher emission at 480 nm which results in a flat slope relative to control and P-PantOH-loaded liposomes at pH 6 and 8 (Figure 3-9 B & D). This is indicative of a membrane “fluidizing” effect by this molecule. All the liposomal preparation had similar spectra at pH 7 which suggests similar membrane phases for all three at this pH (Figure 3-9 C).

The GP values were calculated and used to compare membrane fluidity for all three liposomal preparations under all four conditions (Figure 3-9 D). The GP of the empty POPC-Chol liposome suspended in water is 0.43 ± 0.13 which is indicative of a liquid-crystalline phase as is expected for a membrane of this phospholipid composition. This GP value drops to ~0.3 under buffered conditions which implies the influence of ionic strength on fluidity of this membrane model. P-PantSH-loaded liposomes have a GP value of ~0.4 under all four conditions. This implies a membrane “ordering” effect by P-PantSH, especially under buffered conditions. However, this effect is not pH-dependent since the GP values are similar for all four conditions. Conversely, PantOH-loaded liposomes of 0.26 ± 0.047 water, and this slightly drops to 0.19 ± 0.005 and 0.18 ± 0.003 at pH 6 and 8, respectively, suggesting “fluidizing” effect by PantOH at these pH levels. This dependence on pH is further highlighted by the membrane “ordering” effect indicated by a slightly higher GP value of 0.31 ± 0.006 at pH 7.

#### *3.2.4.2* PantOH has minimal interaction with the bacterial membrane model

Prodan spectra were also recorded for control liposomes and PantOH-loaded liposomes for the bacterial membrane model. Evaluation of the curves of the spectra obtained in water as well as at pH 6, 7 and 8, show similar slopes which suggest minimal change in fluidity as a result of the presence of PantOH (Figure 3-10 A-C). Evaluation of the GP values show that both the control as well as PantOH-loaded liposomes have GP values of 0.13 and 0.12, respectively (Figure 3-10 D) which is lower than the POPC-Chol liposomes which had an average GP value of 0.4 ± 0.13 (Figure 3-9 D). This suggests a higher degree of fluidity in POPE-POPG-CL than POPC-Chol membranes. This can be attributed to a difference in phospholipid head groups since all the phospholipids have the same fatty acyl chains.

On the other hand, a slightly lower value of 0.12 ± 0.0004 for PantOH-loaded liposomes relative to 0.13 ± 0.001 for control POPE-POPG-CL in water was observed. This is indicative of “fluidizing” effect by PantOH which is consistent with the observation for POPC-Chol fluidity analysis (Figure 3-10 D). Nonetheless, these PantOH-induced effects were small, suggesting that the interaction with the membrane is low or minimal. As result, subsequent fluidity evaluations were performed with the eukaryotic membrane model only.

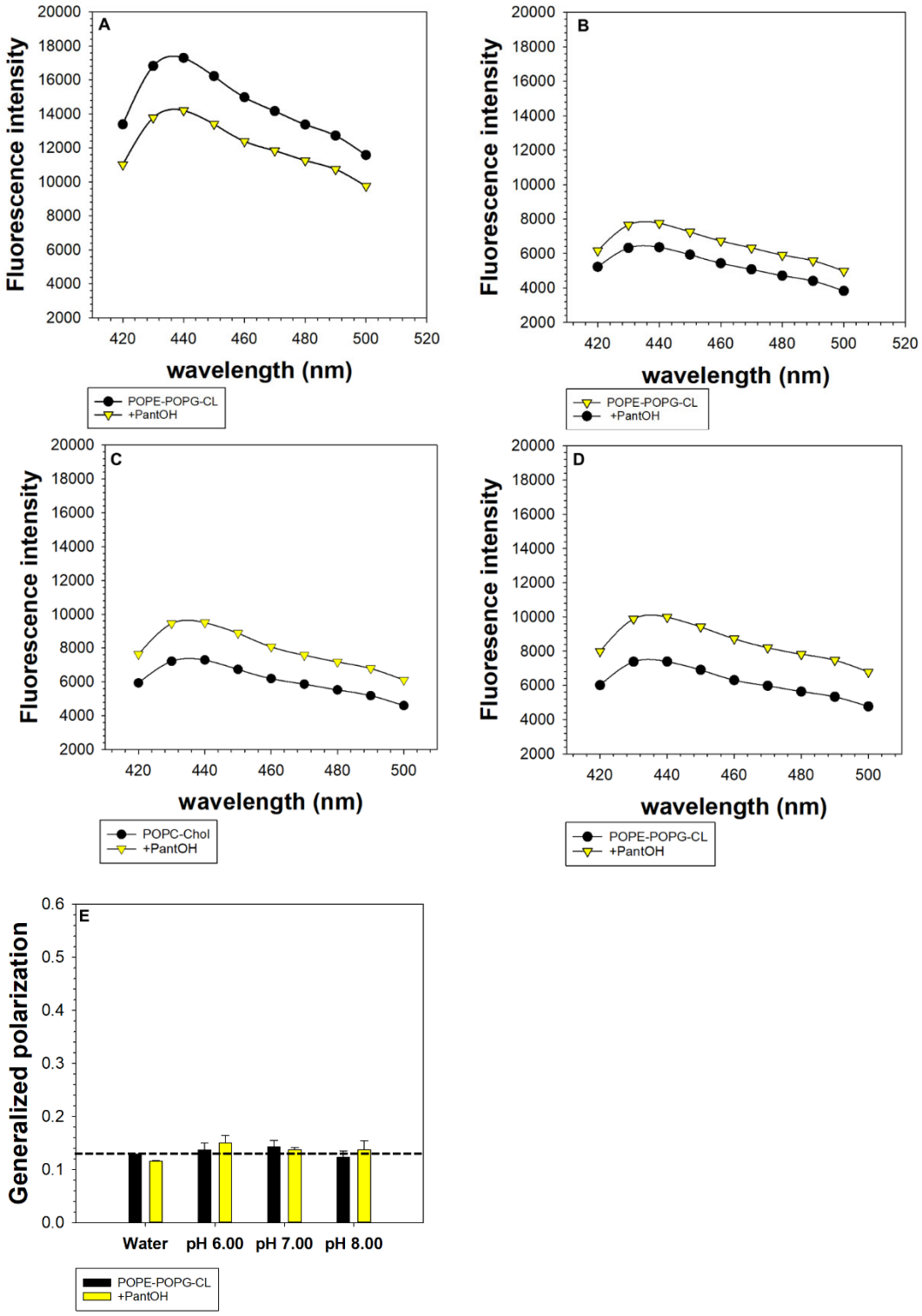


**Figure 3-10: Membrane fluidity of POPE-POPG-CL in the presence of PantOH.** Prodan emission spectra of control as well as PantOH-loaded liposomes were recorded in water (A), pH 6 (B), pH 7 (C) and pH 8 (D), respectively. The GP values were calculated from these spectra and used to evaluate the membrane fluidity for the three liposomal preparations under the different conditions (E). The experiment was performed in triplicate; the bars show the average value and the errors show the standard deviation.

### *3.2.4.3* Ionic strength and composition do not influence interaction of P-PantSH and PantOH with the eukaryotic model membrane

Following the observation that the fluidity of POPC-Chol is influenced by ionic strength, we decided to investigate the influence of ionic composition on membrane fluidity, and whether or not the ions affect the interaction of pantothenate analogues with the membrane. Potassium, sodium and calcium ions ($K^+$, $Na^+$ and $Ca^{2+}$, respectively) are electrochemical gradient components and are important for the membrane translocation of some molecules[170,171]. For this reason, their effects on membrane fluidity were evaluated. Control, P-PantSH- and PantOH-loaded liposomes were prepared as previously described.

Membrane fluidity of the liposomal preparations was determined by the recording prodan spectra in water as well as in the presence of KCl, NaCl and $CaCl_2$ (1 mM of each, Figure 3-11). Though sufficient to perturb membranes, 2 mM $CaCl_2$ was shown to prime liposomal particles start to aggregate at this concentration, and for this reason we elected to use a lower concentration, that would presumably affect fluidity without causing aggregation of liposomal particles[172]. The GP values were calculated from the spectra and the effect of the ions evaluated. The GP value of the control POPC-Chol liposomes was used as a reference (indicated by the dotted line) for comparison. There is a slight increase in GP in the presence of $Ca^{2+}$, suggesting membrane "ordering" effect of this ion compared to control liposomes. P-PantSH also has a membrane "ordering" effect which is consistent with previous findings. However, the presence of ions does not seem to influence this effect. PantOH also has membrane disordering effect which is also consistent with previous findings. Nonetheless, a slight increase in GP value was observed for this liposomal preparation in the presence of the ions. This increase may not be large enough to make any conclusions regarding the effects of ions on interaction of PantOH with the POPC-Chol membrane, however it does justify further investigation of their effect in membrane fluidity permeation by passive diffusion.

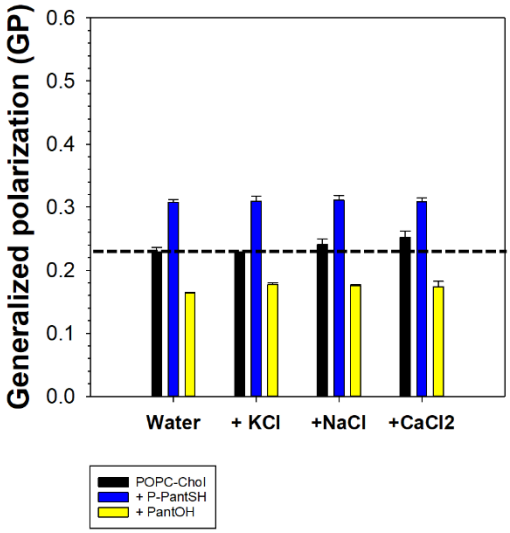


**Figure 3-11: Influence of ionic composition on membrane fluidity of POPC-Chol liposomes.** Membrane fluidity of control, P-PantSH- and PantOH-loaded liposomes was evaluated in the presence of 1 mM of either KCl, NaCl and $CaCl_2$ to evaluate the effect of $K^+$, $Na^+$ and $Ca^{2+}$ on the fluidity. The experiment was performed in triplicate; the bars show the average value and the errors show the standard deviation.

### *3.2.4.4* Membrane fluidity modulates the interaction of pantothenate analogues with the membrane

It is presumed that the effect of P-PantSH and PantOH on membrane fluidity are a result of interaction of these molecules with the membrane. Therefore, we wanted to identify the determinants of this interaction. Was it the chemical identity of the molecule of interest, a specific phospholipid composition, or are the interactions modulated by the fluidity of the membrane? To answer these questions, variations of the eukaryotic membrane models that differed in the degree of fluidity were prepared. Unlike POPC, dipalmitoylphosphatidylcholine (DPPC) has two saturated fatty acyl chains. Consequently, a membrane model of higher rigidity was prepared with DPPC phospholipids. Liposomes made up of POPC and DPPC in a 1:1 ratio were prepared to evaluate membrane fluidity in the absence of cholesterol.

Furthermore, since findings from membrane permeability studies suggest importance of the phosphorylated pantoyl moiety for P-PantSH permeability, we wanted to find out if there was any correlation between this factor and membrane fluidity. We also wanted to determine the reason for differing effects on membrane fluidity upon addition of P-PantSH and PantOH: was the phosphate group or cysteamine moiety responsible for the difference? In order to achieve these objectives, the effects of P-PantSH and PantOH on membrane fluidity were evaluated. In addition, PantSH, P-PantOH, PanCOOH and P-PanCOOH were also included in this experiment as all these compounds contain a pantoyl moiety, and by using the phosphorylated and unphosphorylated counterparts of all the analogues we could investigate the importance of the 4'-phosphate group on fluidity.

Liposomes with no pantothenate analogue loaded in the intraliposomal cavity were prepared as controls (reference membranes) for comparison. Liposomes loaded with one of each of the 6 pantothenate analogues mentioned above was prepared for all three lipid compositions. The liposomes were prepared in 10 mM Tris-HCl, pH 7 since the fluidity was found to be influenced by ionic strength. Prodan spectra were recorded for all preparations and GP values calculated to determine fluidity.

Evaluation of the spectral overlays show relatively flat spectra for POPC-Chol and POPC-DPPC (Figure 3-12 A & B, respectively), and steep slopes as a result of emission at 440 nm for the DPPC membrane. These in turn suggest that DPPC membranes are much more rigid than POPC-Chol and POPC-DPPC membranes. This is further confirmed by GP values of 0.06 ± 0.012 and 0.02 ± 0.01for POPC-Chol and POPC-DPPC control liposomes, respectively, which is lower than GP values of DPPC control liposomes of 0.38 ± 0.012.

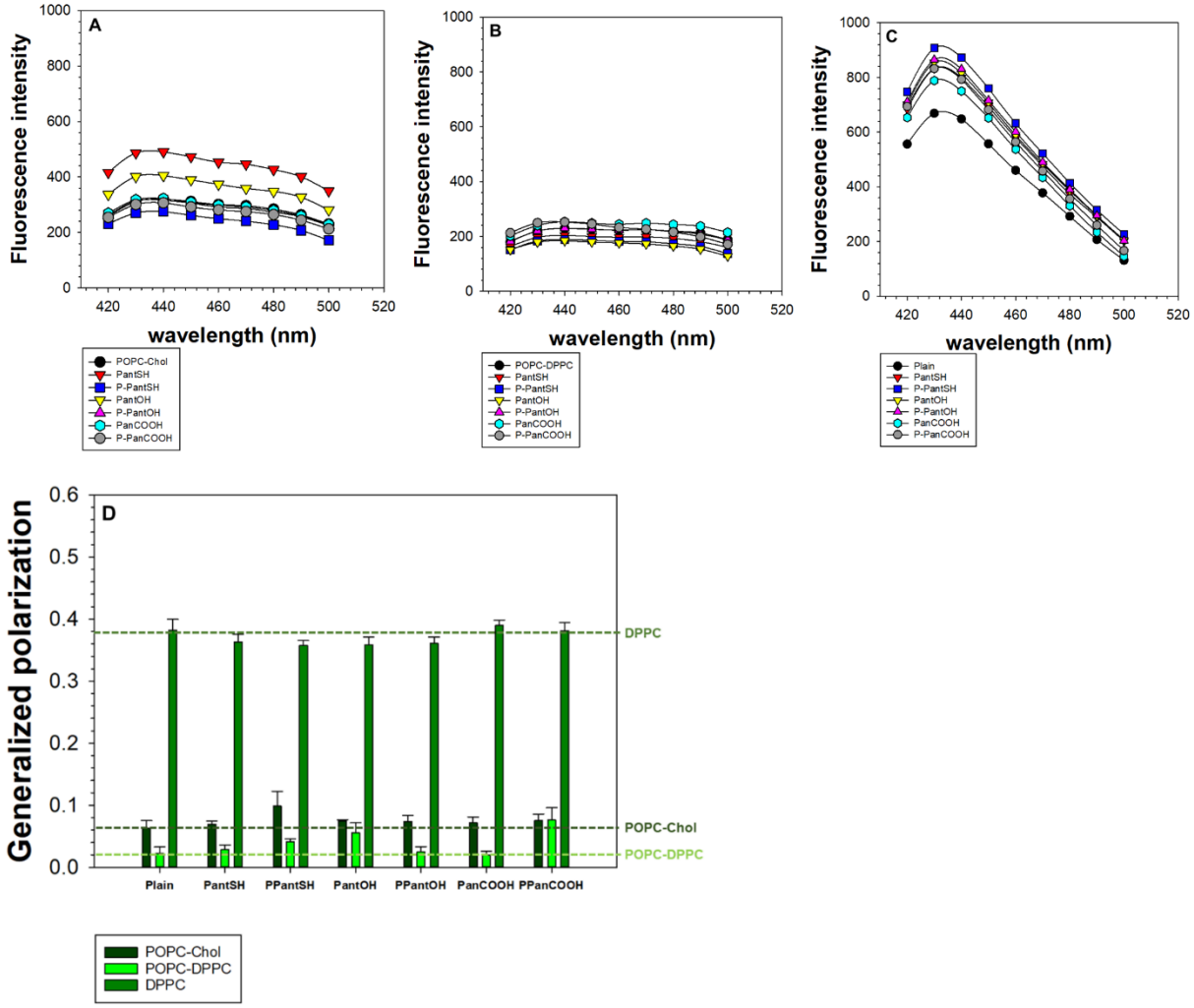


**Figure 3-12: Interaction of pantothenate analogues with the membrane is dependent on the degree of membrane fluidity**. POPC-Chol (A), POPC-DPPC (B) and DPPC (C) represent variations of the eukaryotic membrane model which differ in the degree of fluidity. These were prepared with either P-PantSH, P-PanCOOH and P-PantOH or their non-phosphorylated form loaded in the intraliposomal cavity. The Prodan spectra were then

recorded for all three membrane models and the GP values evaluated (D) to compare the effects of the pantothenate analogues on fluidity.

Evaluation of effect of pantothenate analogues on membrane fluidity suggests a membrane "ordering" effect by P-PantSH, in POPC-Chol and POPC-DPPC membranes. P-PanCOOH also had membrane "ordering" effects in POPC-DPPC membrane. These pantothenate analogue induced changes in membrane fluidity were greater in a membrane model of relatively higher fluidity than the rest. Furthermore, there were marginal effects in the membrane model of lower fluidity. This is in turn suggests a requirement for a certain degree of fluidity for pantothenate analogue interaction.

## 3.3 Discussion

### 3.3.1 Direct molecule quantification improves reproducibility in liposome-based assays

Liposomes were used as an *in vitro* membrane system to perform this study as liposomes are versatile and easy to prepare[54,57,173]. However, these particles are infamous for poor reproducibility and there have been attempts to create alternative membrane models with better reproducibility[136,174]. However, the preparation of these alternatives is cumbersome and are therefore also not very attractive options. As reproducibility is a known challenge, this study went to lengths to optimize the encapsulation efficiency of the liposomes and a reference molecule was also included with all the measurements performed in an effort to circumvent these issues (Chapter 2). We were able to produce meaningful permeability data for low molecular weight thiols associated with CoA using this liposome-based system as a sensitive fluorophore that enables direct measurement of a molecule of interest minimises variability and can improve reproducibility despite the liposomal system. In contrast, the indirect measurement assays used for phosphorylated and non-phosphorylated analogues had poor reproducibility and as a result, no definitive conclusions were made from the data obtained for these molecules.

### 3.3.2 The phosphorylated pantoyl moiety may be important for membrane translocation

Membrane permeability measurements went on to show that P-PantSH permeates the eukaryotic membrane model but not the bacterial model. Charge repulsion between the membrane surface and phosphate group of P-PantSH may play a role in the inability of this molecule to permeate bacterial membranes given that POPG and CL give the liposomal membrane a slightly negative charge since these two lipids both are negatively charged[26,166,167]. Additionally, this is supported by the higher relative liposomal diffusion of PantSH in this membrane model which suggests that the non-phosphorylated form may cross

the bacterial membranes more efficiently but not necessarily fast enough to support growth. On the other hand, the poor permeability demonstrated for PantSH and H-SNAC in the eukaryotic membrane model suggests the importance of the phosphorylated pantoyl moiety in membrane translocation of P-PantSH. Unfortunately, such a structure correlation could not be established with other phosphorylated pantothenate analogues.

### 3.3.3 Membrane fluidity modulates P-PantSH-membrane interactions in the eukaryotic membrane model

We then went on to show that the presence of either P-PantSH or PantOH in the membrane alters the fluidity which suggests interaction of these molecules with the membrane in eukaryotic membrane models. The PantOH interaction is pH dependent as illustrated by the different effects on fluidity at different pH levels. This could be attributed to the dissociation properties of this molecule under different pH conditions. For instance PantOH is known to have hydration effects when applied ectopically[175]. The skin has a pH of ≈ 5.5[176], and we showed a PantOH induced increase in membrane fluidity at pH 6. This phenomenon may therefore be explained as follows: the solubility-diffusion theory describes transient aqueous pockets that exist at the surface of the membrane as well as vicinity of the glycerol backbone. The theory further states that solutes dissolve into these pockets to permeate the membrane. Therefore, the “fluidizing” effect of PantOH suggests that this molecule is able to recruit more of the aqueous pockets to the membrane surface. It would therefore be interesting to find out if co-administration of other small molecules with PantOH improves their permeability as a result of this effect.

The permeability of PantOH across mammalian cells is assumed and though we could not demonstrate this, the liposomal diffusion rate of this molecule in our eukaryotic system suggests the ability of the molecule to cross the in vitro membrane with some efficiency. And since the two molecules produced similar fluidity effects at pH 7, it possible that at physiological pH these two molecules are likely to interact or translocate over the membrane in a similar manner. Which we propose is by a mechanism illustrated in Figure 3-13 which is also supported by the solubility-diffusion theory[39,40].

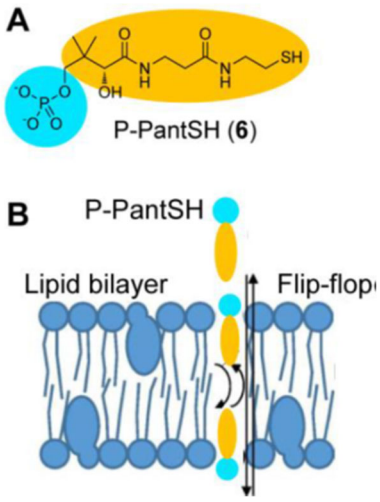


**Figure 3-13: Proposed mechanism of P-PantSH permeation. A**) Structure of P-PantSH, showing the polar (in blue circle) and amphiphilic (in orange) moieties. **B**) Proposed mechanism whereby P-PantSH could pass through a lipid bilayer. The molecule inserts itself in one leaflet in the same orientation as a phospholipid, after which it undergoes a flip-flop exchange to the inner leaflet. From here, it is released to the cytosol. Adapted from [177].

Our findings also show that membrane fluidity modulates the interaction of P-PantSH with the membrane, with the interaction becoming more pronounced in membrane compositions of higher fluidity. Furthermore, P-PanCOOH membrane interaction, as indicated by a change in the fluidity, was also observed in the membrane model of higher fluidity. This is line with the view that a phosphorylated pantoyl moiety is important for membrane translocation of P-PantSH. The membrane fluidity analysis also shows that pH and ionic strength influence membrane fluidity, though not to the extent that it alters the pantothenate analogue induced effects, and perhaps altering the membrane permeability assay to include these factors may yield better outcomes.

## 3.4 Materials and methods

### 3.4.1 Preparation lipid dry films

Lipid stocks of 1-palmitoyl-2-oleoyl-*sn*-glycero-3-phosphophatidylcholine (POPC), 1-palmitoyl-2-oleoyl-*sn*-glycero-3-phosphoethanolamine (POPE), 1-palmitoyl-2-oleoyl-*sn*-glycero-3-phosphoglycerol (POPG) and cardiolipin (CL) and cholesterol were prepared by weighing out the dry lipid powder and dissolving it in chloroform to a concentration of 10 mg/mL for each compound. To prepare the eukaryotic membrane model, POPC and cholesterol were mixed together in a 9:1 (w/w) ratio to a final volume of 1 mL per preparation. The bacterial membrane model was prepared by mixing POPE, POPG and CL in a 7:2:1 ratio (w/w) also to a final volume of 1 mL per preparation. The lipid mixtures were transferred to round bottom flasks after which the organic solvent was removed *in vacuo*. Residual solvent was removed under high vacuum for a period of 12 hours to produce dry lipid films.

### 3.4.2 Preparation of liposomes loaded with thiolated molecules

The dry lipid films of eukaryotic or bacterial membrane model mixtures were rehydrated with 1 mM of either GSH, PPantSH, PantSH, dePCoA, CoA or H-*S*NAC target metabolite, each with 1.5 mM TCEP as a reducing agent. Following rehydration with a solution of GSH and reducing agent, the lipid suspension was incubated at 60˚C for 20 minutes with constant vortexing at 5-minute intervals. The suspension was then flash-frozen in liquid nitrogen (~ 80 °C) and allowed to thaw at room temperature (~ 22 ˚C). The freeze-thaw cycle was repeated five times to promote formation of unilamellar vesicles. The suspension was then subjected to 20 extrusion passages to form SUVs (liposomes) of uniform size using the Avanti™ mini-extruder fitted with two 800 nm polycarbonate filters (Whatman). Excess metabolite was removed by size exclusion chromatography in a Sephadex-G75 column prepared in-house. To prepare the column, 2 g of Sephadex-G75 beads was weighed out and hydrated with MilliQ water. The slurry was allowed to stand at room temperature for 1 hour for full hydration of the beads. The excess buffer was decanted out and the slurry was transferred to a 5 mL syringe column sealed with cotton wool. The column was then placed in a 15 mL centrifugal tube and the beads were packed by centrifugation at 3 000 g for 5 minutes in a benchtop swing bucket centrifuge. The flow through was then discarded and the extruded lipid suspension was then placed on the column bed. The thiol metabolite-loaded liposomes were then harvested by centrifugation at 1 000 g for 5 minutes in a swing bucket rotor. The purified liposome suspension was then collected in the flow through and stored at 4 °C until further use.

### 3.4.3 Preparation of pantothenate analogue-loaded liposomes

POPC-Chol and POPE-POPG-CL liposomes respectively loaded with 5 mM of either PanCOOH, PantSH, N5-Pan, *N*-PE-Pan or PantOH were prepared as described in 3.3.1.1 for thiol molecule-loaded liposomes.

### 3.4.4 Preparation of phosphopantothenate analogue-loaded liposomes

POPC-Chol and POPE-POPG-CL liposomes respectively loaded with 5 mM of either G6P, P-PanCOOH, P-PantSH, P-N5-Pan, P-*N*-PE-Pan or P-PantOH were prepared as described in 3.3.1.1 for thiol molecule-loaded liposomes.

### 3.4.5 Determination of membrane permeability of thiolated molecules by the CPM-based fluorescence assay

A 1 mM solution of either GSH, PPantSH, PantSH, dePCoA, CoA or H-*S*NAC was prepared to represent to determine the “free” metabolite diffusion rate. To each solution, 1.5 mM Tris-2-Carboxyethylphosphine (TCEP) which is reducing agent, was added. Three dialysis membrane units were hydrated for 10 minutes in 3 ×10 mL beaker filled with 900 µL of MilliQ water. Following hydration, 200 µL of a respective solution was placed inside these dialysis

membrane units, and the diffusion rate were then monitored by collecting 20 µL aliquots of each dialysate at 0.5 hour intervals for 2.5 hours, such that the measurements were performed in triplicate. The aliquots were then transferred to a black 96 well plate to which 160 µL MilliQ water and 20 µL of 10 µM CPM were added. The plate was then incubated at room temperature for 30 minutes to allow formation of CPM-adducts. Following this, the fluorescence intensity of each aliquot was measured on the fluorimeter (TECAN spark 10M, Switzerland) at $\lambda_{ex}$ = 387 nm and $\lambda_{em}$ = 465 nm. The liposomal diffusion rate was then determined by placing 3×200 µL of the lipid suspensions prepared in 3.4.2 in dialysis membrane units placed in 3×10 mL beakers. The diffusion rate was determined as described above for "free" metabolite diffusion. The fluorescence intensity values were then plotted against time intervals at which the aliquots were collected. The diffusion rates were then determined by calculating the slopes of respective plots. The liposomal diffusion rate was then normalized to the "free" metabolite diffusion rate to describe relative liposomal diffusion, where a value of 1 would indicate that the liposomal diffusion is equal to the free diffusion rate. The process was repeated for each respective metabolite. The relative permeability of GSH was a set as a reference for the membrane model in question.

### 3.4.6 Determination of membrane permeability Pantothenate analogues by the coupled enzyme (PanK-PK-LDH) assay

A 5 mM solution of either PanCOOH, PantSH, N5-Pan, *N*-PE-Pan or PantOH was prepared to determine the "free" metabolite diffusion rate. Three dialysis membrane units were hydrated for 10 minutes in 3 ×10 mL beaker filled with 900 µL of MilliQ water. Following hydration, 200 µL of a respective solution was placed inside these dialysis membrane units, and the diffusion rate were then monitored by collecting 20 µL aliquots of each dialysate at 0.5 hour intervals for 2.5 hours, such that the measurements were performed in triplicate. The liposomal diffusion rate was then determined by placing 3 × 200 µL of the lipid suspensions prepared in 3.4.3 in dialysis membrane units placed in 3 × 10 ml beakers. The diffusion was monitored by the same method as described above for "free" metabolite diffusion. All aliquots of 20 µL dialysate were transferred to a clear 96 well plate. A reaction mixture containing 1.5 mM ATP, 2 mM PEP, 0.5 mM NADH, *Ec*PanK (2 µg/ 200 µL reaction), 2 U PK, 2 U LDH in a 50 mM Tris-HCl pH-7.4, 20 mM KCl, 20 mM $MgCl_2$. buffer was prepared. Following this, the presence of metabolite of interest in each aliquot was determined by adding 180 µL of the reaction mixture and monitoring change in absorbance at 340 nm to determine NADH consumption from each aliquot. The NADH consumption was then calculated from the resultant slopes for each aliquot. The coupled enzyme assay is set up in such a manner that the NADH consumption rate corresponds to the amount of molecule of interest used as a substrate for the PanK reaction. For this reason, the resultants NADH rates for each aliquot were plotted against the

time interval at which the aliquot was collected to represent the progression of diffusion of the metabolite of interest. The slopes of these plots were then used to calculate the diffusion rate of each of the metabolites included in the study. The relative permeability was calculated from the "free" metabolite and liposomal diffusion rates as described in 3.4.5. The relative permeability of PanCOOH was a set as a reference to determine "true" permeability across the membrane model in question.

### 3.4.7 Determination of membrane permeability of phosphorylated pantothenate analogues by the alkaline phosphatase (ALP) & malachite green assay

A 5 mM solution of either G6P, P-PanCOOH, P-PantSH, P-N5-Pan, P-N-PEPan or P-PantOH was prepared to determine the "free" metabolite diffusion rate. Three dialysis membrane units were hydrated for 10 minutes in 3×10 mL beaker filled with 900 µL of MilliQ water. Following hydration, 200 µL of a respective solution was placed inside these dialysis membrane units, and the diffusion rate was then monitored by collecting 20 µL aliquots of each dialysate at 0.5 hour intervals for 2.5 hours, such that the measurements were performed in triplicate. The liposomal diffusion rate was then determined by placing 3×200 µL of the lipid suspensions prepared in 3.4.4 in dialysis membrane units placed in 3 × 10 ml beakers. The diffusion was monitored by the same method described above for "free" metabolite diffusion. To determine the diffusion rate, a Malachite green solution consisting of 0.034% Malachite green, 3.4% Ethanol, 10 mM ammonium molybdate dissolved in up to 1 M HCL (HPLC grade, 99% Purity, Merck, Germany). A phosphate cleavage reaction was prepared by adding 4 mM $NiCl_2$, 50 mM Tris-HCl, pH 7.6, 0.1 mM $CaCl_2$, BSA (2 mg/mL) and 5 U ALP to each 20 µL aliquot to a final volume of 100 µL. Each reaction mixture was incubated at 37 °C for 2.5 h to allow cleavage of the phosphorylated compound by malachite green assay. Following this, the enzyme was heat inactivated at 65 °C for 15 minutes. The reaction components were then removed by centrifugation at 13 000 g for 5 minutes. The supernatant from each aliquot was transferred to a 96 well plate. To determine the amount of phosphate in each aliquot, 50 µL of the malachite green solution was added was transferred to each well. The plate was allowed to stand at room temperature for 10 minutes for color development. The absorbance for each aliquot was measured at 625 nm and plotted against time to show the diffusion of each molecule of interest over time. The slopes of the resultant plots were then used to calculate the diffusion rate for each molecule of interest. Following this, the relative permeability was calculated as described in 3.4.5. The relative permeability of G6P was set as a reference to determine the "true" permeability across the membrane model.

### 3.4.8 Prodan spectral recording and GP determination

A 1 mM stock of Prodan was prepared in DMSO. Following this, 20 µL of the control POPC/Chol liposomal preparation was transferred to a black 96-well plate. The liposomes were diluted 10 × with 180 µL water. Prodan solution was then added to a final concentration of 10 µM (i.e. ~2 µL of the stock). The plate was then incubated at room temperature for 15 minutes to allow incorporation of the dye into the membrane. The emission spectra were then recorded on the TECAN SPARK 10 M fluorimeter, at $\lambda_{ex}$ = 370 nm with the signal gain manually set to 50%. This procedure was repeated for control POPE/POPG/CL, as well as the P-PantSH and PantOH loaded liposomes. The procedure was repeated again, this time adding 1 mM of either Tris-HCl (pH 7.00), Tris-HCl (pH 8.00) or MES-HCl (pH 6.00) to each liposomal preparation. The spectra were collected at 25 °C for all liposomal preparations. Then finally, the general polarization (GP) value was calculated from each spectrum.

### 3.4.9 Investigation of fluidity of the eukaryotic membrane model

2-palmitoyl-sn-glycero-3-phosphophatidylcholine (DPPC) lipid films were prepared as described in 3.4.1 for POPC-Chol and POPE-POPG-CL. Lipid films POPC: DPPC in a ratio of 1:1 (w/w) were also prepared in the same way. The lipid films were either hydrated with MilliQ water – to represent control membranes, or with 5 mM P-PantSH or 5 mM PantOH. The Prodan spectra were recorded in 10 mM Tris-HCl, pH 7.4 for all membrane models in question. The measurements were performed as described in 3.4.8.

# 4 SLC25A16 transports P-PantSH in an ADP-dependent manner

## 4.1 Introduction

Mitochondrial carriers (MCs) are a superfamily of transporters classified as SLC25 (solute carrier family 25) in mammals[178]. All members of this family have a tripartite structure of tandemly repeating domains of at least 100 amino acid length[179]. A substantial amount of metabolic machinery is compartmentalized into mitochondrion. Therefore, MCs provide a link between organellar and cytoplasmic metabolic activity by catalyzing translocation of numerous solutes across the mitochondrial membranes. Despite the apparent structural similarity, MCs have functional diversity and transport a large variety of solutes that differ in size and chemical properties[178,180,181]. Therefore, the MCs can be further classified into subfamilies based on substrate specificity, mode of transport and kinetic properties. For example, some MCs exclusively transport negatively charged particles, some catalyze a 1:1 substrate exchange (antiport), some are uniporters, some are $H^+$-compensated symporters, and some use a combination of these mechanisms to transport solutes. Some membrane transporters classified as MCs localize to other organelles such as the peroxisome and chloroplast[178].

At least three MCs associated with the transport of CoA have been identified in mammals. These include SLC25A16, SLC25A17 and SLC25A42. SLC25A16 was originally thought to be associated with Grave's disease and was accordingly named Grave's disease carrier protein. However, it was later shown that a missense mutation of this transporter leads to the reversal of CoA levels between the cytosol and mitochondrion suggesting its role in the maintenance of mitochondrial CoA pools[178,182]. Nonetheless, direct characterisation of this protein is yet to be performed. SLC25A16 is closely related to SLC25A42 and the latter is highly expressed in most mammalian tissues[124] (Figure 4-1). A *Homo sapiens* isoform of SLC25A42 was characterized and found to function by a counter exchange mechanism in which uptake of one substrate requires efflux of another. It has the highest affinity towards adenosine 3',5'-diphosphate (PAP), with a $K_m$ value of 50 ± 7 µM. This transporter also has affinity towards dePCoA and CoA, with $K_m$ values of 64 ± 9 µM and 71 ± 10 µM, respectively. A missense mutation in the gene that encodes this protein causes mitochondrial myopathy associated with lactic acidosis and muscle weakness which highlights its importance in the regulation of metabolic activity inside the mitochondrion[183].

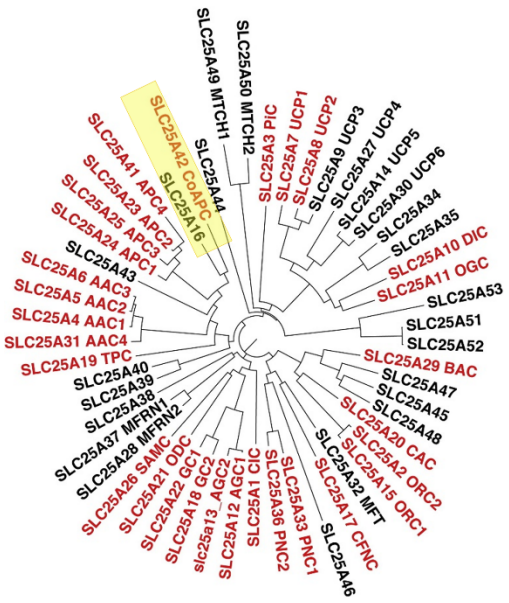


**Figure 4-1: Phylogenetic analysis of mammalian mitochondrial carriers.** The analysis indicates that SLC25A16 and SLC25A42 clusters together (indicated by the yellow rectangle). This suggests functional homology between the two carriers. Adapted from Palmieri et al.[178]

Unlike the other two, SLC25A17 localises to the peroxisome[125]. *H. sapiens* SLC25A17 has also been characterized and was also shown to function by a counter-exchange mechanism. Its transport affinity was determined to be 19 ± 3 μM for [$^{14}$C] AMP/AMP exchange at 25 ºC. Amongst others, CoA and dePCoA were found to be competitive inhibitors of [$^{14}$C] AMP uptake, with $K_i$ values of 19.6 ± 3.8 μM and 14.4 ± 5.4 μM, respectively. This transporter also demonstrates affinity towards the flavin cofactors FAD and FMN, the adenosine nucleotides ADP and PAP, as well as folate and NAD$^+$[125].

SLC25A42 exhibits high sequence homology towards carriers of ADP/ATP as well as ATP-Mg/$P_i$, while SLC25A17 exhibits high sequence similarity towards other pyrimidine nucleotide carriers and the folate/NAD$^+$ carrier. Therefore, the rationale for screening free CoA, acetyl-CoA and dePCoA as substrates for these proteins was informed by its apparent homology towards nucleotide-recognizing carriers[124,125].The observed affinity of these transporters towards CoA and dePCoA (**3**) is consequently attributed to the ability to recognize the adenylyl moiety (**2**) present in all these molecules (Figure 4-2).

However, it would be interesting to find out if these MCs exhibit any affinity towards the P-PantSH moiety (**1**), especially in SLC25A17 which shares sequence homology with a folate transporter. This is because both folate and PanCOOH are vitamin molecules, and the latter is a precursor of CoA and a structural analogue of P-PantSH. Furthermore, the probability of transport of these molecules was ruled out in SLC25A42 on the premise that CoA biosynthesis took place exclusively in the cytoplasm. However, we now know that enzymes involved in CoA

salvage, i.e. PANK2 and CoASy, localize to the mitochondrion[118,122]. This in turn suggests that any of the CoA precursors (PanCOOH, PantSH, P-PantSH or dePCoA) could potentially cross the mitochondrial membranes[63], and transport by the MCs associated with CoA transport would be an effective way in which this would be achieved.

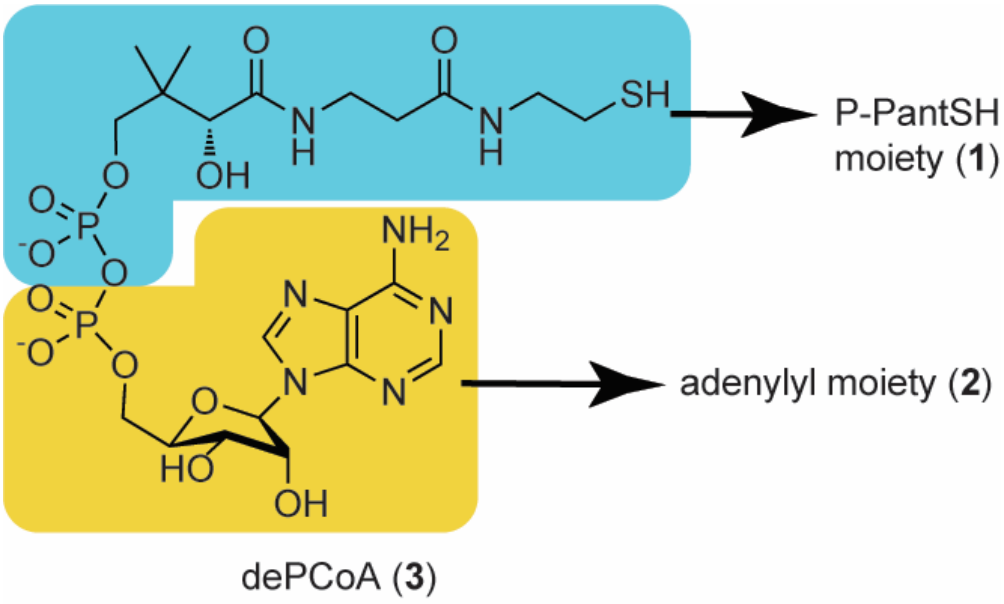


**Figure 4-2: Affinity of the MC towards a substrate depends on its ability to recognize either the P-PantSH (1) or adenylyl moiety (2).** Among the molecules identified as substrates for SLC25A42 and SLC25A16 is dePCoA (**3**) which has both the adenylyl and P-PantSH moieties. ATP, ADP and AMP are examples of molecules containing the adenylyl moiety and that are common substrates of some transporters in the SLC25 class.

Kinetic characterisation of SLC25A42 and SLC25A17 was previously done using *in vitro* homo-exchange assays using proteoliposomes reconstituted with the transporter in question. The proteoliposome was preloaded with one component and then the uptake of another was measured[124,125]. For these assays, the intraliposomal component was a non-labelled compound, with the radiolabeled form being placed outside the liposome so that the uptake could be determined by monitoring the increase of radioactivity inside the liposome.

Performing transport assays in this manner requires access to the radiolabeled versions of the compound of interest. A wide variety of radiolabeled compounds are commercially available; however if a required compound is not available, it can be synthesized in house if there is capacity to do so. There are financial implications in either case, but the major drawback of the latter is the time spent on chemical synthesis. Therefore, availability of a radiolabeled compound can limit the size and diversity of sample set for transport screening. It may therefore be useful to have an alternative method that does not require the use of radiolabeled compounds to study the transport kinetics of a membrane protein. The discontinuous liposomal assay for membrane permeability measurement described in chapter

2 is one such alternative. The assay was designed in such a manner that detection methods can be changed as required to accommodate molecules with a diversity of chemical structures.

Therefore, the main aim of this part of the study was to investigate the transport kinetics of SLC25A16 using the discontinuous liposomal assay for permeability measurements. SLC25A16 is a particularly interesting candidate to characterize because no direct kinetic characterisation of this transporter has been performed to date. Furthermore, of the three transporters, it is the only one for which there is evidence directly linking it to CoA levels in the mitochondrion. Based on previous research, we have proposed a key regulatory role of P-PantSH in the maintenance of subcellular CoA pools of which the mitochondrion is one. Therefore, the affinity of SLC25A16 towards this molecule was investigated. Moreover, since this transporter exhibits sequence similarity towards SLC25A42, dePCoA and the adenosine nucleotides ATP and ADP were also included. The finding that CoASy (which uses dePCoA as substrate) to the mitochondrion provides further rationalization for inclusion of dePCoA in the sample set. PantSH, which is a precursor of CoA salvage, was also included such that all potential precursors of CoA in the mitochondrion were screened. Taken together, this part of the study provides the first insights into the substrate preference of the human SLC25A16 carrier.

## 4.2 Results

### 4.2.1 Expression, purification and functional reconstitution of SCL25A16

Identification and characterization of a solute carrier requires identification of suitable substrates[178]. The most successful strategies for this include gene expression and purification of recombinant proteins and reconstitution into liposomes followed by direct protein assays[184]. This strategy appears simple but can fail for numerous reasons. Some of these reasons include difficulties experience with expression and subsequent purification of the protein, mainly because these proteins are often found in inclusion bodies in the cytoplasm of *E. coli* cells due to their foreign nature as well as the need to be included in membranes. This can lead to extensive efforts to resolubilize and refold the protein before it can be incorporated in proteoliposomes. Therefore, the first objective of the study was to express and purify the SLC25A16 protein to apparent homogeneity.

The gene construct encoding *H. sapiens* SLC25A16 cloned into a high copy expression vector (pRUN) was expressed in *E. coli* C41 (DE3) cells. This cell line was preferred over BL21(DE3) cells as mitochondrial carrier proteins tend to become toxic towards this strain, while the C41(DE3) strain is engineered to be more tolerant of such potentially toxic proteins [184]. Starter cultures were prepared by inoculating 4×5 ml LB media with a colony of transformed C41(DE3)

cells, and incubation at 37 ºC, shaking at 150 g for ~16 hours. The starter cultures were transferred to 4×500 ml LB media, and incubated at 37 ºC, shaking at 150 g until $OD_{600}$ ~0.6. Following this, overexpression of the recombinant protein was induced with 1 mM IPTG, and the protein was expressed at 37 ºC, shaking at 150 g for ~5 hours. At the end of this period 1 ml aliquots were collected from each flask and cells from these aliquots were harvested and lysed with BugBuster® reagent, and the insoluble extracts were collected by centrifugation. The supernatants were discarded and pellets collected and screened for protein expression since the MCs are expected to express into inclusion bodies. Protein expression was screened by 12% SDS-PAGE and the gel was stained with Coomassie brilliant blue for visualization (Figure 4-3). Bands of relatively high intensity were observed just below the 40 kDa marker, which is close to the expected size of the protein of ~35kDa. Cells were harvested from the rest of the culture by centrifugation, discarding the supernatants and collecting the pellets. These were stored at -20 ºC until further use.

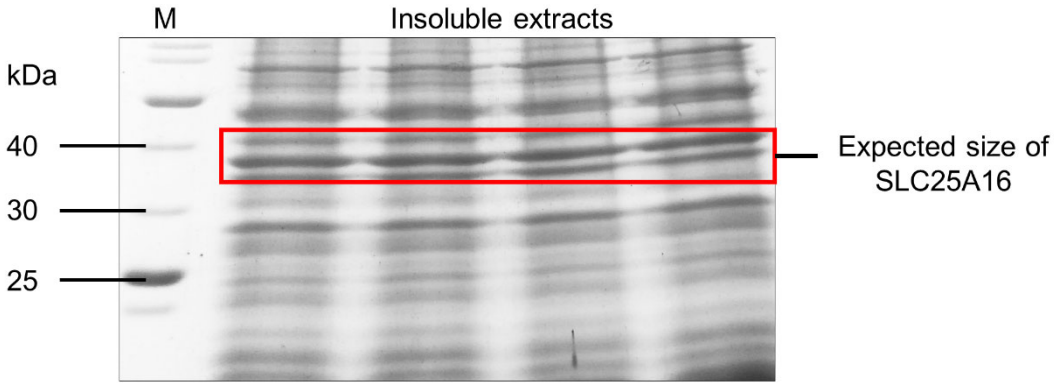


**Figure 4-3: Expression of the SCL25A16 protein in *E. coli* C41 (DE 3) cells.** The insoluble extracts were harvested from cell lysates and screened for overexpression of SLC25A16. M denotes the molecular weight marker (Broad range Page ruler, NEB). Expression was induced with 1 mM IPTG (concentration indicated at the bottom panel). Protein expression was screened by 12% SDS/PAGE and the gel was stained with Coomassie brilliant blue.

The pellets were thawed at 4 ºC and resuspended in lysis buffer containing Triton X-114 detergent. The cells were lysed by sonication, and the insoluble extracts were collected by centrifugation. The supernatant was discarded and the pellet was resuspended by pulse sonication for 3×30 s with more detergent. Following this, the suspension was subjected to another centrifugation cycle. The process was repeated until the pellet was homogenous (i.e.: no “halo” around the pellet). Two intense bands between 30 and 40 kDa were subsequently observed upon SDS-PAGE analysis (Figure 4-4). The smaller one of the two bands was postulated to be an *E. coli* membrane protein which is a common contaminant in purification of recombinant membrane proteins[184,185]. The protein suspension was the subjected to ultracentrifugation on a density gradient to harvest what would presumably be “homogenous”

inclusion bodies. Unfortunately, the preparation still contained contaminants. As stated above, these contaminants are presumed to be endogenous *E. coli* membrane proteins that are quite difficult to remove at this point in the purification process. Such contaminants are usually a result of suboptimal cell lysis. A French press is a more efficient technique for cell lysis, but we did not have access to such an instrument at the time of performing this study. Therefore, we opted to continue with the partially pure preparation to perform an initial characterization.

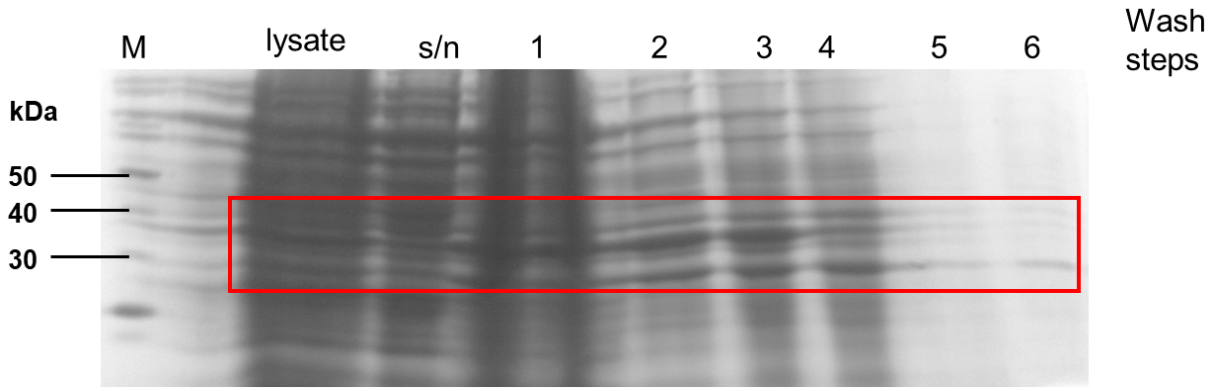


**Figure 4-4: Purification of SLC25A16 inclusion bodies.** The inclusion bodies were harvested by progressive wash steps with Triton X-114. The insoluble extract was collected by centrifugation at each step. The purification was screened by 12% SDS-PAGE and the gel was stained with Coomassie brilliant blue.

The process of resolubilization involves protein denaturation by progressive addition of a detergent. Up to 2% of sarkosyl was added to the SLC25A16 preparation, as its inclusion yields the most satisfactory outcome relative to other detergents[185]. Following resolubilization, the detergent is usually removed by centrifugation. Subsequently, 12% SDS-PAGE was performed to confirm presence of the resolubilized protein in the supernatant. The resulting gel is shown in Figure 4-5, in which two bands can be seen, one 30 kDa in size, and the other just below 40 kDa in the resolubilized fraction. These are at the same positions previously observed in the purification evaluation gel. These bands were presumed to be the target protein together with the *E. coli* membrane protein contaminant. Due to the difficulties encountered in removing the endogenous protein contaminants and the low overall yield, we decided to proceed to reconstitute the resolubilized protein into liposomes.

The now denatured protein folds back into its native conformation during reconstitution and the process must occur gradually. This was done by preparing a lipid suspension of α-phosphatidylcholine in the presence of small amounts of detergent (~2% Triton X-114), then systematically adding cardiolipin and the resolubilized protein. Excess protein and detergent was then removed by slow passage through an Amberlite-XAD column prepared in house[184,185]. This process was repeated about 13 times. Following this, the suspension was

subjected to freeze-thaw cycles and extrusion to promote formation of unilamellar proteoliposomes containing the SLC25A16 in a presumably functional state.

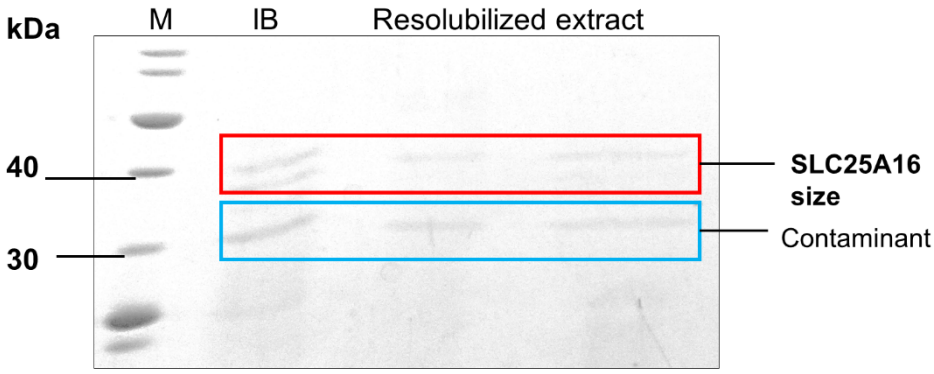


**Figure 4-5: 12% SDS-PAGE of resolubilized SLC25A16 extracts.** Inclusion bodies containing SLC25A16 were purified by progressive addition of Triton X-114. Following this, the inclusion bodies were resolubilized with ~2% sarkosyl. M denotes the broad range molecular weight marker (Broad range page ruler, NEB). The gel was stained with Coomassie brilliant blue.

### 4.2.2 Functional characterization of SLC25A16: Efflux measurements with PantSH, P-PantSH and dePCoA

For functional characterization of SLC25A16, we prepared proteoliposomes loaded with dePCoA, PantSH or P-PantSH, respectively. The efflux of respective molecules from the liposomes was measured using the discontinuous CPM-based assay described in chapter 2 (Figure 4-6). The diffusion rate of the free metabolite was not measured as it was already demonstrated that all three molecules can freely diffuse over the dialysis membrane. Furthermore, the time intervals used here are much shorter than the intervals used to measure passive diffusion as was done in the studies described in chapter 3. This was done due to the expectation—informed by previous studies—that protein-mediated membrane transport would occur more rapidly than permeation by passive diffusion.

Apart from measuring the efflux of the thiolated molecules of interest directly, we were also interested in establishing if this efflux was affected (positively or negatively) by the presence of adenosine nucleotides. This interest was based on the findings that other SLC25 carriers often use counter-exchange mechanisms for transport. Consequently, the efflux of the CoA biosynthetic precursors were measured from the proteoliposomes both in the absence and the presence of either ATP or ADP (Figure 4-7). Any changes in the observed efflux rate could then be attributed to the presence of the nucleotide, indicating a counter-exchange or other transport mechanism.

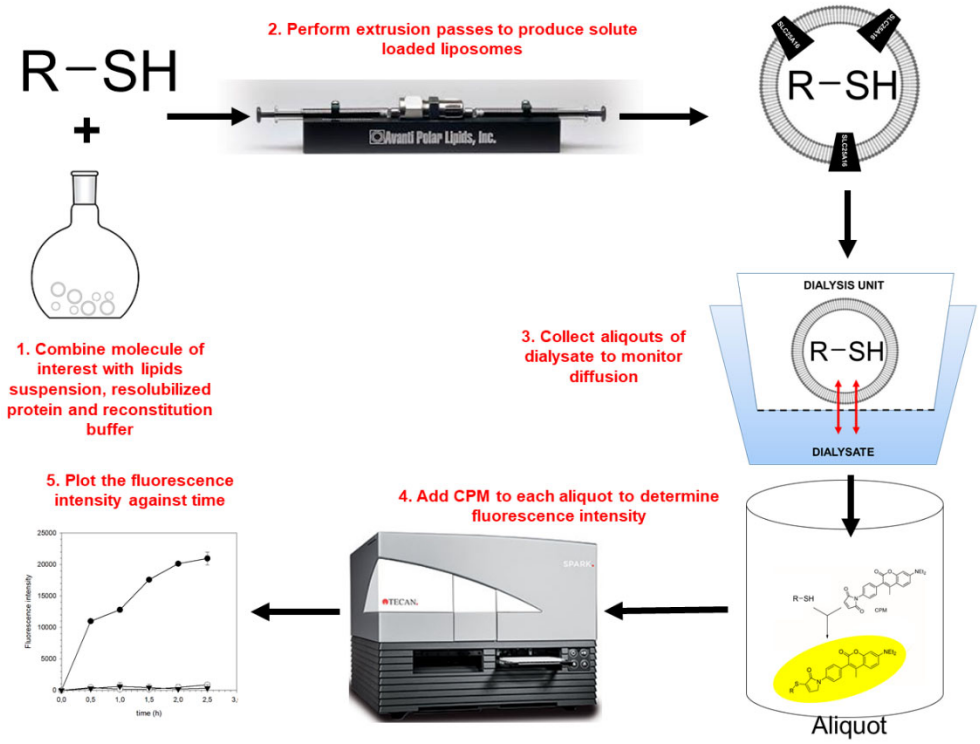


**Figure 4-6: Work flow for measuring efflux from SLC25A16 proteoliposomes.** Proteoliposomes were prepared by in the presence of a detergent by the extrusion. These were prepared with either PantSH, P-PantSH or dePCoA loaded in the intraliposomal cavity. The efflux was the measured by the discontinuous liposomal assay for permeability measurement described earlier.

The results show rapid efflux of dePCoA from the liposomes in the absence of the nucleotides. The presence of either ATP or ADP does not seem to affect the efflux rate of this molecule (Figure 4-7 A). The CPM adducts formed with the respective thiol molecules have varying fluorescence emission signals and this is the reason for difference in fluorescence intensity between Figure 4-7 A to C. PantSH efflux could also be observed in the absence of nucleotides, although this was not to the same extent as for dePCoA. However, ATP and ADP seemed to inhibit the efflux of this molecule (Figure 4-7 B). On the other hand, no efflux was observed for P-PantSH unless ADP was present (Figure 4-7 C).

The lack of distinction in dePCoA in the presence of absence of adenosine nucleotides is in line with the view that the transporter recognises the adenylyl moiety of dePCoA for transport. Conversely, the diminished efflux of PantSH in the presence of either ATP or ADP suggests that these molecules compete for the same binding site on the transporter, and that the transporter possibly has stronger affinity for the adenosine nucleotides resulting in inhibition of PantSH efflux. On the other hand, the ADP-dependent P-PantSH efflux suggests that there may be a counter-exchange transport mechanism in its case. However, this cannot be confirmed with current assay, as it exclusively measures efflux.

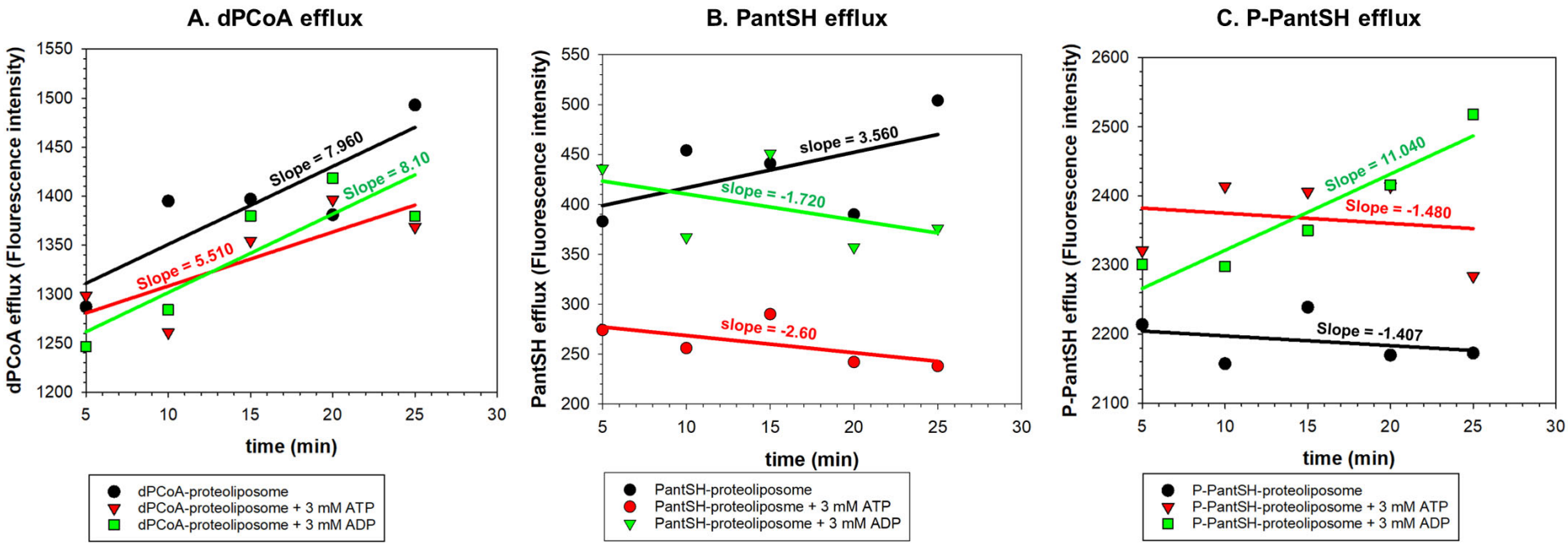


**Figure 4-7: Efflux measurements of PantSH, P-PantSH and dePCoA from SLC25A16 proteoliposomes.** The efflux of dePCoA, PantSH, P-PantSH from SLC25A16 proteoliposomes was measured in the absence (black), as well as presence of 3 mM of either ATP (red) or ADP (green).Linear curve fits were performed on sigmaplot-14.0, and the slopes derived from these fits indicate the average efflux rate for each condition.

## 4.3 Discussion

This study provided the first data on the substrate specificity of the human SLC25A16 carrier. In particular, we demonstrate efflux of that dePCoA regardless of the presence of any external nucleotides. In addition, the observed differences in efflux of P-PantSH in the presence of ADP indicates that this molecule of interest likely occurs by a counter-exchange mechanism. This change would not have occurred if the observed efflux was due to passive diffusion, or due to non-specific leakage. Furthermore, the main component of the liposomes used in this study is phosphatidylcholine, which was also the main constituent of the eukaryotic membrane model described in chapter 3. P-PantSH was shown to efficiently cross the latter by passive diffusion. Therefore, the observed dependence on ADP of P-PantSH efflux in the current study, is evidence that the two process are distinct from each other. However, a control experiment using liposomes devoid of a transporter would have been ideal to ascertain that the observed efflux is true result of protein-mediated membrane transport.

Finally, our results indicate that the protein purification method should be optimised to improve confidence in the observed results. As stated, a more efficient lysis method would ensure minimal contamination. Furthermore, the identity of the protein could be confirmed by mass spectrometry or western blot since SLC25A16 antibodies are commercially available. Amino acid analysis could also be performed to determine absolute protein concentration in purified inclusion bodies – this would simplify the process of quantifying resolubilized protein extracts, which will in turn be useful for the purposes of reporting kinetic data. Microscopy techniques, which were instrumental for confirming encapsulation efficiency of the liposomal preparation described in chapter 2 and 3, could also be useful for confirming protein reconstitution.

## 4.4 Conclusion

We were able to demonstrate transport kinetics of SLC25A16 with the discontinuous liposomal assay describe in chapter 2, which is further evidence of the versatility of this assay. We also provide first evidence that SLC25A16 may be a P-PantSH/ADP transporter. This supports the proposition that P-PantSH plays a regulatory role in maintenance of subcellular CoA pools since this transporter is implicated, at least in the regulation of mitochondrial CoA levels.

## 4.5 Materials and methods

Agar, Tryptone, Sodium chloride (NaCl), Yeast extract, , Sodium dodecyl sulphate (SDS), , Tris, HCl, Ethylenediaminetetraacetic acid (EDTA), Dithiothreitol (DTT), sucrose, Tris(2-carboxyethyl)phosphine hydrochloride (TCEP), Sodium sulphate ($Na_2SO_4$), CPM, 3'-Dephospho Coenzyme A (dePCoA), Amberlite®-XAD®, Triton-X114™, Adenosine 5'-mono-phosphate (AMP), Adenosine 5'-diphosphate (ADP), Adenosine 5'-triphosphate (ATP) and

thiamine pyrophosphate (TPP) all had a purity of 95 % or higher and were purchased from Sigma-Aldrich, Germany. 30% acrylamide monomer solution for electrophoresis (PAGE) was also purchased from Sigma-Aldrich. Methanol (99% Purity for HPLC) was purchased from Merck, Germany. Coomassie® Brilliant blue R 250 was purchased from Merck, Germany. Glass Pasteur pipettes and black 96 well plates were purchased from Lasec. Sephadex G-75 was from (GE Healthcare, USA). The unstained broad range page ruler (P7717) was purchased from NEB (U.S.A).The Beckman J-26 XPI centrifuge and Optima L-80 XP ultracentrifuge were used to perform the centrifugation steps.

### 4.5.1 Sub-cloning and expression of SLC25A16 protein

The gene construct for SLC25A16 cloned into a high copy pRUN plasmid was a gift from G. Fiermonte, Bari University – Italy. Chemically competent *E. coli* C41 (DE3) cells were transformed with the plasmid using heat shock. The cells were then transferred to LB-Agar solid media (20 g agar, 10 g tryptone, 10 g NaCl and 5 g yeast extract 1 L MilliQ water), and incubated at 37 ºC for ~16 hours. One colony was picked from the agar plate and transferred to 2 × 5 mL LB-media (10 g tryptone, 10 g NaCl and 5 g Yeast extract 1 L MilliQ water). This was also incubated at 37 ºC for ≈16 hours for maximum growth of the transformed cells. These starter cultures were then transferred to 2 × 1 L LB media and incubated at 37 ºC, shaking at 150 g until the $OD_{600}$ ~0.6–0.8. Following this, 1 mL aliquots were collected as pre-induction controls from each flask. Overexpression of the recombinant protein was induced with IPTG to the final concentration of 0.5 and 1 mM for each respective flask. The protein was expressed at 37 ºC, shaking at 150 g for 16–20 hours, but two aliquots were collected at 3 hours post-induction as well as at the end of the incubation period. All the aliquots collected were treated with bug buster reagent to lyse the cells. The insoluble cell extracts were harvested by centrifugation and screened for protein expression with 12% SDS-PAGE. Cells were harvested from the rest of the cultures by centrifugation at 8 000 g, 4 ºC for 20 minutes in a fixed angle rotor (Beckman JA-10). The supernatant was discarded, and the pellet collected and stored at -20 ºC until further use.

### 4.5.2 SDS-PAGE

The expression and purification evaluation of the proteins were achieved The separation gel solution was prepared with Acrylamide/bis (30% 37.5:1, Sigma-Aldrich) and Sodium dodecyl sulphate (SDS) 10 % (w/v) in 1.5 M Tris-HCl at pH 8.8. The polymerization reaction was initiated with Ammonium persulfate (APS), 10% (w/v) and *N*,*N*,*N*′,*N*′-tetramethylethylene-diamine (TEMED) according to the method described in[186]. The solution was prepared as indicated in Table 4-1.

Table 4-1: The 12% separation gel solution

| Component | Volume (mL) |
|---|---|
| Water | 1.4 |
| Acrylamide/bis (30%) | 3.3 |
| 1.5 M Tris-HCl, pH 8.8 | 2.5 |
| SDS (10% w/v) | 0.1 |
| APS (10% w/w) | 0.1 |
| TEMED | 0.032 |

The stacking solution was prepared as indicated in *Table 4-2*.

Table 4-2: The 4% stacking gel solution

| Component | Volume (mL) |
|---|---|
| Water | 6.1 |
| Acrylamide/bis (30%) | 1.3 |
| 0.5M Tris-HCl, pH 6.8 | 2.5 |
| SDS (10% w/w) | 0.1 |
| APS (10% w/w) | 0.01 |
| TEMED | 0.1 |

### 4.5.3 Coomassie brilliant blue stain

All the SDS-PAGE gels were stained with Coomassie brilliant blue stain according to a protocol described by [187]. The following four solutions with varying concentrations of the Coomassie brilliant blue stain were used to stain each gel:

Solution A: Isopropanol 25% (v/v), Acetic Acid 10% (v/v), Coomassie R-250 0.05% (w/v).

Solution B: Isopropanol 10% (v/v), Acetic Acid 10% (v/v), Coomassie R-250 0.005% (w/v).

Solution C: Acetic Acid 10% (v/v), Coomassie R-250 0.002% (w/v).

Solution D: Acetic Acid 10% (v/v).

Each gel was first immersed in solution A, heated in the microwave for 20 seconds, and then placed on an orbital shaker for 5 minutes. The solution was then discarded and the gel rinsed with MilliQ water. The gel was then immersed in solution B and then subjected to the same process this continued progressively until the gel was finally immersed in Solution D which is the “destaining” solution.

### 4.5.4 Purification of SLC25A16 inclusion bodies

The SLC25A16 inclusion bodies were purified based on the method described by [185].The lysis buffer was prepared as follows: 1% (v/v) Triton-X114, 10 mM Tris-HCL, pH 7.00, 0.1 mM EDTA and 1 mM DTT. Specifically, a 10 × stock solution of this buffer was prepared, which

was then diluted prior to each preparation. A previously prepared protein pellet was thawed at room temperature. This was resuspended with 20 mL of the lysis buffer described above. The cells were lysed with 5 sonication cycles with 30 sec pause between each. The inclusion bodies were harvested by centrifugation at 20 000 g for 15 min in a fixed angle rotor (Beckman JA-25.50). The supernatant was discarded and the pellet resuspended in another 20 mL of lysis buffer. The sonication and centrifugation cycles were repeated six times as described above. The pellet from the final cycle was resuspended in 5 ml of lysis buffer without Triton X-114 and stored at 4 ºC until further use.

A sucrose density gradient was prepared as follows: 4 mL of 70% (w/v) sucrose, 9 mL 53% (w/v) sucrose and 4.5 mL 40% (w/v) sucrose. Each solution was prepared with MilliQ water. The gradient was loaded and allowed to stand for about 12 hours to settle. The inclusion bodies were then harvested by placing 2 mL of the suspension onto the gradient bed. Centrifugation was performed at 141 000 g for 5 hours in a preparative ultracentrifuge to fractionate the inclusion bodies. The target protein separated as a brown-gold disk in between the 70 and 53% layers. It was collected by further centrifugation at 13 000 g for 15 minutes in 2 mL reaction tubes. The supernatant was discarded and the pellet resuspended in 2mL of 1 M NaCl, 10 Mm Tris-HCL, pH 7.00, 1 mM DTT, 0.1 mM EDTA. Centrifugation was performed again at 13 000 g for 15 minutes. The pellet resuspension and centrifugation was repeated three times to remove excess sucrose. Following this, the pellet was resuspended in MilliQ water and the centrifugation step was repeated. The resuspension in water and centrifugation was also repeated several times to remove the excess NaCl. Finally, the pellet was resuspended in 1 mL Tris-HCl, pH 7.00, 10 mM $Na_2SO_4$, 1 mM DTT, and 0.1 mM EDTA. The suspension was then aliquoted into 100 µL portions and flash frozen in liquid nitrogen and store at -80 °C.

### 4.5.5 Resolubilization

One 100 µL aliquot of inclusion bodies was thawed on ice. Then, 60 µL of resolubilization buffer containing (1.67% sarkosyl, Tris-HCL, pH 7.00, 0.1 mM EDTA, and 1 mM DTT) was added to the aliquot. The suspension was then cooled on ice for another 5 minutes. The protein was resolubilized by pipetting up and down on ice for about 10 minutes or until the solution was clear. The solution was then diluted with 500 µL water in a stepwise manner (this is: 100 µL at a time). The sarkosyl was removed by centrifugation at 12 000 ×g for 10 minutes and the solubilized protein was collected in the supernatant.

### 4.5.6 Reconstitution

Liposomes were prepared from α-phosphatidylcholine by sonication for 20 seconds. The sonication was repeated 5 times with 30 second pause between cycles. The following

components were then added to the liposomal suspension: 60 µL soluble protein, 3% Triton X-114, 10 mM Tris-HCL, pH 7.00, 0.1 mM EDTA and 5 mM dePCoA (or P-PantSH) + 7.5 Mm TCEP. Following this, 500 µL of 2 mg/ml cardiolipin were added. The suspension was then mixed by vigorous vortexing. It was then flash frozen in liquid nitrogen and thawed at ~ 16 °C in a water bath. This cycle was repeated 5 times to promote formation of unilamellar vesicles. The unilamellar vesicles were then prepared by performing 20 extrusion passes on the Avanti Polar Lipids® mini-extruder fitted with 2 × polycarbonate filters.

### 4.5.7 Proteoliposome purification

An Amberlite-XAD column was prepared as follows: A 2 mL glass Pasteur pipette was sealed with cotton wool. Following this, 600 mg of Amberlite beads were placed in the column. The column was then washed with 13 passages of methanol (Merck, Germany) and then left in the methanol overnight. The methanol was then washed off with Tris-HCL buffer described in 4.5.7. Thereafter 1 ml of the reconstitution mixture was then passed through the column and eluted with the solubilization buffer. The first two 500 µL fractions were collected. These were pooled and the passage was repeated about 5 more times. Following this, excess metabolite was removed by size exclusion on a Sephadex G-75 (Amerscham, GE Healthcare) column prepared in house. The beads were hydrated with 10 mM Tris-HCL, pH 7.00, 0.1 mM EDTA and 5 mM NaCl +7.5 mM TCEP. Excess moisture was removed and the slurry was packed in a 5 mL syringe column sealed with cotton wool. The column was placed in a 15 mL centrifugal tube and residual buffer was removed by centrifugation at 3 000 g for 5 minutes. The flow-through was removed and the proteoliposomes suspension was loaded onto the column bed. The “pure” liposomes were then harvested by centrifugation at 1000 g for 5 minutes and collected in the flow through.

### 4.5.8 Efflux measurements

Efflux of dePCoA was measured by hydrating a dialysis unit with 900 µL of 10 mM Tris-HCl, pH 7.00 with 0.1 mM EDTA. Subsequently, 200 µL of the proteoliposome suspension was placed inside the dialysis unit and efflux was monitored by collecting 20 µL aliquots at 5 minute intervals for 25 minutes. Solutions of AMP, ADP, ATP and TPP were prepared to a final concentration of 100 mM each. Four dialysis unit were then hydrated with 4 × 900 µL of 10 mM Tris-HCl, pH 7.00 with 0.1 mM EDTA. The proteoliposome was added to each dialysis unit this time with 0.5 mM of respective adenosine nucleotide, to the final concentration of 200 µL. The efflux of dePCoA in the presence of the adenosine nucleotides was then measured by collecting 20 µL aliquots of each dialysate at 5 minute intervals for 25 minutes. The process was repeated for 3 mM and 6 mM adenosine nucleotides. Each 20 µL aliquot collected was transferred to a black 96-well plate to which 170 µL of Tris-HCl pH 7.00 and 10 µL of CPM

(100 μM) was added. The fluorescence intensity was then measured at $\lambda_{ex}$ = 387 and $\lambda_{em}$ = 465 nm of each aliquot such that the efflux could be reported as a fluorescence intensity time course. The slope of each time course was obtained from a linear curve-fit performed on the Sigma-plot version 14.0 software. This was such that the efflux rate was slope ± standard error of the fit. Efflux measurements of P-PantSH were performed in a similar manner using P-PantSH-loaded proteoliposome.

# Chapter 5: Concluding remarks and future studies

Membrane permeability of small molecules is an important but often neglected part of drug discovery. This can mainly be attributed to a lack of adequate investigational tools. Therefore, we described a discontinuous assay for measuring membrane permeability of CoA-related small molecules in an effort to address this limitation in the context of thiolated molecules like CoA. In addition, we were able to demonstrate the versatility of this assay setup by expanding it to molecules with other functionalities such as phosphorylated and non-phosphorylated pantothenate analogues. This was achieved by modification of the detection method used to quantify the molecules in question. Moreover, we demonstrated that the assay is also amenable to the study of membrane carriers, and was therefore applied to the study of a mitochondrial membrane carrier.

The most reproducible outcomes were observed with the CPM-based fluorescence detection method used to determine the diffusion rates of thiolated molecules. This method enables direct measurement of the molecule in question, while the other two methods used entailed measurement of a secondary factor related to the concentration of the molecules of interest. Unfortunately, this resulted in pronounced variability which made the measurements less reliable. This difference in reproducibility between the CPM-based and the coupled enzyme assay-based measurements is an indication that it would be worthwhile to identify other chromophores that work by a mechanism similar to that of CPM but recognise different reactive groups like the phosphate or amine moiety. Moreover, techniques like LC-MS could also be considered for more accurate measurements of the diffusion rates, since these are more sensitive than standard spectroscopic techniques. However, the drawback with such techniques include the cost implications.

The second aim of the study was to identify the molecular determinants that confer permeability by passive diffusion in pantothenate analogues. This was achieved by measuring membrane permeability across *in vitro* models of mammalian and bacterial membrane models. This was done in an effort to find out if there was any correlation between permeability and structure of the molecule of interest. We investigated the role of membrane composition in the ability of the molecules to cross membranes by passive. Unfortunately, no direct correlation was found between the permeability and the molecule's structure. However, the relevance of the phospho-pantoyl moiety in promoting permeability could at least be inferred from the data. On the other hand, the membrane fluidity analysis indicates that the permeability of P-PantSH more likely correlates with the fluidity of the membranes in question. This in turn suggests that manipulation of membrane composition to affect membrane fluidity

may offer a new mechanism to regulate the maintenance of CoA levels from exogenous sources.

Our final objective was to characterize a mitochondrial carrier associated with regulation of CoA – SLC25A16. Two other transporters with affinity towards CoA and dePCoA have been identified. However, in both cases the affinity was determined using homo-exchange experiments which measure the exchange of a radiolabelled molecule for the non-radiolabelled form. On the other hand, our results constitute the first report of the transport of a CoA-related molecule through direct measurement of its efflux. Specifically, dePCoA efflux was observed from SLC25A16 regardless of the presence of adenosine nucleotides, while the presence of ADP was required for P-PantSH efflux. Since this transporter is associated with regulation of mitochondrial CoA, its demonstrated affinity towards dePCoA and P-PantSH supports the view that homeostatic regulation of CoA is mediated by CoA biosynthetic intermediates in eukaryotic cells. This is useful information regarding the transporter and CoA homeostasis in general; however, a more comprehensive characterisation that includes other potential substrates would provide a more complete picture. The preparation of the proteoliposome also has to be optimised to eliminate doubt regarding the observed outcomes related to the presence of bacterial contaminant proteins. Furthermore, it may be worthwhile to re-visit the other two MCs associated with CoA transport—SLC25A17 and SLC25A42—to understand the involvement of all three in this process.

Taken together, these findings provide evidence that P-PantSH may indeed be a nexus metabolite of CoA metabolism, and this may have important implications for the development of drugs that target CoA biosynthesis and utilization. This may be in the context of human diseases for the treatment of (or delaying the onset of) neurodegenerative diseases, or alternatively as antimicrobials for the treatment of infectious diseases. Therefore, in order to improve our insight regarding the aspects of membrane permeability and transport of CoA as addressed in this dissertation, we have set out the following objectives for future studies:

1. Since the importance of the phospho-pantoyl moiety in promoting membrane permeability is suggested by our findings, the membrane permeability measurements of the phosphorylated and non-phosphorylated pantothenate analogues should be repeated with more sensitive detection methods in an effort to identify such a structure-permeability relationship.

2. To verify the correlation between membrane fluidity and permeability observed for P-PantSH, the membrane fluidity should also be examined using other biophysical techniques, such as differential scanning calorimetry (DSC) and SAXS, and the results compared to the permeability outcomes. This work should ideally be done by using a

range of liposomal formulations that differ in lipid identity and fluidity from those described in this study.

3. To optimise the purification of SLC25A16 and verify its identity with mass spectrometry, and to directly confirm its reconstitution in proteoliposomes with a multiplatform technique such as correlated light and electron microscopy (CLEM) that uses different detection techniques to create contrast between particles in a single micrograph.

4. The crystallization of SLC25A16 nano-disks to study the binding/substrate recognition site of the carrier protein – this will aid in identifying the true substrate for this mitochondrial carrier.

5. To perform the same analysis done on SLC25A16 on SLC25A42 and SLC25A17 using the membrane permeability assay described in chapter two, so as to directly confirm the transport of CoA and CoA-related metabolites by these carriers. This will complement the results achieved in previous studies that inferred their transport from exchange studies with labelled nucleotides.

# References


1. Pollastri, M. P. Overview on the Rule of Five. *Curr. Protoc. Pharmacol.* **49**, (2010).
2. Swinney, D. C. & Anthony, J. How were new medicines discovered? *Nat. Rev. Drug Discov.* **10**, (2011).
3. Hughes, J. P., *et al*. Principles of early drug discovery. *Brit. J. Pharm.* **162**, (2011).
4. Lindsay, M. A. Target discovery. *Nat. Rev. Drug Discov.* **2**, (2003).
5. Imming, P., *et al.* Drugs, their targets and the nature and number of drug targets. *Nat. Rev. Drug Discov.* **5**, (2006).
6. Overington, J. P., *et al.* How many drug targets are there? *Nat. Rev. Drug Discov.* **5**, (2006).
7. Boppana, K., *et al*. Knowledge based identification of MAO-B selective inhibitors using pharmacophore and structure based virtual screening models. *Eur. J. Med. Chem.* **44**, (2009).
8. McInnes, C. Virtual screening strategies in drug discovery. *Curr. Opi. Chem.Biol.***11**, (2007).
9. Law, R. *et al.* The multiple roles of computational chemistry in fragment-based drug design. *J. Comput. Aided. Mol. Des.* **23**, (2009).
10. Fox, S. *et al.* High-throughput screening: Update on practices and success. *Journal of Biomol. Scr.* **11**, (2006).
11. Torrance, C. J., *et al*. Use of isogenic human cancer cells for high-throughput screening and drug discovery. *Nat. Biotechnol.* **19**, (2001).
12. Veber, D. F. *et al.* Molecular properties that influence the oral bioavailability of drug candidates. *J. Med. Chem.* **45**, (2002).
13. Lipinski, C. A. Drug-like properties and the causes of poor solubility and poor permeability. *J. Pharmacol. Toxicol. Meth.* **44**, (2000).
14. Ertl, P., *et al*. Fast calculation of molecular polar surface area as a sum of fragment-based contributions and its application to the prediction of drug transport properties. *J. Med. Chem.* **43**, (2000).
15. Yang, N. J. & Hinner, M. J. Getting across the cell membrane: an overview for small molecules, peptides, and proteins. *Methods in molecular biology (Clifton, N.J.)* **1266**, (2015).
16. Subczynski, W. K., *et al*. Oxygen permeability of phosphatidylcholine-cholesterol membranes. *Proc. Natl. Acad. Sci. U. S. A.* **86**, (1989).
17. Orbach, E. & Finkelstein, A. The nonelectrolyte permeability of planar lipid bilayer membranes. *J. Gen. Physiol.* **75**, (1980).
18. Toyoshima, C., *et al*. First crystal structures of Na +,K +-ATPase: New light on the oldest ion pump. *Structure.* **19**, (2011).
19. Mueckler, M. & Thorens, B. The SLC2 (GLUT) family of membrane transporters. *Molecular Aspects of Medicine.* **34**, (2013).

20. Enyedi, P. & Czirják, G. Molecular background of leak K+ currents: Two-pore domain potassium channels. *Physiol. Rev.* **90**, (2010).

21. Duax, W. L. *et al.* Molecular structure and mechanisms of action of cyclic and linear ion transport antibiotics. *Biopolymers.* **40**, (1996).

22. Andrade, S. L. A. & Einsle, O. The Amt/Mep/Rh family of ammonium transport proteins (Review). *Mol. Mem. Biol.* **24**, (2007).

23. Amin, M. L. p-glycoprotein Inhibition for Optimal Drug Delivery. *Drug Tar. Ins.* ***7*** (2013).

24. Stein, E. D. Do Dietary Levels of Pantothenic Acid Regulate Its Intestinal Uptake in Mice? *Artic. J. Nutr.* **119** (1989).

25. Zachowski, A. Phospholipids in animal eukaryotic membranes: transverse asymmetry and movement. *Biochem. J.* **294**, (1993).

26. van Meer, G., *et al.* Membrane lipids: where they are and how they behave. *Nat. Rev. Mol. Cell Biol.* **9**, (2008).

27. Armbruster, B. N. *et al.* Molecular cell biology. *Science.* **101**, (2009).

28. Spector, A. A. & Yorek, M. A. Membrane lipid composition and cellular function. *J. Lipid Res.* **26**, (1985).

29. Hancock, R. E. W. Alterations in structure of the cell envelope. *Ann. Rev. Microbiol.* **38**, (1984).

30. J.Silhavy, T., Kahne, D. & Walker, S. The bacterial cell envelope. *Cold Spring Harb. Perspect. Biol.* **2**, (2010).

31. Sohlenkamp, C. & Geiger, O. Bacterial membrane lipids: Diversity in structures and pathways. *FEMS Microbiol. Rev.* **40**, (2015).

32. Delcour, A. H. Outer membrane permeability and antibiotic resistance. *BBA - Prot. Proteom.* **1794**, (2009).

33. Graef, F. *et al.* The bacterial cell envelope as delimiter of anti-infective bioavailability – An in vitro permeation model of the Gram-negative bacterial inner membrane. *J. Contl. Rel.* **243**, (2016).

34. Blanco, P., *et al.* Bacterial multidrug efflux pumps: much more than antibiotic resistance determinants. *Microorganisms*, **4,** (2016).

35. Blair, J. M. A. & Piddock, L. J. V. How to Measure Export via Bacterial Multidrug Resistance Efflux Pumps. *mBio*. **7**, (2016).

36. Du, D. *et al.* Multidrug efflux pumps: structure, function and regulation. *Nat. Rev. Microbiol.* **16**, (2018).

37. Andersen, C., *et al*. Protein export and drug efflux through bacterial channel-tunnels. *Curr. Opi. Cell Biol.* **13**, (2001).

38. Piddock, L. J. V. Multidrug-resistance efflux pumps? Not just for resistance. *Nat. Rev. Microb.* **4**, (2014).

39. Finkelstein, A. Water and nonelectrolyte permeability of lipid bilayer membranes. *J. Gen. Physiol.* **68**, (1976).

40. Lande, M. B. The relationship between membrane fluidity and permeabilities to water, solutes, ammonia, and protons. *J. Gen. Physiol.* **106**, (1995).

41. Ingólfsson, H. I. *et al.* Lipid organization of the plasma membrane. *J. Am. Chem. Soc.* **136**, (2014).

42. Ernst, R., *et al.* Homeoviscous Adaptation and the Regulation of Membrane Lipids. *J. Mol. Biol.* **428**, (2016).

43. van Blitterswijk, W. J., *et al*. Quantitative Contributions of Cholesterol and the Individual Classes of Phospholipids and Their Degree of Fatty Acyl (Un)Saturation to Membrane Fluidity Measured by Fluorescence Polarization. *Biochemistry* **26**, (1987).

44. Paula, S., *et al*. Permeation of protons, potassium ions, and small polar molecules through phospholipid bilayers as a function of membrane thickness. *Biophys. J.* **70**, (1996).

45. Hidalgo, I. J., *et al*. *Characterization of the Human Colon Carcinoma Cell Line (Caco-2) as a Model System for Intestinal Epithelial Permeability*. *Gastroenterology.* **96**, (1989).

46. Hilgers, A. R., *et al*. Caco-2 Cell Monolayers as a Model for Drug Transport Across the Intestinal Mucosa. *Pharm. Res. An Off. J. Am. Assoc. Pharm. Sci.* **7**, (1990).

47. Augustijns, P., *et al.* Evidence for a polarized efflux system in Caco-2 cells capable of modulating cyclosporine A transport. *BBRC.* **197**, (1993).

48. Artursson, P., *et al.* Caco-2 monolayers in experimental and theoretical predictions of drug transport. Adv. *Drug del. Rev.* **46***,*(2012).

49. Regazzo, D.,*et al*. The (193–209) 17-residues peptide of bovine β-casein is transported through Caco-2 monolayer. *Mol. Nutr. and food Res.* **54***,* (2010).

50. Teksin, Z. S., *et al*. Comparison of Drug Permeabilities and BCS Classification: Three Lipid-Component PAMPA System Method versus Caco-2 Monolayers. *AAPS J.* **12**, (2010).

51. Petit, C. *et al.* Prediction of the Passive Intestinal Absorption of Medicinal Plant Extract Constituents with the Parallel Artificial Membrane Permeability Assay (PAMPA). *Planta Med.* **82** (2016).

52. Campbell, S. D., *et al*. Significance of lipid composition in a blood-brain barrier-mimetic PAMPA assay. *J. Biomol. Screen.* **19***,* (2014).

53. Akbarzadeh, A. *et al.* Liposome: Classification, preparation, and applications. *Nanoscale Res. Lett.* **8**, (2013).

54. Lasic, D. D. Novel applications of liposomes. *Trends Biotech.* **16**, (1998).

55. Deng, N.-N., *et al.* Monodisperse Uni-and Multicompartment Liposomes. ACS. **138,** (2016).

56. Tan, G. *et al.* Bioadhesive chitosan-loaded liposomes: A more efficient and higher permeable ocular delivery platform for timolol maleate. *Int. J. Biol. Macromol.* **94**, (2017).

57. Batzri, S. & Korn, E. D. Single bilayer liposomes prepared without sonication. *BBA - Biomembr.* **298**, (1973).

58. Novelli. C.D., The involvement of coenzyme A in acetate oxidation in yeast. *J. Biol. Chem.* **171**, (1947).

59. Rufer, A. C., *et al*. Structural insight into function and regulation of carnitine palmitoyltransferase. *Cell. Mol. Sci.* **66**, (2009).

60. Hollebeke, J.,*et al*. N-terminal acetylation and other functions of Nα-acetyltransferases. *Biol. Chem.* **393**, (2012).

61. Choudhary, C., *et al*. The growing landscape of lysine acetylation links metabolism and cell signalling. *Nat. Rev. Mol. Cell Biol.* **15**, (2014).

62. Cotter, D. G., *et al*. Ketone body metabolism and cardiovascular disease. *American J. Physiol - Heart Circ.Physiol.* **304**, (2013).

63. Begley, T. P., *et al.* The biosynthesis of coenzyme a in bacteria. *J. Biol. Chem*. **61**, (2001).

64. Rgen Stolz, J. & Sauer, N. The Fenpropimorph Resistance Gene FEN2 from *Saccharomyces cerevisiae* Encodes a Plasma Membrane H-Pantothenate Symporter. *J. biol. Chem.* **274**, (1999).

65. Augagneur, Y. *et al.* Identification and Functional Analysis of the Primary Pantothenate Transporter, PfPAT, of the Human Malaria Parasite *Plasmodium falciparum. J. Biol. Chem. **288**,* (2013).

66. Uchida, Y. *et al.* Major involvement of $Na^+$-dependent multivitamin transporter (SLC5A6/SMVT) in uptake of biotin and pantothenic acid by human brain capillary endothelial cells. *J. Neurochem.* **134**, (2015).

67. Huang, L. *et al.* A plastidial pantoate transporter with a potential role in pantothenate synthesis. *Biochem. J.* **475**, (2018).

68. Vallari, D. S. & Rock, C. O. *Isolation and Characterization of Escherichia coli Pantothenate Permease (panF) Mutants*. *J. Bact.* **164**, (1985).

69. Reizer, J., Reizer, A., The Na+/pantothenate symporter (PanF) of *Escherichia coli* is homologous to the Na+/proline symporter (PutP) of *E. coli* and the Na+/glucose symporters. *Microbiol. Res.* (1990).

70. Saliba, K. J. & Kirk, K. pH regulation in the intracellular malaria parasite, *Plasmodium falciparum*. H+ extrusion via a V-type H+-ATPase. *J. Biol. Chem.* **274**, (1999).

71. Desai, S. A., *et al*. A nutrient-permeable channel on the intraerythrocytic malaria parasite. *Nature* **362**, (1993).

72. Cronan, J. E., *et al. Genetic and Biochemical Analyses of Pantothenate Biosynthesis in Escherichia coli and Salmonella typhimurium*. *J. Bact.* **149** (1982).

73. Vallari, D. S. & Rock, C. O. *Pantothenate Transport in Escherichia coli*. *J. Bact.* **162**, (1985).

74. Gerdes, S. Y. *et al.* From Genetic Footprinting to Antimicrobial Drug Targets: Examples in Cofactor Biosynthetic Pathways. *J. Bacteriol.* **184**, (2002).

75. Fleischmann, R. D. *et al.* Whole-genome random sequencing and assembly of *Haemophilus influenzae* Rd. *Science.* **269**, (1995).

76. Parkhill, J. *et al.* Complete genome sequence of a multiple drug resistant *Salmonella enterica* serovar Typhi CT18. *Nature* **413**, (2001).

77. Wang, H. *et al.* Human placental Na+-dependent multivitamin transporter. Cloning, functional expression, gene structure, chromosomal localization. *J. Biol. Chem.* **274**, (1999).

78. Prasad, P. D. *et al.* Molecular and functional characterization of the intestinal Na+-dependent multivitamin transporter. *Arch. Biochem. Biophys.* **366**, (1999).

79. Prasad, P. D. *et al.* Cloning and Functional Expression of a cDNA Encoding a Mammalian Sodium-dependent Vitamin Transporter Mediating the Uptake of Pantothenate, Biotin, and Lipoate*. J. Biol. Chem.* **277**, (1998).

80. Saliba, K. J., *et al*. Provitamin B5 (Pantothenol) inhibits growth of the intraerythrocytic malaria parasite. *Antimicrob. Agents Chemother.* **49**, (2005).

81. Spry, C., *et al*. Coenzyme A biosynthesis: An antimicrobial drug target. *FEMS Microbiol. Rev.* **32**, (2008).

82. Kirk, K., *et al.* Transport of Diverse Substrates into Malaria-infected Erythrocytes via a Pathway Showing Functional Characteristics of a Chloride Channel*. J. Biol. Chem*. **269**, (1994).

83. Ginsburg, H., *et al.* How many functional transport pathways does Plasmodium falciparum induce in the membrane of its host erythrocyte? new permeability pathways induced in the membranes of *Plasmodium falciparum*. *Mol. Biochem. Parasitol.* **8**, (2005).

84. Strauss, E. & Begley, T. P. The Antibiotic Activity of N-Pentylpantothenamide Results from Its Conversion to Ethyldethia-Coenzyme A, a Coenzyme A Antimetabolite. *J. Biol. Chem.* **277**, (2002).

85. Barnard, L., et al. Developing Pantetheinase-Resistant Pantothenamide Antibacterials: Structural Modification Impacts on PanK Interaction and Mode of Action. *ACS Infect. Dis.* **4**, (2018).

86. Leonardi, R., et al. Coenzyme A: Back in action. *Prog. Lipid Res.* **44**, (2005).

87. Zhang, Y.-M. *et al.* Acyl Carrier Protein Is a Cellular Target for the Antibacterial Action of the Pantothenamide Class of Pantothenate Antimetabolites. *J. Biol. Chem.* **279**, (2004).

88. Spry, C., *et al*. Pantothenate Utilization by Plasmodium as a Target for Antimalarial Chemotherapy. *Infect. Disord. - Drug Targets* .**10**, (2012).

89. Macuamule, C. J. *et al.* A pantetheinase-resistant pantothenamide with potent, on-target, and selective antiplasmodial activity. *Antimicrob. Agents Chemother.* **59**, (2015).

90. de Villiers, M. *et al.* Antiplasmodial Mode of Action of Pantothenamides: Pantothenate Kinase Serves as a Metabolic Activator Not as a Target. *ACS Infect. Dis.* **3** (2017).

91. Song, W.-J. & Jackowski, S. Cloning, Sequencing, and Expression of the Pantothenate Kinase *(coaA)* Gene of *Escherichia coli*. *J. Biol. Chem.* **174**, (1992).

92. Dunnt, S. D. & Snell, E. E. Isolation of Temperature-Sensitive Pantothenate Kinase Mutants of *Salmonella typhimurium and* Mapping of the *coaA Gene J.Biol Chem.* **140**, (1979).

93. Strauss, E., et al. Phosphopantothenoylcysteine Synthetase from *Escherichia coli* identification and charcaterisation of the last unidentified Coenzyme A biosynthetic enzyme in bacteria. *J. Biol. Chem.* **276**, (2001).

94. Daugherty, M. *et al.* Complete Reconstitution of the Human Coenzyme A Biosynthetic Pathway via Comparative Genomics. *J. Biol. Chem.* **277,** (2002).

95. Izard, T. A Novel Adenylate Binding Site Confers Phosphopantetheine Adenylyltransferase Interactions with Coenzyme A. *J. Bacteriol.* **185**, (2003).

96. Strauss, E., et al. Biocatalytic Production of Coenzyme A Analogues. *ChemCatChem.* **2**, (2010).

97. Vallari, D. S., *et al.* Regulation of pantothenate kinase by coenzyme A and its thioesters. *J. Biol. Chem.* **262**, (1987).

98. Song, W.-J. & Jackowski S.O., Kinetics and Regulation of Pantothenate Kinase from *Escherichia coli . J. Biol. Chem.* **269**, (1994).

99. Brand, L. A. & Strauss, E. Characterization of a New Pantothenate Kinase Isoform from *Helicobacter pylor*i. *J. Biol. Chem.* **280**, (2005).

100. Dansie, L. E. *et al.* Physiological roles of the pantothenate kinases. *Biochem. Soc. Trans*. **42**, (2014).

101. Leonardi, R. *et al.* A pantothenate kinase from *Staphylococcus aureus* refractory to feedback regulation by coenzyme A. *J. Biol. Chem.* **280**, (2005).

102. Choudhry, A. E. *et al.* Inhibitors of Pantothenate Kinase: Novel Antibiotics for Staphylococcal Infections. *Antimicrob. Agents Chemother.* **47**, (2003).

103. Kupke, T. *et al.* Molecular Characterization of Lantibiotic-synthesizing Enzyme EpiD Reveals a Function for Bacterial Dfp Proteins in Coenzyme A Biosynthesis. *J. Biol. Chem.* **275** (2000).

104. Genschel, U. Coenzyme A Biosynthesis: Reconstruction of the Pathway in Archaea and an Evolutionary Scenario Based on Comparative Genomics. *Mol. Biol. Evol.* **21**, (2004).

105. Begley, T. P., Kinsland, C. & Strauss, E. The biosynthesis of coenzyme A in bacteria. *Vitam. Horm.* **61**, (2001).

106. Worrall, D. M. & Tubbs, P. K. A bifunctional enzyme complex in coenzyme A biosynthesis: purification of pantetheine phosphate adenylyltransferase and dephospho-CoA kinase. *Biochem. J* .**215**, (1983).

107. Martin, D. P. & Drueckhammer, D. G. Separate enzymes catalyze the final two steps of coenzyme A biosynthesis in Brevibacterium ammoniagenes: Purification of pantetheine phosphate adenylyltransferase. *BBRC.* **192**, (1993).

108. Sibon, O. C. M. & Strauss, E. Coenzyme A: to make it or uptake it? *Nat. Rev. Mol. Cell. Biol.* **17**, (2016).

109. Hayflick, S. J. Coenzyme A and Its Derivatives in Cellular Metabolism and Disease Defective pantothenate metabolism and neurodegeneration. *Bioch. Soc. trans.* **42** (2014).

110. Sharma, L. K. *et al.* A therapeutic approach to pantothenate kinase associated neurodegeneration. *Nat. Commun.* **9**, (2018).

111. Huang, L. *et al.* A family of metal-dependent phosphatases implicated in metabolite damage-control. *Nat. Chem. Biol.* **12**, (2016).

112. Balibar, C. J.,*et al.* Pantethine rescues phosphopantothenoylcysteine synthetase and phosphopantothenoylcysteine decarboxylase deficiency in *Escherichia coli* but not in *Pseudomonas aeruginosa*. *J. Bacteriol.* **193**, (2011).

113. Zhou, B. *et al.* A novel pantothenate kinase gene (PANK2) is defective in Hallervorden-Spatz syndrome. *Nat. Genet.* **28**, (2001).

114. Rana, A. *et al.* Pantethine rescues a *Drosophila* model for pantothenate kinase-associated neurodegeneration. PNAS, **17,** (2003).

115. Srinivasan, B. *et al.* Extracellular 4′-phosphopantetheine is a source for intracellular coenzyme A synthesis. *Nat. Chem. Biol.* **11**, (2015).

116. Wittwer, C. T., et al. Metabolism of pantethine in cystinosis. *J. Clin. Invest.* **76**, (1985).

117. Leonardi, R., *et al*. Pantothenate kinase 1 is required to support the metabolic transition from the fed to the fasted state. *PLoS One* **5**, (2010).

118. Alfonso-Pecchio, A., *et al*. Compartmentalization of Mammalian Pantothenate Kinases. *PLoS One* **7**, (2012).

119. Kotzbauer, P. T., *et al*. Neurobiology of Disease Altered Neuronal Mitochondrial Coenzyme A Synthesis in Neurodegeneration with Brain Iron Accumulation Caused by Abnormal Processing, Stability, and Catalytic Activity of Mutant Pantothenate Kinase 2. *J. Neurosci*. **5**, (2005).

120. Johnson, M. A. *et al.* Mitochondrial localization of human PANK2 and hypotheses of secondary iron accumulation in pantothenate kinase-associated neurodegeneration. *Ann. N. Y. Acad. Sci.* **1012**, (2004).

121. Hörtnagel, K., et al. An isoform of hPANK2, deficient in pantothenate kinase-associated neurodegeneration, localizes to mitochondria. *Human mol. gen.* **12**, (2003).

122. Zhyvoloup, A. *et al.* Subcellular Localization and Regulation of Coenzyme A Synthase. *J. Biol. Chem.* **278**, (2003).

123. Vozza, A. *et al.* Biochemical characterization of a new mitochondrial transporter of dephosphocoenzyme A in *Drosophila melanogaster*. *BBA - Bioenerg.* **1858**, (2017).

124. Fiermonte, G., *et al.* A novel member of solute carrier family 25 (SLC25A42) is a transporter of coenzyme A and adenosine 3',5'-diphosphate in human mitochondria. *J. Biol. Chem.* **284**, (2009).

125. Agrimi, G., *et al*. The human gene SLC25A17 encodes a peroxisomal transporter of coenzyme A, FAD and NAD. *Biochem. J* . **443**, (2012).

126. Dusi, S. *et al.* Exome sequence reveals mutations in CoA synthase as a cause of neurodegeneration with brain iron accumulation. *Am. J. Hum. Genet.* **94**, (2014).

127. Meo, I. Di, *et al.* Acetyl-4′-phosphopantetheine is stable in serum and prevents phenotypes induced by pantothenate kinase deficiency. *Sci. Rep.* ***9,*** (2017).

128. Jackowski, S. & Rock, C. Metabolism of 4 ’ -Phosphopantetheine in *Escherichia coli. J. Bact.* **158**, (1984).

129. Jackowski, S. & Rock, C. O. Regulation of coenzyme A biosynthesis. *J. Bact.* **148**, (1981).

130. Kallinteri, P. *et al.* Dexamethasone incorporating liposomes: An *in vitro* study of their applicability as a slow releasing delivery system of dexamethasone from covered metallic stents. *Biomaterials* **23**, (2002).

131. Szoka, F. Comparative Properties and Methods of Preparation of Lipid Vesicles (Liposomes) Bioresponsive vectors View project comparative properties and methods of preparation of lipid vesicles. *Annu. Rev. Biophys. Bioeng.* ***9,*** (1980)

132. Crosasso, P. *et al.* Preparation, characterization and properties of sterically stabilized paclitaxel-containing liposomes. *J. Conl. Rel.* **63**, (2000).

133. Nichols, J. W., et al. measurement of the net proton-hydroxyl permeability of large unilamellar liposomes with fluorescent probe 9-aminoacridine.*BBA-Biomem*, **596**, (1980).

134. Nikaido, H; Varra, M. Molecular basis of bacterial outer membrane permeability. *Microbiol. Mol. Biol. Rev.* **67**, (1985).

135. Di, L. *et al.* Development of a new permeability assay using low-efflux MDCKII cells. *J. Pharm. Sci.* **100,** (2011).

136. Graef, F. *et al.* The bacterial cell envelope as delimiter of anti-infective bioavailability – An in vitro permeation model of the Gram-negative bacterial inner membrane. *J. Contl. Rel.* **243**, (2016).

137. Sani, M. A. & Separovic, F. How Membrane-Active Peptides Get into Lipid Membranes. *Acc. Chem. Res.* **49,** (2016).

138. Jesorka, A. *et al.* Generation of phospholipid vesicle-nanotube networks and transport of molecules therein. *Nat. Protoc.* **6**, (2011).

139. Eyer, K. *et al.* A liposomal fluorescence assay to study permeation kinetics of drug-like weak bases across the lipid bilayer. *J. Contl. Rel.* **173**, (2014).

140. Ong, S. G. M., *et al.* Evaluation of extrusion technique for nanosizing liposomes. *Pharmaceutics.* **8**, (2016).

141. Campos, M. *et al.* A constant size extension drives bacterial cell size homeostasis. *Cell.* **159**, (2014).

142. Ross, F. M. Opportunities and challenges in liquid cell electron microscopy. *Science.* **350**, (2015).

143. Ryabov, A. & Baum, P. Electron microscopy of electromagnetic waveforms. *Science.* **353**, (2016).

144. Stetefeld, J., *et al.* Dynamic light scattering: a practical guide and applications in biomedical sciences. *Biophy. Rev.* **8**, (2016).

145. Goosen, R. & Strauss, E. Simultaneous quantification of coenzyme A and its salvage pathway intermediates in in vitro and whole cell-sourced samples. *RSC Adv.* **7**, (2017).

146. Ribas, V., *et al*. Glutathione and mitochondria. *Front. Pharmacol*. **5** (2014).

147. Chattoraj, S., *et al*. Role of Red-Ox Cycle in Structural Oscillations and Solvation Dynamics in the Mitochondria of a Live Cell. *J. Phys. Chem. B.* **119**, (2015).

148. Yi, J.-R. *et al.* Expression Cloning of a Rat Hepatic Reduced Glutathione Transporter with Canalicular Characteristics. *J. Clin. Invest.* **93**, (1994).

149. Zhang, M.-Y. *et al.* A Novel Family of Transporters Mediating the Transport of Glutathione Derivatives in Plants . *Plant Physio.* **134**, (2004).

150. Pittman, M. S., *et al.* A Bacterial Glutathione Transporter (*Escherichia coli* CydDC) Exports Reductant to the Periplasm *J. Biol. Chem*. **280,** (2005).

151. de Villiers, M., *et al*. Variation in pantothenate kinase type determines the pantothenamide mode of action and impacts on coenzyme A salvage biosynthesis. *FEBS J.* **281,** (2014).

152. Rgen Stolz, J. & Sauer, N. The Fenpropimorph Resistance Gene FEN2 from *Saccharomyces cerevisiae* Encodes a Plasma Membrane H-Pantothenate Symporter. *J. Biol. Chem.* **274**, (1999).

153. Lowe, D. & John, S. *Alkaline Phosphatase*. *Stat Pearls* (2019).

154. Geladopoulos, T.,*et al.* A malachite green colorimetric assay for protein phosphatase activity. *Anal. Biochem.* **192,** (1991).

155. Baykov, A. A., *et al*. A malachite green procedure for orthophosphate determination and its use in alkaline phosphatase-based enzyme immunoassay. *Anal. Biochem.* **171**, (1988).

156. Sonna, L. A., *et al.* The Mechanism of Glucose 6-Phosphate Transport by *Escherichia coli*. *J. Biol. Chem* **263**, (1988).

157. Kammerer, B. *et al.* Molecular Characterization of a Carbon Transporter in Plastids from Heterotrophic Tissues: The Glucose 6-Phosphate/ Phosphate Antiporter. *The Plant Cell* **10**, (1998).

158. Srinivasan, B. & Sibon, O. C. M. Coenzyme A, more than 'just' a metabolic cofactor. *Biochem. Soc. Trans.* **42**, (2014).

159. Wesołowska, O., *et al.* Interaction of the chemopreventive agent resveratrol and its metabolite, piceatannol, with model membranes. *BBA - Biomem.* **9** (2009).

160. Sułkowski, W. W., *et al*. The influence of temperature, cholesterol content and pH on liposome stability. *J. Mol. Struct.* **744**, (2005).

161. Ladbrooke, B. D., *et al.* Studies on lecithin-cholesterol-water interactions by differential scanning calorimetry and X-ray diffraction. *BBA - Biomem.* **150**, (1968).

162. Svergun, D.I & Koch M.H.J., Small angle scattering of small molecules *Rep. Prog. Phys.* **66**, (2003).

163. Krasnowska, E. K., *et al.* Prodan as a Membrane Surface Fluorescence Probe: Partitioning between Water and Phospholipid Phases. *Biophys. J.* **74**,(1998).

164. Suhaj, A. *et al.* Prodan differentially influences its local environment. *Phys. Chem. Chem. Phys.* **20**, (2018).

165. Phosphatidylethanolamine - an overview | ScienceDirect Topics. Available at: https://www.sciencedirect.com/topics/agricultural-and-biological-sciences/phosphatidylethanolamine. (Accessed: 12th December 2019)

166. Phosphatidylglycerol - an overview | ScienceDirect Topics. Available at: https://www.sciencedirect.com/topics/medicine-and-dentistry/phosphatidylglycerol. (Accessed: 12th December 2019)

167. Cardiolipin - an overview | ScienceDirect Topics. Available at: https://www.sciencedirect.com/topics/neuroscience/cardiolipin. (Accessed: 12th December 2019)

168. Bogs, J. *et al.* Functional characterization and expression analysis of a glutathione transporter, BjGT1, from *Brassica juncea*: Evidence for regulation by heavy metal exposure. *Plant, Cell Environ.* **26** (2003).

169. Parasassi, T., et al. Phase fluctuation in phospholipid membranes revealed by Laurdan fluorescence. *Biophys. J.* **57**, (1990)

170. Cafiso, D. S. & Hubbell, W. L. Estimation of Transmembrane Potentials from Phase Equilibria of Hydrophobic Paramagnetic Ions. *Biochemistry*. **17**, (1978).

171. Gouaux, E. & MacKinnon, R. Principles of Selective Ion Transport in Channels and Pumps. *Science.* **310**, (2005).

172. Lind, T. K., *et al*. Formation and Characterization of Supported Lipid Bilayers Composed of Phosphatidylethanolamine and Phosphatidylglycerol by Vesicle Fusion, a Simple but Relevant Model for Bacterial Membranes. *ACS Omega.* **4**, (2019).

173. Gruner, S. M., *et al*. Novel Multilayered Lipid Vesicles: Comparison of Physical Characteristics of Multilamellar Liposomes and Stable Plurilamellar Vesicles. *Biochemistry.* **24**, (1985).

174. Graef, F. *et al. In Vitro* Model of the Gram-Negative Bacterial Cell Envelope for Investigation of Anti-Infective Permeation Kinetics. *ACS Infect. Dis.* **4**, (2018).

175. Ebner, F., *et al.* Topical use of dexpanthenol in skin disorders. *A. J. Clin. Dermat.* **3**, (2002).

176. Lambers, H., *et al.* Natural skin surface pH is on average below 5, which is beneficial for its resident flora. *Int. J. Cosmet. Sci.* **28**, (2006).

177. Krämer, S. D., *et al.* Lipid-bilayer permeation of drug-like compounds. *Chem. Biodivers.* **6**, (2009).

178. Palmieri, F. & Monné, M. Discoveries, metabolic roles and diseases of mitochondrial carriers: A review. *BBA - Mol. Cell Res.* **1863**, (2016).

179. Palmieri, F. Mitochondrial carrier proteins. *FEBS Letters* **346**, (1994).

180. Palmieri, F. & Pierri, C. L. Mitochondrial metabolite transport. *Essays Biochem.* **47**, (2010).

181. Palmieri, F., *et al.* Evolution, structure and function of mitochondrial carriers: A review with new insights. *Plant J.* **66**, (2011).

182. Khan, S. *et al.* A homozygous missense mutation in SLC25A16 associated with autosomal recessive isolated fingernail dysplasia in a Pakistani family. *Brit. J. Derm.* **178,** (2018).

183. Shamseldin, H. E. *et al.* Mutation of the mitochondrial carrier SLC25A42 causes a novel form of mitochondrial myopathy in humans. *Hum. Genet.* **135**, (2016).

184. Fiermonte, G., *et al.* Expression in *Escherichia coli*, functional characterization, and tissue distribution of isoforms A and B of the phosphate carrier from bovine mitochondria. *J. Biol. Chem.* **273**, (1998).

185. Fiermonte, G., *et al.* Abundant bacterial expression and reconstitution of an intrinsic membrane-transport protein from bovine mitochondria. *Biochem. J.* **294**, (1993).

186. Smith, B. J. SDS Polyacrylamide Gel Electrophoresis of Proteins. *Methods Mol. Biol.* **1,** (1984).

187. EE Fairbanks. A modification of Lemberg's staining method. *J. earth Planet. Sci.* **10**, (1925).